Engineering Journal

American Institute of Steel Construction

Second Quarter 2014 Volume 51, No. 2

ENGINEERING JOURNAL

AMERICAN INSTITUTE OF STEEL CONSTRUCTION

Dedicated to the development and improvement of steel construction, through the interchange of ideas, experiences and data.

ENGINEERING JOURNAL (ISSN 0013-8029) is published quarterly. Subscriptions: Members: one subscription, $40 per year, included in dues; Additional Member Subscriptions: $40 per year. Non-Members U.S.: $160 per year. Foreign (Canada and Mexico): Members $80 per year. Non-Members $160 per year. Published by the American Institute of Steel Construction at One East Wacker Drive, Suite 700, Chicago, IL 60601.

Periodicals postage paid at Chicago, IL and additional mailing offices. **Postmaster:** Send address changes to ENGINEERING JOURNAL in care of the American Institute of Steel Construction, One East Wacker Drive, Suite 700, Chicago, IL 60601.

Message from the Editor

Anytime I run across statistics about our nation's bridge infrastructure, I am staggered by the numbers. For example, the Federal Highway Administration's National Bridge Inventory statistics for 2012 indicate that there are 607,000 bridges in the United States and that 24% of them are either structurally deficient or functionally obsolete. Those numbers imply that a significant amount of bridge construction is in our future.

Most bridges are not signature spans like New York's Tappan Zee Bridge—a steel truss structure currently being replaced with twin cable-stayed steel structures. Rather, they are the highway bridges we drive over and under every day. The National Steel Bridge Alliance is always on the lookout for innovations that further increase the cost effectiveness of these types of steel bridges. One such concept is called "simple-made-continuous" or "simple for dead load–continuous for live load" (SDCL for short). The SDCL concept combines the constructability of simple-span structures with the in-service performance of continuous spans through the use of a unique field connection between adjacent girders. This field connection has been the focus of several studies investigating the ease of construction and long-term durability of effective connection details.

This year, the second and third quarter issues of *Engineering Journal* contain a collection of peer-reviewed papers highlighting some of this SDCL research. In a slight departure from our regular format, one paper in each issue presents a successful SDCL steel bridge case study.

For more information on SDCL steel bridge solutions, visit the National Steel Bridge Alliance at www.steelbridges.org.

Sincerely,

Keith A. Grubb, P.E., S.E.
Editor

Simple for Dead Load–Continuous for Live Load Steel Bridge Systems

ATOROD AZIZINAMINI

ABSTRACT

This paper presents the development of design, fabrication, erection and construction procedures for a new steel bridge system referred to as simple for dead and continuous for live loads (SDCL). The economy of the SDCL system depends on several factors, including the use of economical and efficient details over the interior supports. Extensive experimental, numerical and analytical work was conducted to develop economical details and efficient ways of using the SDCL steel bridge system for straight and minimally skewed bridges in which the skew angle is less than 10°. Several bridges were then designed using the research results, and their performance from the time of fabrication to construction and their long-term behavior were studied. This knowledge was then used to provide detailed information on design, fabrication, erection and construction procedures for steel bridges using the SDCL system. This paper provides a summary of the entire work, including design recommendations and economical details to be employed in conjunction with the SDCL steel bridge system.

Keywords: steel bridges, steel girders, SDCL, simple for dead load–continuous for live load.

INTRODUCTION

The simple for dead and continuous for live load (SDCL) system is providing steel bridges with new horizons and opportunities for developing economical bridge systems, especially in cases for which accelerating the construction process is a priority. The system has many advantages over conventional methods of constructing straight and minimally skewed steel bridges in which the skew angle is less than 10°, including lower initial and life-cycle costs, easier inspection and reduced maintenance. The key to economic application of the system lies in selecting appropriate connection details over interior supports to provide live load continuity. Due to the lack of guidelines, unnecessarily complicated details are often used in practice. The SDCL steel bridge system also provides an attractive alternative for application in highly seismic areas, but additional research is necessary.

The objective of this paper is to provide complete information for design, fabrication and construction of straight and slightly skewed steel bridges using the SDCL concept. The information presented is based on more than 10 years of comprehensive research, parts of which are published in the form of final research reports (Azizinamini, Lampe and Yakel, 2003; Azizinamini, Yakel and Farimani, 2005; Azizinamini et al., 2005). The investigation included the development of an economical concept for the SDCL system for use in both conventional and Accelerated Bridge Construction (ABC), development of design provisions and field application and long-term monitoring of SDCL systems that are open to traffic. Additional results of this comprehensive research effort are summarized and published in the research dissertations of six graduate students (Lampe, 2001; Mossahebi, 2004; Otte, 2006; Farimani, 2006; Kowalski, 2007; Javidi, 2009). This paper provides a summary of the overall work that was carried out, with references to more detailed information on various aspects of the research study.

The following briefly describes four significant aspects of the research study:

Experimental Investigation. Full-scale tests were carried out to develop practical details for joining girders over the interior supports for live load continuity using conventional construction practices (Lampe et al., 2014).

Force Transfer Mechanism. Comprehensive numerical and analytical studies were carried out to provide an understanding of the force transfer mechanism for the details that were developed to connect the steel girders in the SDCL system over the interior supports (Farimani et al., 2014). A detailed design approach was then developed that provided an excellent comparison with the test results. This detailed design method was then used to develop a more practical and simplified design approach that gives conservative results and is suitable for use in a design office. The simplified design steps for one recommended connection detail are provided in this paper.

Monitoring of In-Service SDCL Bridges. Several bridges were constructed using the recommended details developed in these research projects. The behavior of

Atorod Azizinamini, Ph.D., P.E., Professor and Chair, Civil and Environmental Engineering Department, Florida International University, Miami, FL. E-mail: aazizina@fiu.edu

these bridges during construction and their long-term performance were monitored (Yakel and Azizinamini, 2014). Monitoring of the in-service behavior of SDCL steel bridges ranged from two to more than five years.

SDCL S ystem f or A ccelerated B ridge C onstruction. Additional work was carried out to customize the SDCL steel bridge systems for accelerated bridge construction (Javidi, Yakel, and Azizinamini, 2014). Work included developing suitable details over the interior supports; conducting experimental, numerical and analytical studies; field application using the ABC philosophy of construction; and short- and long-term monitoring of an in-service SDCL bridge system constructed using ABC principles.

BACKGROUND

The latter half of the 20th century saw many changes in the design of bridges, one of the most significant of which resulted from the introduction of alternative construction materials. Prestressed concrete has become increasingly popular since its introduction in the 1950s (Dunker and Rabbat, 1992). The increase coincided with a decrease in the use of steel in short- to medium-span bridges. Several factors contributed to this trend, among them costly details such as bolted splices. The contemporary trend in steel bridge design and construction is to eliminate unnecessary details that contribute both to cost and decreased service life. Following a series of discussions with designers, steel fabricators and contractors in the late 1990s and early 2000s, it was concluded that the development of a steel bridge system for multi-span bridges, with each span having maximum lengths of about 150 ft, would benefit the bridge industry the most. Review of National Bridge Inventory (NBI) data indicates that about 90% of the bridges in service have a maximum single-span length of less than or equal to 150 ft (Lampe et al., 2014). Two factors were identified to help improve the economy of steel bridges: eliminating bolted splices and simplifying the construction sequences. It was concluded that what was needed was a system in which the girders would act as simple spans during deck casting and then act as continuous girders for live load.

The idea of using a simple-span girder for dead load and then making the girder continuous for live load was originally developed in the 1960s for precast, prestressed concrete girders to prevent leakage through the deck joints in simple beam spans (Freyermuth, 1969). However, there are some major differences between the application of this system to prestressed concrete girder bridges and to steel girder bridges.

Figure 1 shows a conventional two-span continuous steel bridge girder. The construction sequence consists of erecting the middle section and then connecting the two end sections using either bolted or welded field splices. This type of construction usually requires two cranes on site with possible traffic interruptions.

Another possibility is to place two simple-span girders between the abutments and pier, cast the deck slab and provide the continuity for live load and superimposed dead loads only (e.g., barriers and the future wearing surface). Figure 2 shows a schematic of such a system.

In the case of both prestressed and steel girder bridges, continuity for live and superimposed dead load is typically accomplished by placing reinforcing bars over the pier and casting concrete diaphragms over the pier. In both cases, the bottom portion of the concrete diaphragms in the vicinity of the girders is subjected to a compressive force transferred from adjacent girders. These compressive forces are generated by negative moments produced by traffic loads and superimposed dead loads. In the case of prestressed girders, the bottom flanges of the girders generally have large areas and are able to distribute the compressive force and prevent crushing of the concrete. However, in the case of steel girder bridges, the bottom flanges of the girder have smaller areas and a higher modulus of elasticity than the flanges of

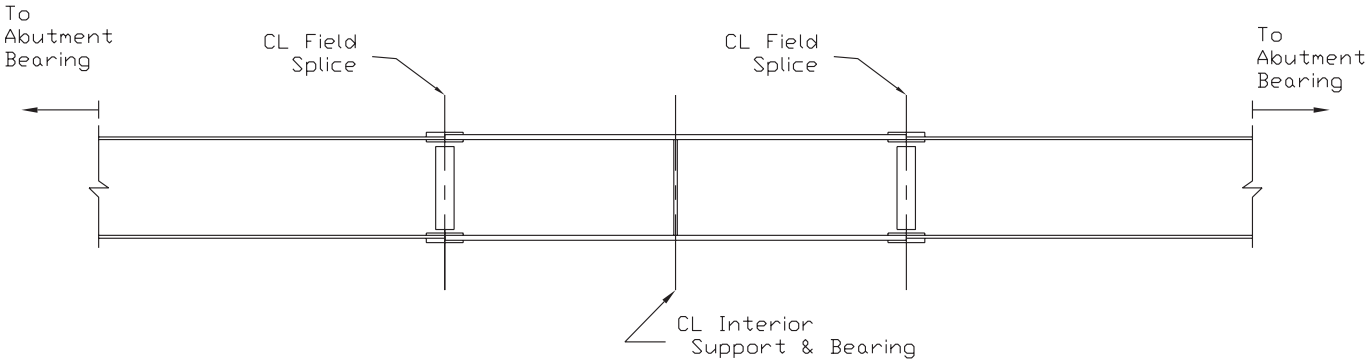

Fig. 1. Conventional two-span continuous steel bridge girder.

concrete girders. These two factors combined can result in crushing of the concrete in the diaphragm in the vicinity of the steel girder bottom flanges when the load is transferred.

In the initial stages of the development of the system, a series of preliminary finite element analyses was conducted (Lampe et al., 2014), which indicated that the level of these compressive stresses is large. For instance, for a two-span bridge with a span length of 100 ft and girder spacing of 10 ft, the resulting compressive stress in the bottom of the concrete diaphragm due to traffic loads could exceed the compressive strength of the concrete by a factor of 4 or higher (assuming 4000-psi concrete is placed in the diaphragms). Therefore, in the case of steel bridges utilizing the SDCL concept, there is a need to develop a detail that could eliminate the possibility of crushing of the concrete in the concrete diaphragm immediately adjacent to the bottom flanges of the girders.

OVERALL STRUCTURAL CHARACTERISTICS

Figures 3 and 4 compare the maximum positive and negative moments, respectively, for two-span steel bridges with equal length spans, analyzed assuming conventional and SDCL systems. In the conventional case, the girders were assumed continuous for both dead and live loads. In the SDCL system, the girders were analyzed as simple spans for the dead weight of the girders and wet concrete deck and as continuous spans for superimposed dead and live loads. Three two-span bridges were considered. The span lengths for these three bridges were 100, 120 and 150 ft. The girder spacing in all cases was 10 ft (Lampe et al., 2014). The solid line in each graph corresponds to the conventional case, whereas the dashed line corresponds to the SDCL system. As indicated in Figure 3, the maximum positive moment in the SDCL system is larger than in the conventional case. This is expected because the girders resist the noncomposite dead loads as a simple span. On the other hand, as shown in Figure 4, the maximum negative moment for the SDCL system is decreased. This behavior is a result of the fact that the noncomposite dead load does not produce any negative moment at the pier.

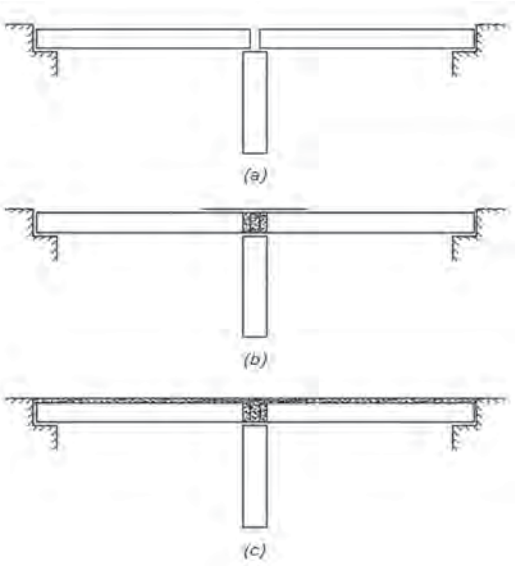

Fig. 2. Construction sequence for SDCL bridge systems.

RECOMMENDED CONNECTION DETAIL FOR CONVENTIONAL CONSTRUCTION METHODS

A possible connection detail to provide live load continuity over the pier in an SDCL steel girder system for the case of conventional methods of construction is to use a concrete diaphragm over the piers to connect the girders. Figure 5 shows the recommended connection detail over the pier. The following are the various elements of the connection detail:

- Concrete diaphragm, which should be cast at least a few days prior to casting the deck.
- Steel slab reinforcement to provide live load continuity. This reinforcement is placed before casting the deck.
- End plates welded to the ends of each girder.
- Steel blocks welded toward the bottom of each end plate.
- Elastomeric pads where the steel girders seat.
- A small gap is needed between the bottom of the steel flanges and the top surface of the cap beams. The gap should be filled with soft material, such as expanded polystyrene, to allow the rotation of the entire detail once the concrete diaphragm is cast and cured.
- Dowel reinforcement could also be placed to connect the cap beam to the concrete diaphragm in order to prevent longitudinal movement of the superstructure at the connection point.

The detail shown is applicable to both I- and box-girder bridges. Figures 6 and 7 show photos of the recommended detail used in I- and box-girder bridges, respectively. In both cases, a steel block is provided near the bottom flanges. In the case of the box girder, an additional steel plate is welded to the top flanges, as shown in Figure 7, to prevent pull-out of the tension flanges of the girder from the concrete diaphragm.

Figure 8 shows a portion of the recommended connection detail over the pier. Minimal steel reinforcement is needed within the concrete diaphragm. For the sake of clarity, not all of the reinforcement is shown in Figure 8. Figure 9 shows an example of the steel reinforcement that could be provided inside the concrete diaphragm.

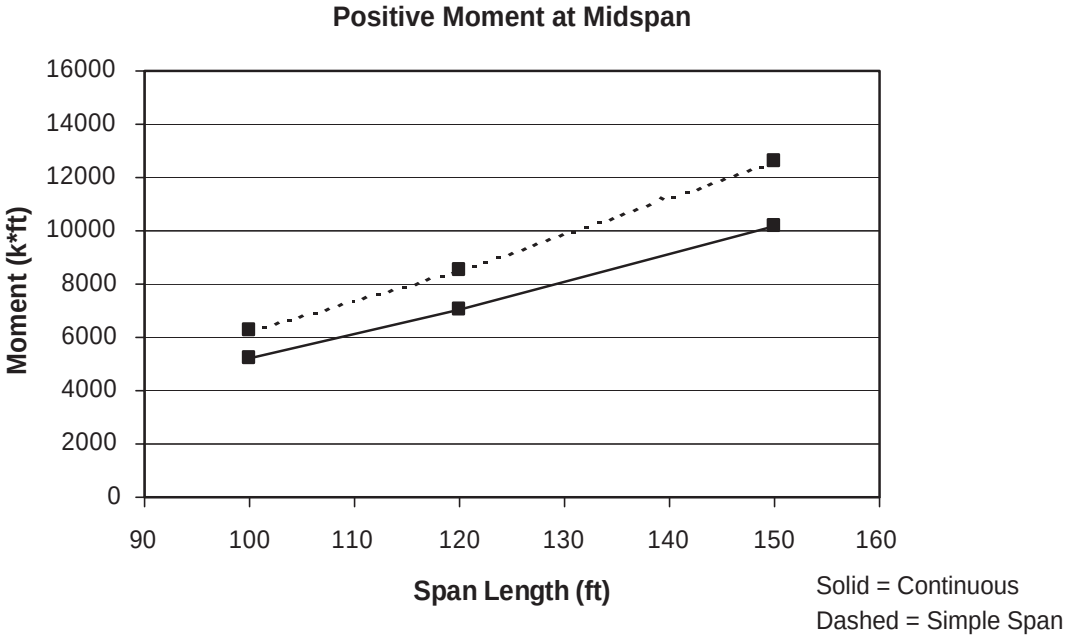

Fig. 3 Maximum positive moment comparison.

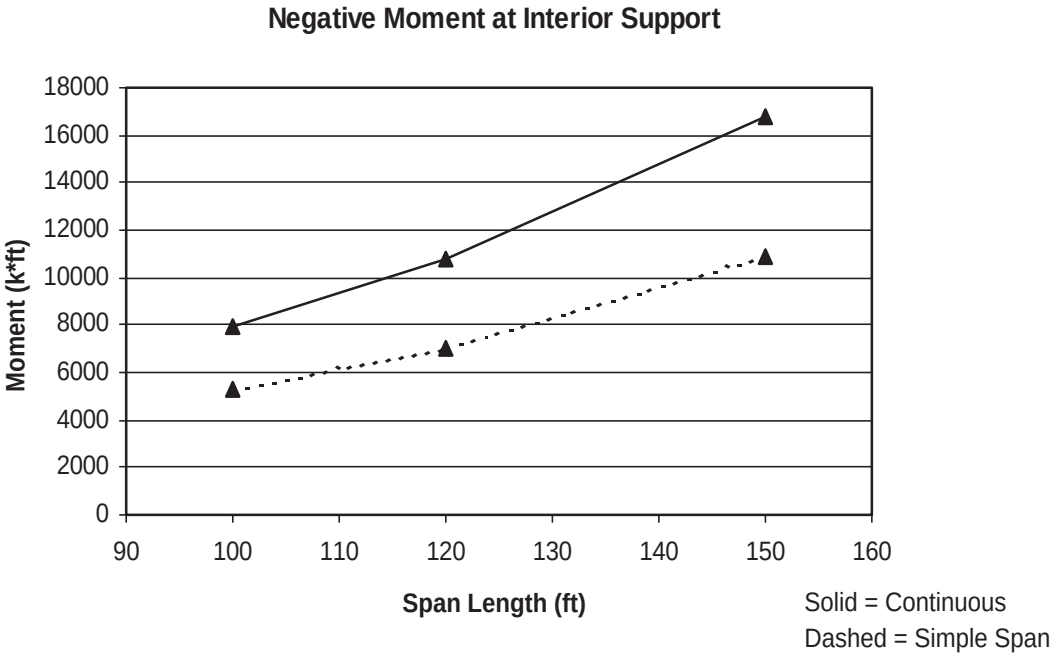

Fig. 4. Maximum negative moment comparison.

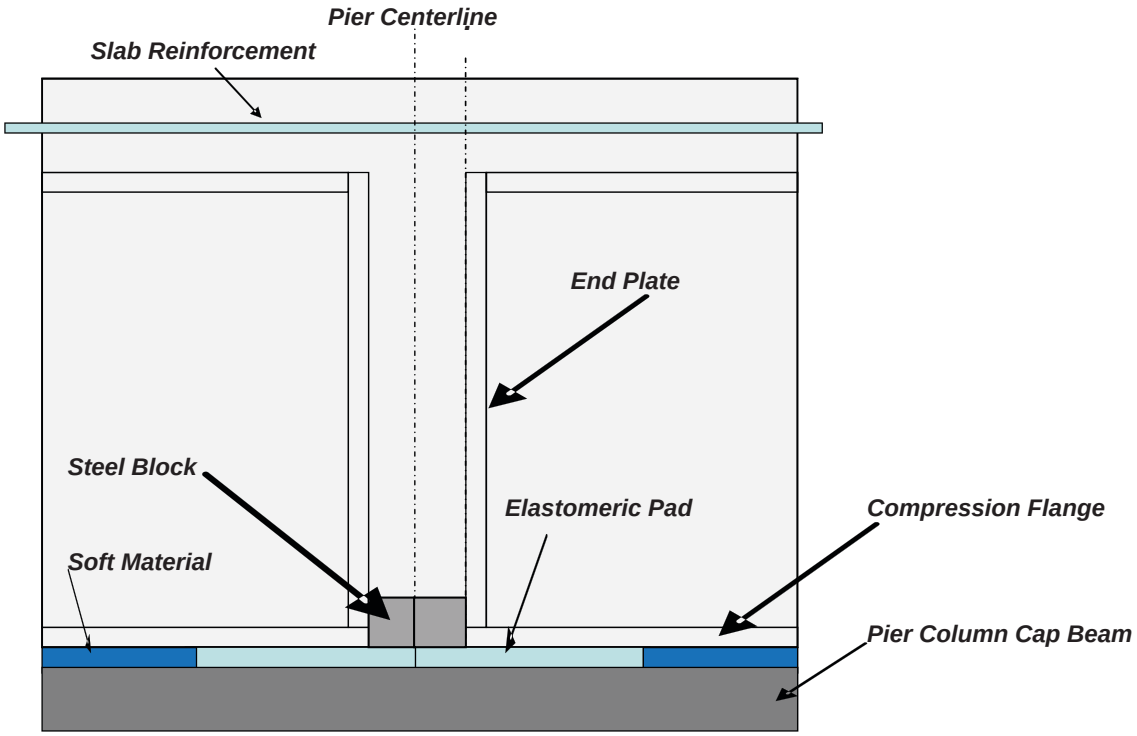

Fig. 5. Concrete diaphragm detail over the pier for conventional methods of construction.

Fig. 6. Recommended detail on an I girder.

Fig. 7. Recommended detail on a box girder.

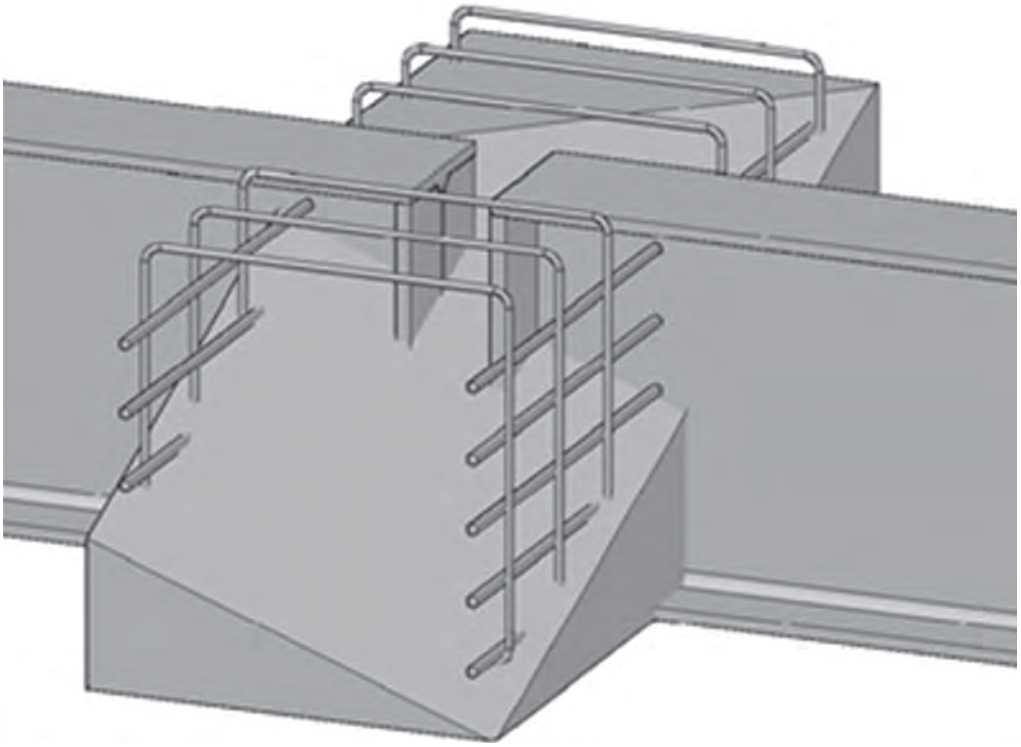

Fig. 8. A partial schematic of the steel reinforcement in the concrete diaphragm.

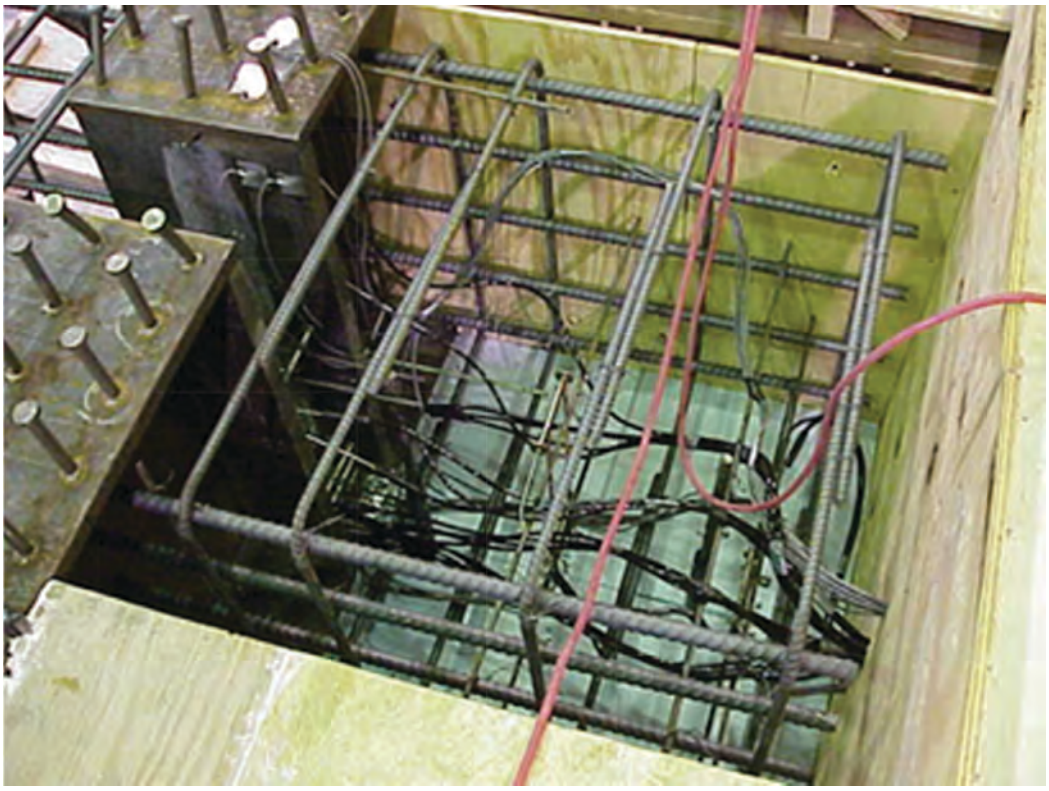

Fig. 9. Example of the required minimal reinforcement in the concrete diaphragm.

For the recommended connection detail shown in Figure 5, the bottom flanges will be subject to a compression force under traffic live loads. Where the number of spans exceeds two, bottom flanges could also be subject to a tensile force. However, the level of this tensile force is generally small. In cases where the tension force becomes significant, it might be necessary to positively attach the bottom portion of the connection shown in Figure 5 to enhance the tension capacity of the connection.

Research results show that for the recommended detail, the compressive force created by the live loads is capable of crushing the concrete in the vicinity of the compression flanges of the steel girder. To demonstrate this aspect of the connection detail, Figure 10 shows results of three full-scale tests. Each test utilized different connection details. Figure 10 shows the details used in each test along with a resulting moment versus deflection curve for each test specimen. The only difference among the three test specimens was the details used at the end of the steel girders. In test 2, the ends of the girder were simply embedded in the concrete diaphragm, which resulted in the lowest capacity. Welding end plates to the end of the girders, as was the case in test 3, resulted in a larger capacity. Connecting the bottom flanges and welding end plates to the ends of girders, as was the case for test 1, proved to achieve the best performance. Note that for clarity, curved segments associated with unloading and subsequent reloading of the specimen have been removed from the plots in Figure 10. This has resulted in the appearance of a jagged response, particularly for the case of test 1. The reasons for unloading varied, but were typically to deal with fixture and load system issues. Additional details can be found in the referenced research reports.

The main reason for the significant capacity reduction observed in the case of test 2, as compared to tests 1 and 3, is that the bottom flanges crushed the concrete adjacent to the bottom flanges and prevented the development of adequate compression capacity in the connection. With the moment capacity of the connection being equal to total compressive force times the moment arm (i.e., the distance between the resultant compressive force located near the bottom flanges and the resultant tensile force located near the tension reinforcement), a reduction in compression resistance near the

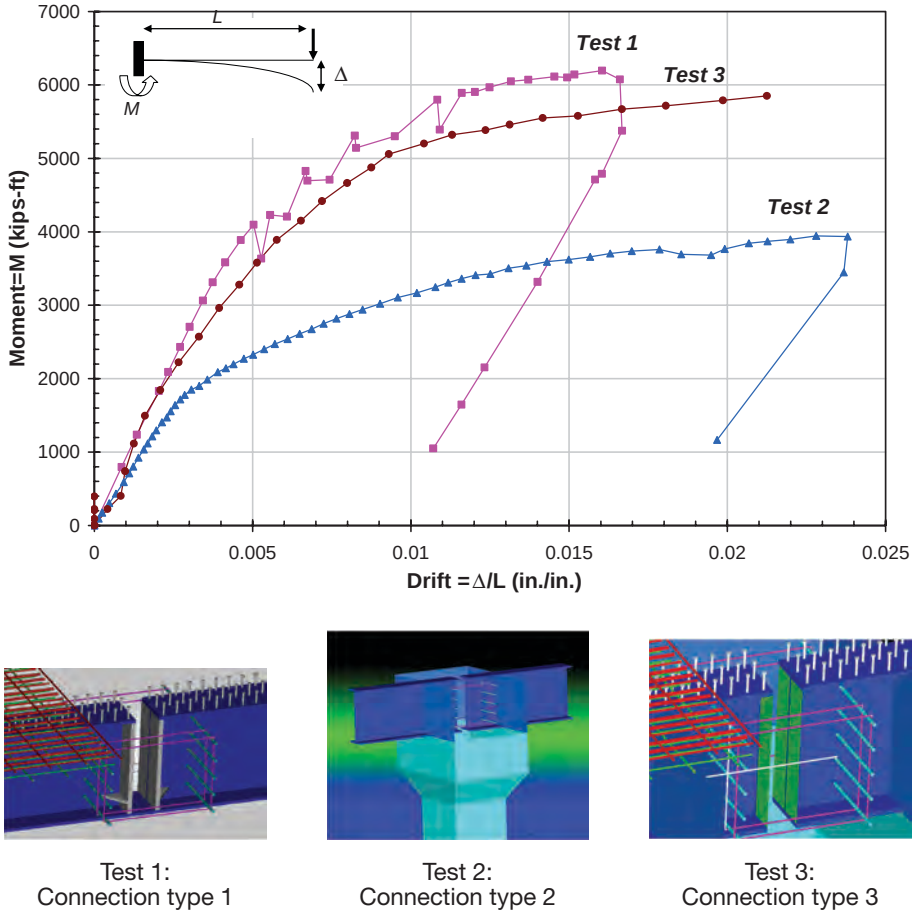

Fig. 10. Effect of end details on moment-deflection performance.

bottom flange translates into a lower moment capacity. Therefore, preventing the crushing of the concrete near the bottom flanges enhances the moment capacity of the connection.

The principal consideration in selecting the connection detail for the SDCL system when a concrete diaphragm is used is the transfer of the compressive force from the compression flange of one steel girder to the compression flange of the adjacent girder without going through the concrete diaphragm. An example of a practical solution used in several bridges is shown in Figure 11. As mentioned previously, in the case of multi-span bridges and in cases in which bottom flanges could be subjected to significant tensile forces, positively attaching the bottom portion of the recommended connection will be needed (see Figure 11).

Figure 11 shows the recommended detail for providing live load continuity over the pier before casting the diaphragm concrete. The recommended detail to transfer the compression force from one girder to the next without going through the concrete diaphragm is to weld the end plate to the end of each girder and then weld a steel block to the end plate near the bottom of the connection, as shown in Figures 5, 6, 7 and 11. These steel blocks are about 2 in. thick by 4 in. high and as wide as the width of the girder flanges. Although the steel blocks need to touch each other, they do not need to be perfectly in contact, as shown in Figure 11. The holes shown in the webs of the steel girders, visible in Figure 11, are provided to accommodate the steel reinforcement needed in the concrete diaphragm (see also Figures 8 and 9).

The use of concrete to connect the two girders provides several advantages. Based on research and field observations, it is recommended that about ½ to ⅔ of the depth of the concrete diaphragm be cast and cured for about seven days before casting the deck and the remainder of the diaphragm. Casting ½ to ⅔ of the depth of the diaphragm provides excellent torsional bracing for the ends of the girders, which is required with respect to flexural capacity and during casting of the deck. This eliminates the need to provide a steel diaphragm at each girder end simply for construction purposes. Indeed, the load stiffener visible in Figure 11 is technically unnecessary but is an artifact from conventional design requested to be left in by the owner. The use of concrete over the support encases the girder ends and protects them against corrosion, enhancing the service life of the girder ends.

DESIGN PROVISIONS FOR CONVENTIONAL CONSTRUCTION METHODS

A combination of experimental and numerical studies was carried out to better comprehend the contribution of the various elements of connection types 1, 2 and 3 shown in Figure 10. Connection type 2 (no end details) was used as a reference point and should be avoided. Research results indicated that connection type 3 could still experience crushing of the concrete in the vicinity of the compression flange and inside the concrete diaphragm. Classes of connection details resembling connection type 1 are recommended for use in practice. The main characteristics of connection type 1 are that the compression flanges of the girder inside the concrete diaphragm are in contact, and the possibility of crushing of the diaphragm concrete is eliminated. Table 1 shows the contribution of each connection element to the overall moment capacity of connection types 1 and 3 as determined by finite element analysis. The moment of each element was computed about the centerline of the bottom plate.

Every element within the concrete diaphragm contributes

Fig. 11. Typical live load continuity detail used in field application; overall view on the left, close-up view on the right.

Table 1. Contribution of Each Resisting Element to Overall Moment Capacity		
Resisting Element	**Connection Type 1**	**Connection Type 3**
Tension reinforcement in slab	60.82%	66.77%
Stirrups in tension	5.09%	5.42%
Concrete in tension	4.35%	6.03%
Stirrups in compression	0.00%	1.58%
Concrete in compression	12.37%	20.20%
Bottom plate in compression	17.37%	NA
Total	100.00%	100.00%

to the overall moment capacity of the connection; however, the contribution of some elements could conservatively be ignored. It is recommended to use connection types that would resemble type 1, which is the focus of the following discussion. The design procedure for connection type 3 is more complex and is provided in Farimani et al. (2014). It is not recommended to use connection type 3 in practice since some level of crushing of the concrete adjacent to the compression flange was observed in the experimental tests.

Closer examination of the information provided in Table 1 indicates that the flexural capacity for connection type 1 is predominantly (approximately 77%) provided by a couple created by the tension reinforcement placed in the deck and the compression steel block located at bottom of the connection. Based on the research findings, it is suggested that simplified design provisions be followed for calculating the flexural capacity of connection type 1. The same procedure can also be used to calculate the area of steel reinforcement needed in the slab to provide live load continuity.

As mentioned previously, based on the values shown in Table 1, the effect of the stirrups and diaphragm concrete can be ignored when calculating the moment capacity of connection type 1. This leaves only the bottom compression block and slab tension reinforcement to provide the moment-resisting capacity. The capacity is then simply the tension capacity of the slab reinforcement multiplied by the moment arm. Because the bottom compression block will be sized so that it will not yield, the resulting moment arm is equal to the distance between the slab tension reinforcement and the center of the bottom compression block. The steel blocks are in contact (bearing) and can resist stresses well beyond the yield stress.

Research has shown that failure of connection detail type 1 coincides with the slab tension reinforcement reaching its ultimate capacity. Research has also shown that all tension reinforcement within the effective width will yield. The resulting equation for calculating the capacity of the connection is therefore:

$$M_n = A_s f_y (d - H/2) \quad (1)$$

where

M_n = nominal moment capacity of the connection, in.-kip
A_s = area of the slab tension reinforcement, in.^{2}
f_y = yield stress of the slab tension reinforcement, ksi
d = distance between the bottom of the girder and the centroid of the slab tension reinforcement, in.
H = height of the steel block, parallel to the girder depth, in.
t_{pl} = thickness of the steel block, parallel to the girder length, in.

The use of the recommended design procedures is demonstrated using a two-span bridge consisting of two 97-ft spans with the following design information:

Required live load moment capacity, M_u(LL)	34,770 in.-kip
Steel beam	W40×249
Depth of the steel beam	43.375 in.
Width of compression flange, b_f	15.75 in.
Bottom of girder to centroid of rebar, d	47.75 in.
Effective width of concrete slab, b_e	92 in.
Slab thickness	8.5 in.
Strength reduction factor, ϕ	0.9

The nomenclature used to describe the size of the steel blocks is as follows:

- The dimension of the steel block parallel to the depth of the girder will be referred to as the height of the steel block and is designated as H.
- The dimension of the steel block parallel to the width of the girder flange will be referred to as the steel block width and is designated as b_f.
- The dimension of the steel block parallel to the length of the girder is referred to as t_{pl}. This dimension could vary and it is suggested to be at least 2 in.

To begin, a steel block with a height of 2 in. will be assumed. After calculating the required area of the slab tension reinforcement, the adequacy of this block will be checked. To calculate the required area of the reinforcement,

Equation 1 can be set equal the required strength and solved for A_s:

$$A_s = \frac{M_u}{\phi f_y \left(d - H/2\right)} \tag{2}$$

Using Equation 2, the required area of slab tension reinforcement is calculated as shown:

$$A_s = \frac{34,770}{0.9(60)(47.75 - 2/2)}$$
$$= 13.8 \text{ in.}^2$$

In order to ensure that the bottom compression block remains elastic when the ultimate capacity of the connection is reached, the required minimum height of the steel block can be found using Equation 3. Note that the ultimate strength of the tension reinforcement is used. Based on the results of the research, the ultimate strength is assumed to be 1.7 times the yield strength.

$$H_{\min} = \frac{1.7A_s f_y}{b_f F_{ypl}} \tag{3}$$

where

H_{min} = minimum height of the bottom compression block, parallel to the depth of the girder, in.
F_{ypl} = yield strength of the steel block, ksi
b_f = width of the girder flange, in.

The width of the block is assumed to be equivalent to the width of the girder bottom flange and the area of reinforcement is assumed to be equivalent to the required area calculated with Equation 1. If the actual area of reinforcement is larger based on the arrangement of bars selected, the thickness of the block should be re-evaluated.

$$H_{\min} = \frac{1.7(13.8)(60)}{15.75(50)}$$
$$= 1.79 \text{ in.} < 2 \text{ in.}$$
$$\therefore \text{ assumed block height acceptable}$$

Therefore, using steel blocks with dimensions of 2 in. by 2 in. by 15.75 in. is adequate.

FABRICATION AND CONSTRUCTION RECOMMENDATIONS FOR CONVENTIONAL CONSTRUCTION METHODS

For the recommended connection detail shown in Figure 11, test results indicated that minimum size fillet welds could be used to attach the end plates to the girder ends. In addition, the attachment between the steel blocks and the steel end plate could be achieved using minimum size fillet welds. As shown in Figure 11, the steel blocks need to touch each other; however, they do not need to be in full contact. During construction, the longitudinal movement of the girders could create a gap between the steel blocks due to thermal loads. This should not be a concern, however, because concrete paste can fill the space between the steel blocks and create a smooth load transfer path. This recommendation is based on observed test results and field experiences.

One of the critical steps during the construction stage is the casting of the concrete diaphragm prior to the casting of the deck. This involves two opposing requirements. First, the ends of the girders must be prevented from twisting during the casting of the deck to ensure stability of the girders. This is a requirement for using the flexural design provisions of the *LRFD Bridge Design Specifications* (AASHTO, 2012). In this regard, casting the full depth of the concrete diaphragm would be ideal. However, field measurements indicate that full-depth casting of the concrete diaphragm can provide about 50% moment continuity during deck casting. This unintended continuity can result in cracking of the concrete diaphragm during deck casting. This behavior was observed in the construction of Highway N-2 over the I-80 bridge in Nebraska (Yakel and Azizinamini, 2014) for which the concrete diaphragm was completely cast and cured before casting the deck. After removing the formwork, cracks were observed on the face of the concrete diaphragm, as shown in Figure 12. Formation of cracks in the concrete diaphragm resulted in a reduction in the level of continuity moment. The cracks were later filled with epoxy. It should be noted that these cracks did not pose any safety hazard or potential for failure—they can be repaired with epoxy filling—rather, the issue was more of an aesthetic problem and possibly a service-life issue. Nevertheless, departments of transportation generally do not favor the formation of such cracks.

Field experience indicates that the level of unintended continuity is significantly reduced if the concrete diaphragm is cast to about ½ to ⅔ of its full depth before placing a thin steel sheet between the end plates running across the entire width of the concrete diaphragm. Figure 13 shows the suggested detail that was used in construction of a bridge using an SDCL steel bridge system in Montana.

The thin cold-formed steel sheet shown in Figure 13 should be extended to near the bottom flange of the girders and secured while casting the partial-depth concrete diaphragm. Other details or approaches may also be feasible to reduce this unintended continuity. The main objective is to secure the ends of the girder in concrete and provide good torsional bracing while, to the extent possible, allowing the girder ends to rotate when casting the deck without subjecting the concrete diaphragm to tensile forces. The incorporation of cold-formed thin steel sheet, as shown in Figure 13,

Fig. 12. An example of cracking in the concrete diaphragm if it is cast full depth.

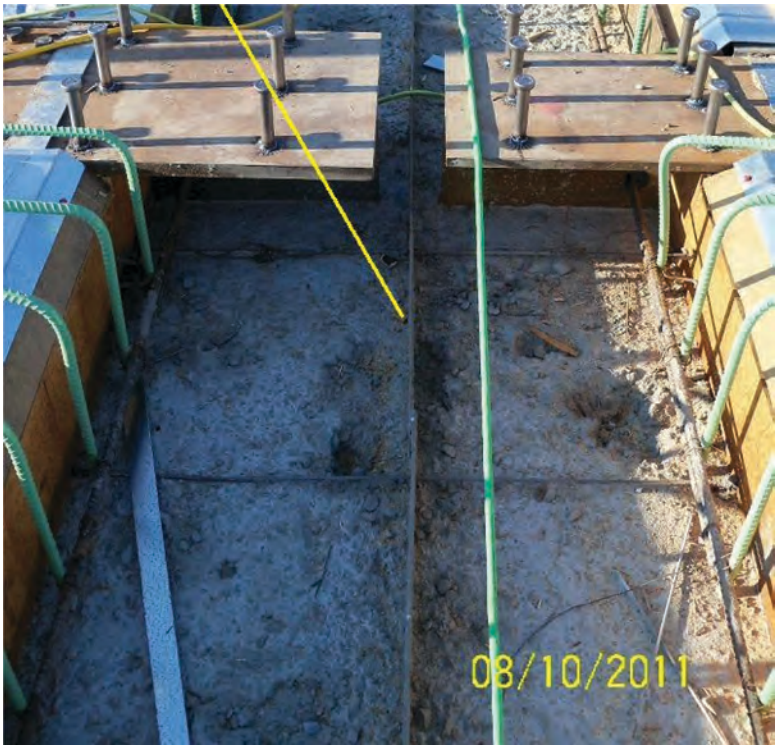

Fig. 13. Recommended solution for reducing unintended continuity over the pier.

also controls the direction of cracking, if any, in the concrete diaphragm while casting the deck. It is recommended that about 25% dead load continuity should be assumed, despite precautionary measures that may be taken to avoid the development of unintended dead load continuity during the design process.

Although this discussion focused on I-shaped steel girders, the same conclusions are applicable to box-shaped girders.

DESIGN AND CONSTRUCTION ADVANTAGES USING CONVENTIONAL CONSTRUCTION METHODS

SDCL steel bridge systems present several advantages when used in conjunction with conventional construction methods, including:

1. Eliminating the need for bolted splices.
2. Allowing the use of the same cross-section throughout the girder length. The positive moment along the girder length is increased slightly, while the negative moment in the same span near the interior supports is decreased. Investigated cases that included span lengths of 90 to 150 ft, which are typically found in simple-grade crossings, have shown that the resulting moments allow the use of the same cross-section throughout the girder length. This observation favors the use of rolled beams where possible.
3. Reducing negative moment near the interior pier. This allows for increasing the spacing between the interior pier and first cross frame, which can in turn reduce the number of cross frames. Casting the ends of the girder in concrete creates a boundary condition that is fixed against torsion, which can allow a further increase in the distance between the interior support and first cross frame. However, this additional fixity is usually ignored in routine design.
4. Providing a stable configuration during construction. The recommended detail and construction procedure, as described earlier, simplifies the bridge details while producing a stable configuration during deck casting. This is achieved by rigidly securing the ends of the girder in the partially cast concrete diaphragm.
5. Allowing the sequence of casting for multi-span bridges to be ignored since the deck may be cast from one end of the bridge to the other end in a single cast. This advantage is a reflection of the fact that each span acts as a simply supported span when casting the deck; the number of spans is not a design consideration.
6. Providing protection of the girder ends against possible corrosion by using the recommended detail over the pier, which enhances the service life of the bridge. Eliminating the bolted splices also enhances the service life by reducing the risk of corrosion.

DESIGN, FABRICATION AND CONSTRUCTION RECOMMENDATIONS FOR ACCELERATED CONSTRUCTION

Accelerated Bridge Construction (ABC) is a response to public demand for avoiding traffic interruption. The SDCL steel bridge system provides an excellent opportunity for accelerating the construction process. This objective can be achieved in several ways. One approach is to use the adjacent girder concept as described later. The concept can be implemented using either I-shaped girders or box girders. However, the following discussion focuses on using steel box girders in applying the SDCL system to ABC. The application of the SDCL system to ABC is further explained using as an example the bridge over I-80 at 262nd Street in Nebraska.

The adjacent girder concept utilizes prefabricated units consisting of an individual steel box girder pre-topped by a portion of deck slab, as shown in Figure 14. In this discussion, each steel section with a pre-topped deck will be

Fig. 14. Single (interior) box girder and deck unit.

referred to as a unit. With this approach, the units are prefabricated and then shipped to the job site. The portion of the deck shown in Figure 14 is cast at the fabrication shop or temporary staging location. Once on site, the individual units are set into place on the supports adjacent to one another (see Figure 15). A longitudinal deck closure strip between the individual units is then cast, joining them together. At the same time, the concrete diaphragm over the interior pier is cast. The interior concrete diaphragm connects the spans and provides continuity between them for subsequent loading (e.g., live load). Step-by-step details of the procedure are described as follows.

Construction Sequence

Step 1. Steel Box-Girder Fabrication. The first step is to fabricate the steel box girders. One option is to have webs perpendicular to the flanges. This allows fabricators to use standard I-girder techniques and jigs. Often, webs of box girders are sloped, which can be costly to fabricate and can require special modifications to equipment.

Step 2. Cast the Deck onto the Girders. This operation can be performed in a precast concrete facility or some other temporary location. Two available options for formwork are conventional form jacks or a shored deck bed. The chosen system depends on fabricator preference and the nature of the job.

Figure 16 shows the fabrication of pre-topped units for the bridge over I-80 at 262nd Street. A primary advantage of ABC is that most of the construction activities can be accomplished off site, away from traffic zones, eliminating the risk associated with exposing workers to work zone hazards.

Given the inherent stability of the steel box section, conventional form jacks can be used for the deck forming. The steel girder is placed on temporary supports, and construction is carried out using conventional methods. Depending on the fabricator's preference, the segments can be constructed individually or all at once.

Other options include placing the steel girder on a flat bed and fully supporting the unit while casting the deck.

Step 3. Placement of the Units on Supports. After casting the deck, the individual pre-topped units can be picked up using regular cranes and placed on the supports, as shown in Figure 17. The main advantage of steel box girders is their significantly lower weight compared to concrete box girders, especially for longer span lengths. Use of lightweight concrete can further reduce the total weight of the pre-topped units if necessary.

Figure 18 shows the photo of the bridge over I-80 at 262nd Street after placement of all the pre-topped units side by side.

Another major advantage of using steel box girders in the adjacent girder system is the ability to match the elevation of different units and achieve the overall geometry. In the case of concrete girders, creep and shrinkage deflections cause different pre-topped units to experience different displacements, and it is almost impossible to match the elevation of adjacent units. Further, in the case of prestressed concrete girders, attaching them over the pier for live load continuity can result in cracking in the concrete diaphragm because of creep and shrinkage-related deformation of the girders, which is not an issue for steel girders. These issues can result in serious field challenges and job delays, especially for longer span lengths.

Step 4. Detail for the Interior Supports and Longitudinal Closure Pour. The detail recommended for ABC application of SDCL steel bridge systems is shown in Figure 19 and is similar to that used for conventional methods of construction.

The longitudinal reinforcement extending from the pre-topped deck can be developed over shorter distances by hooking the bars inside the concrete diaphragm. This particular detail was investigated extensively—including a full-scale test—by Javidi, Yakel, and Azizinamini (2014) and was found to provide good performance. It is recommended that development of the extended longitudinal reinforcement using straight splices be avoided. Developing the longitudinal reinforcement extending from pre-topped girders is not recommended, unless the bars are terminated in the region of the deck subjected predominantly to compression. Ending tension reinforcement in a tension zone will create stress concentrations and develop cracking in the deck, adversely affecting the service life of the bridge deck.

The detail to be used for longitudinal closure pour is a critical aspect of using pre-topped adjacent girder systems.

Fig. 15. Three adjacent box-girder units.

Figure 20 shows the longitudinal closure pour detail used for the 262nd Street Bridge, which utilized headed bars.

Ultra-high-performance concrete (UHPC) provides better alternatives for longitudinal closure pours. In the case of the bridge over I-80 at 262nd Street, the width of the closure pour was 13 in. The headed bars that were used allowed for development of the deck transverse reinforcement over a shorter length. Using UHPC, the width of the closure pour region could further be reduced to 8 in., eliminating the need for the headed bars. The shortcoming is that very tight tolerances need to be specified, which could create challenges in the field. From the standpoint of durability and service life, the width of closure pours needs to be as small as practical. However, from the standpoint of tolerance, the width needs to be as wide as possible. It is recommended to use a narrow width (about 8 in.) and take measures to ensure good quality control during construction.

The fresh concrete that is placed in the closure pour will be restrained by concrete that is already hardened on the either side of the closure pour region (i.e., the pre-topped deck over the girders). This restraint will result in the development of tensile stresses in both the longitudinal and transverse directions in the concrete that is placed in the closure pour. These tensile stresses can easily exceed the modulus of rupture of the concrete and result in the development of longitudinal and transverse cracking at close intervals along the closure pour region. Field observations indicate that these transverse cracks can be 1 or 2 ft apart. The narrower the closure pour region, the lower the severity of these transverse and longitudinal cracks. The restraining phenomenon

Fig. 16. Preparing the formwork for casting the deck on the unit.

Fig. 17. Pickup and placement of pre-topped units on the supports.

described earlier is very similar to the behavior of a closure pour in phase-constructed bridges. A detailed description of the behavior of closure pours in phased constructed bridges and recommended design provisions are provided elsewhere (Azizinamini, Yakel and Swendroski, 2003).

In the case of the 262nd Street Bridge over I-80, a partial-depth pre-topped deck was used necessitating placement of an overlay as the last step of the construction. The use of an overlay allows the addressing of minor adjustments that might be needed during construction.

OTHER DETAILS USED FOR IN-SERVICE BRIDGES

Several states have used SDCL steel bridge systems (Talbot, 2005; Stone, Lindt and Chen, 2011; Morales, 2004; Wasserman, 2005) and some have used modified versions of the recommended details discussed herein. In the sections that follow, these details are presented along with brief discussions of their effectiveness based on research and field observations.

Fig. 18. Completing the placement of the pre-topped units for the bridge over I-80 at 262nd Street in Nebraska.

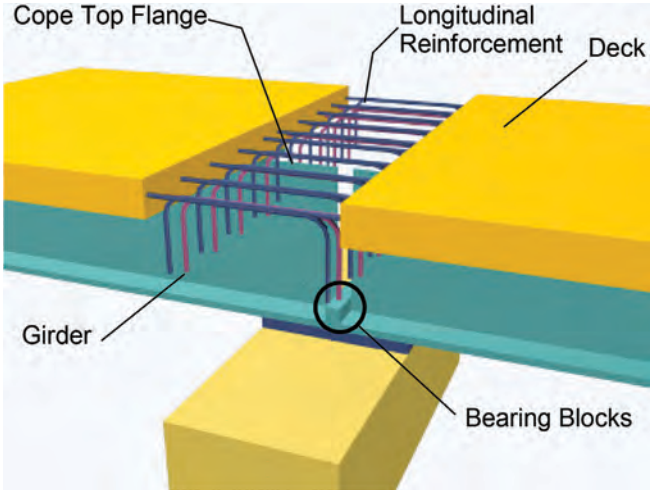

Fig. 19. Recommended interior support detail for an SDCL system used in an ABC application.

The Ohio DOT used the detail shown in Figure 21 in the construction of State Route 22 in Circleville, Ohio (Morales, 2004). The entire connection detail shown was cast in concrete forming the concrete diaphragm. The holes shown in Figure 21 are provided to pass through the transverse reinforcement that extends along the entire width of the concrete diaphragm.

The major difference between this detail and the detail recommended in this study is the gap that is left between the bottom (compression) flanges bearing directly on the concrete diaphragm. Based on the research results presented, this detail—which is similar to the type 3 detail described earlier—can result in crushing of the concrete in the vicinity of the compression flange. In construction of the bridge, the diaphragm and deck were cast simultaneously. This would require providing a steel diaphragm at each end of the girder to act as torsional bracing. It is not clear whether this was provided or not.

The Tennessee DOT has used two different details with an SDCL steel bridge system (Wasserman, 2005). For construction of the State Route 35 Bridge in Maryville, Tennessee, the detail used was very similar to the recommended detail in this paper. This detail is shown in Figure 22.

The detail shown in Figure 22 is similar to connection type 3 described in this paper, except that the girders are anchored to the cap beam using anchor rods. The behavior of this type of detail was investigated by Farimani et al. (2014). However, this detail is not recommended for field application because there was evidence of crushing of the concrete adjacent to the compression flange. A positive aspect of this detail is the attachment of the compression flange to the cap beam using anchor rods, which can be beneficial if moment reversal is a possibility and the bottom flange is placed in tension. However, during construction, the longitudinal movement of the girders due to thermal loading before casting the concrete diaphragm should be evaluated. Restraining both ends of the girder against longitudinal movement before casting the diaphragm can result in failure of the anchor rods. As noted in Figure 22, half of the concrete diaphragm was first cast and cured to secure the girder ends before casting the deck and the rest of the diaphragm. As described earlier, this is an excellent approach for securing the end of the girders against twist and eliminating the need for a steel diaphragm at the girder ends. As recommended previously, somewhere between ½ to ⅔ of the concrete diaphragm should be cast first to provide torsional bracing at the girder ends, and to reduce any unintended moment continuity for dead load.

The second class of details used in Tennessee in conjunction with SDCL steel bridge systems is shown in Figure 23.

This detail was used in the construction of the DuPont Access Road Bridge in New Johnsonville, Tennessee. The major variation from the recommended detail in this case is the cover plate that is provided to connect the top flanges before pouring the concrete diaphragm and deck; thereby providing the continuity for the deck dead load. Bolts connecting the top flanges of the girders are not shown in Figure 23. Such a practice could help reduce the camber that is needed and the deflection of the girder due to the dead weight of the wet concrete.

A variation of the detail shown in Figure 23 was used earlier in New Mexico in the construction of the Las Cruces and Hatch Bridges (Morales, 2004), with the exception that the bolts in the top cover plates were tightened after pouring a portion of the deck in order to provide continuity for the live load only. Such a practice could potentially result in construction complexities. Tightening of the cover plate bolts after deck casting has started could be challenging in

Fig. 20. Possible detail for longitudinal closure pour.

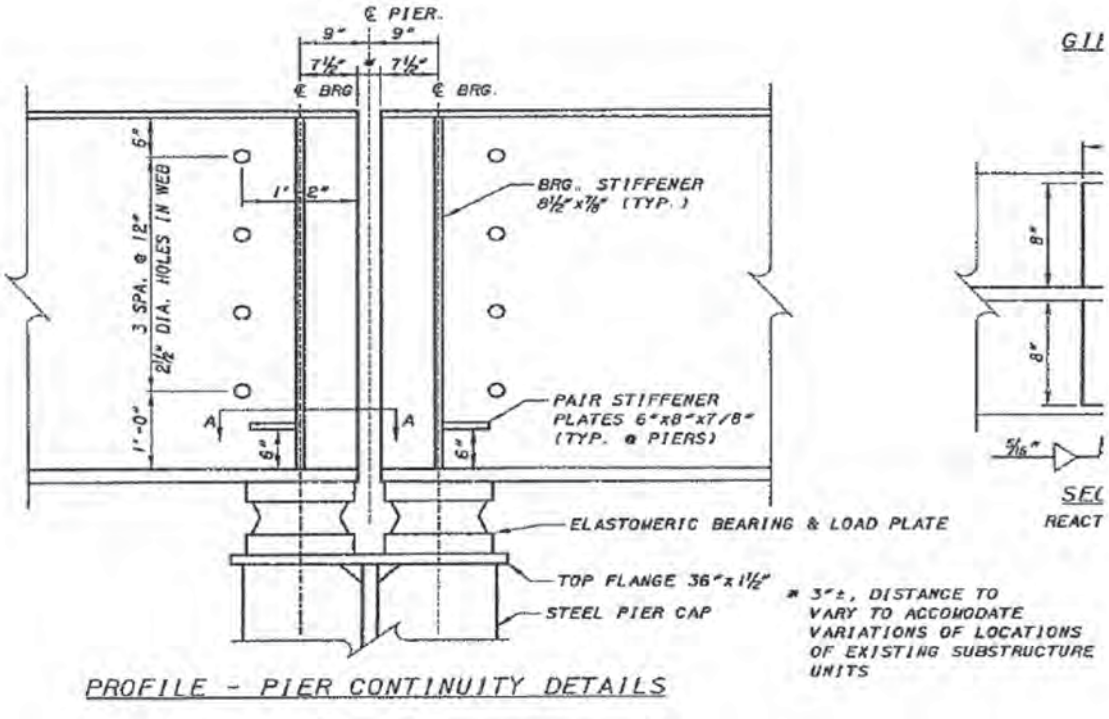

Fig. 21. Detail used by the Ohio DOT.

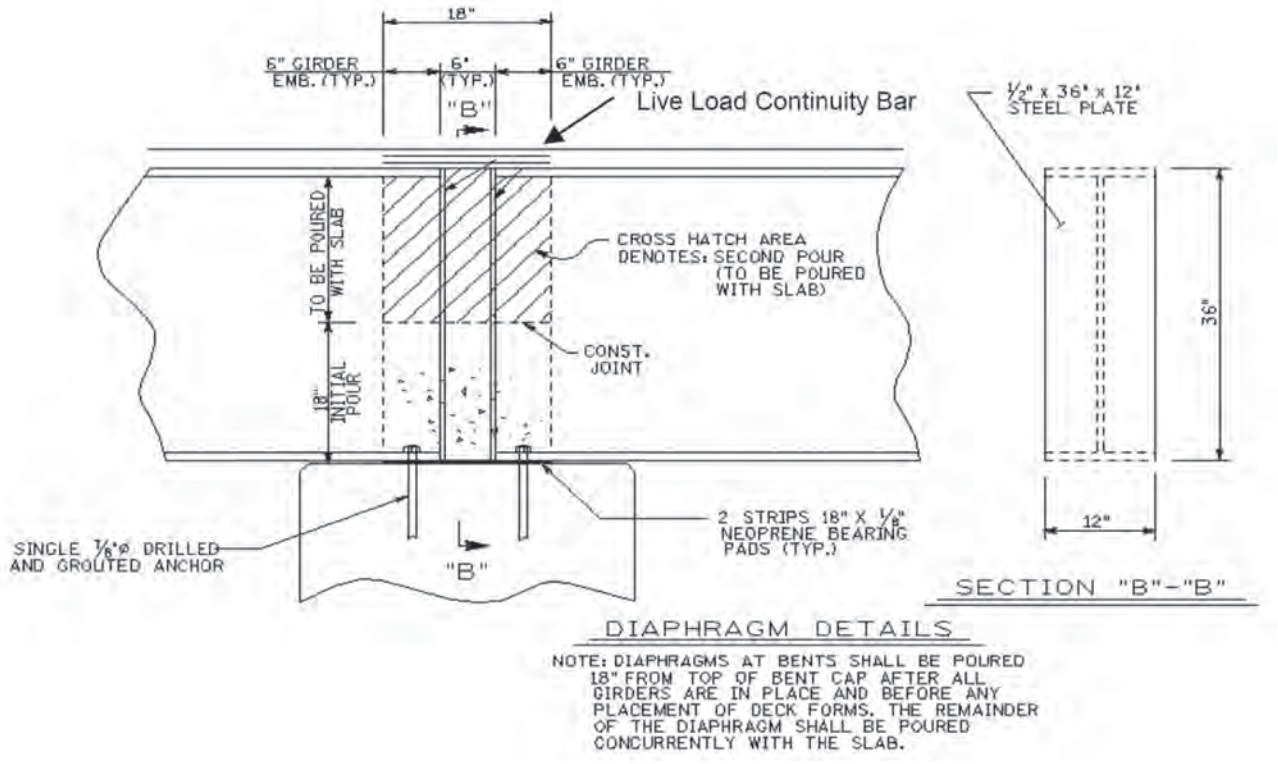

Fig. 22. Detail used in construction of the State Route 35 Bridge in Maryville, Tennessee.

the field. Research results indicate that there is no need for a top cover plate, and field experience indicates that contractors do not favor this detail.

Another detail that was used on a SDCL steel bridge system is a detail used by the Colorado DOT (Stone, Lindt and Chen, 2011) and illustrated in Figure 24. This detail was used in the construction of a six-span, 470-ft long bridge on U.S. Route 36 near Denver, Colorado. A concrete diaphragm was not used in this detail. The girders were seated on an elastomeric bearing pad along with a 30 in. by 14 in. by 1 in. steel plate. The bottom flanges of the girders were welded to the plate to provide compression-flange continuity. Heavy cross frames were provided (W27×84 sections) for the girders (W33×152 sections) near each girder end and over the pier to provide torsional bracing for the girder ends during deck casting. Webs of the two girders over the pier were not connected, which raises a question about the type of connection that was developed. To develop a full-moment connection, flanges and webs need to be spliced and connected. The type of detail used by the Colorado DOT falls in the category of a semi-rigid-type connection and would need experimental verification to assess its rotational stiffness for analysis purposes. Simply assuming that this detail is rigid and the girders are continuous for the purpose of live load analysis is not correct. Further, the transverse weld attaching the bottom flanges of the girders to the 30 in. by 14 in. by 1 in. plate is a Category E or E′ detail for fatigue. The deck detail used over the pier could also develop cracks during its service life and result in moisture leaking over the girder ends. Further, having too many unprotected steel elements over the pier, created by the presence of a heavy steel diaphragm, can further lower the service life and durability of the bridge. One of the major benefits of casting a concrete diaphragm over the girder ends at the pier is enhancing the service life of the bridge by eliminating joints.

In summary, variations of the recommended details in this study have been used by other DOTs for bridges that are in service. From the experiences gained from this study and the use of SDCL steel bridge systems in several states, the following conclusions may be drawn with respect to the characteristics that a preferred detail should possess for joining girders over interior piers in SDCL steel bridge systems:

1. There is a need to provide a continuous load path for transferring the compression force from one bottom flange to the adjacent bottom flange, without crushing the concrete in the diaphragm.
2. The detail to be used should be selected with consideration given to service life and durability. Casting the ends of the girder in concrete can protect the end of the girder against corrosion and eliminate joints over the pier.
3. Details that could potentially create construction challenges should be avoided. Otherwise, the simplicity of the SDCL system will be compromised. Details such as a cover plate for attaching the top flanges of the girder should be avoided. Research results indicate that there is no need to provide a cover plate for continuity

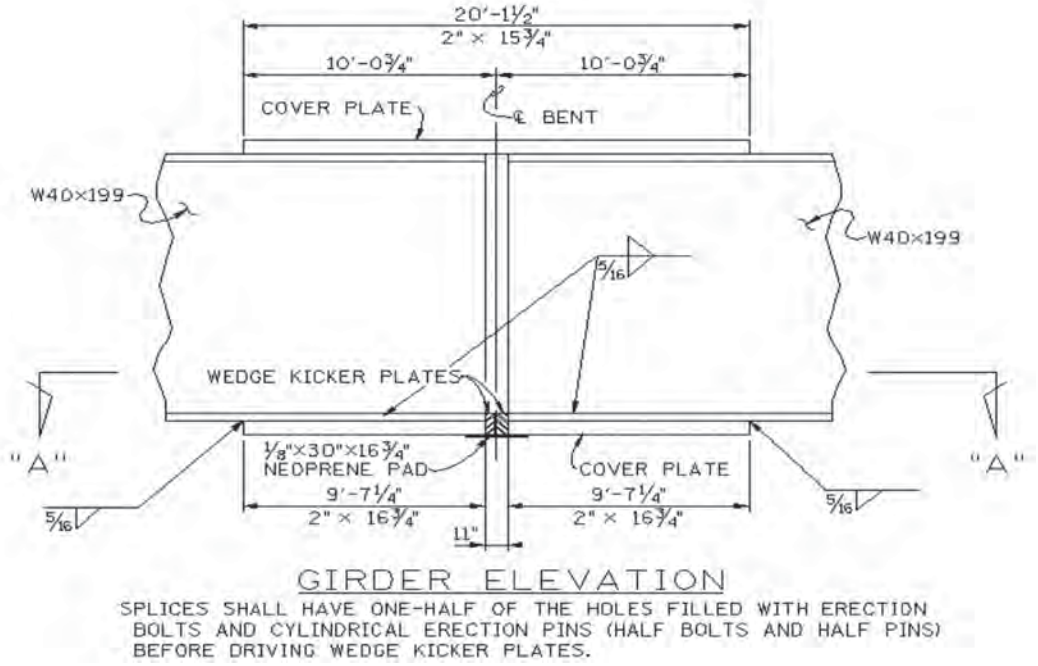

Fig. 23. Second detail for an SDCL steel bridge system, used for the DuPont Access Road Bridge in New Johnsonville, Tennessee.

or any other reason. Prestressed concrete bridges have used SDCL systems for years without any need for connecting the top flanges for continuity or any other reasons.

4. The ends of the girders during deck casting need to be torsionally braced. An effective way to provide this is to partially cast the ends of the girder in concrete, as described earlier.
5. For analysis purposes, the type of connection used over the pier needs to be identifiable with respect to rigidity. Connection details that are chosen should be classified as rigid, providing a full-moment connection to reduce efforts in the analysis stage.
6. Low-category fatigue details should be avoided.

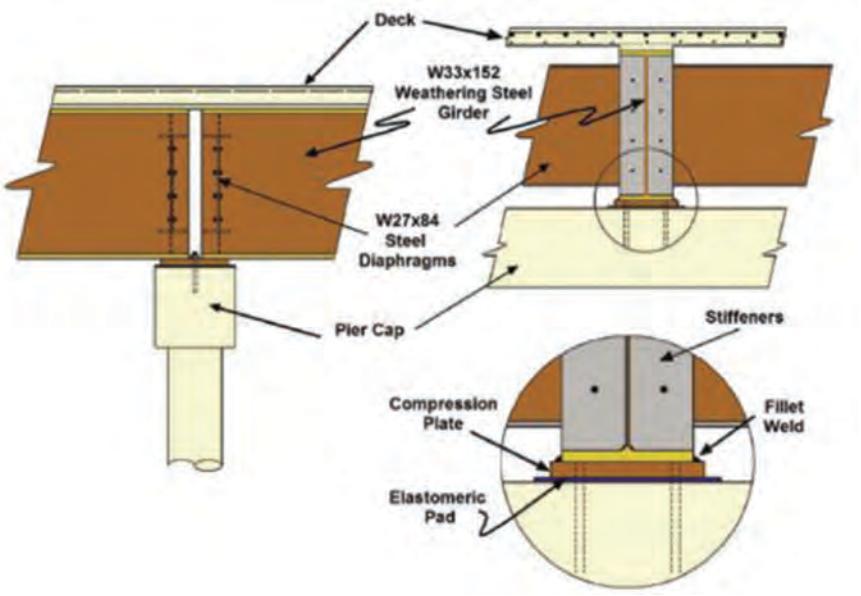

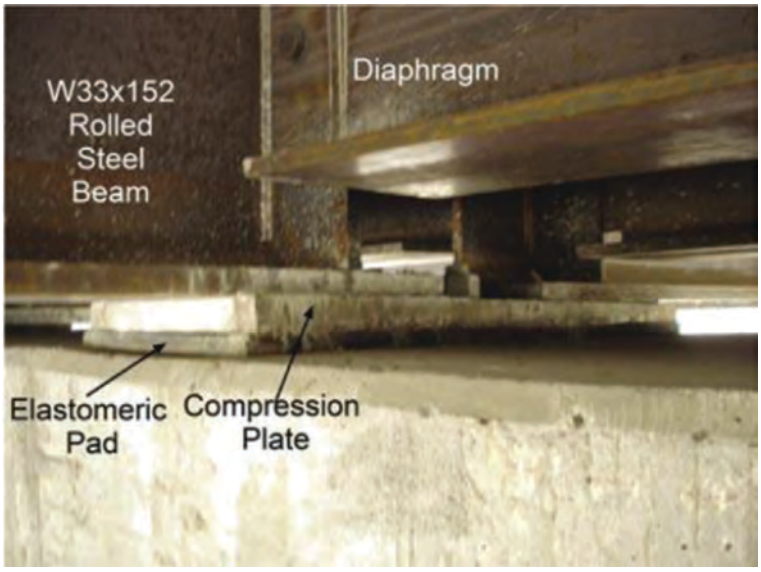

Fig. 24. Detail used by the Colorado DOT for a bridge located on U.S. Route 36 near Denver, Colorado.

SEISMIC APPLICATION

The recommended detail combined with additional research could provide an economical steel bridge system alternative in highly seismic areas; however, to date, no research studies have been carried out to extend the application of SDCL system to these areas. The following is a brief discussion of the issues involved and recommendations for further research, which could allow application of the recommended detail to highly seismic areas. Limited efforts by the author of this paper are under way to expand application of SDCL steel bridge systems to high seismic areas.

Steel bridges are lighter (about 40%) than concrete alternates and can provide better performance in a major earthquake. However, observations from a past earthquake (Astaneh-Asl et al., 1994) demonstrate that use of incorrect details or systems could result in steel bridges sustaining major damage. In the case of the 1995 Hyogoken-Nanbu earthquake in Kobe, Japan (Bruneau, Wilson, and Tremblay, 1996; Chung 1996; Shinozuka et al., 1995; Azizinamini and Ghosh, 1997), steel bridges suffered damage to superstructure elements (e.g., inadequate cross-frame detailing led to lateral bending of the girder webs near the girder ends), resulting in major retrofit activities and the closing of major highways, such as the Hanshin Expressway, for more than a year. The Kobe experience demonstrated that even relatively minor damage to steel bridges in seismic events can result in types of damage that could be very difficult to repair. Among the lessons learned is that critical elements of the bridge that are difficult to inspect and repair must be protected from any level of damage and remain elastic during the entire seismic excitation.

Seismic input is largely unknown; therefore, the design philosophy for buildings and bridges is to work on behavior of the structure under known conditions. Specifically, the design objective is to predefine the damage locations and design them accordingly by providing adequate levels of ductility. In the case of bridges, the preferred damage locations are at the ends of pier columns (formation of plastic hinges). In the direction of traffic, it is preferred to put columns in double curvature as shown in Figure 25. This allows larger portions of the pier column (two plastic hinges versus one for single curvature) to participate in energy dissipation.

Under longitudinal excitation, plastic hinges are located near the top and bottom of the columns, while under transverse excitation, the plastic hinge is located near the bottom of the pier column as shown in Figure 26.

The main design feature in the seismic design of bridges is to keep the superstructure elements completely elastic during an entire seismic event. These elements are called protected elements. The inelasticity is then forced to take place at predefined locations within the substructure. The predefined damage locations are the weak links or fuses that control the level of forces to be transmitted to superstructure elements. This design approach is referred to as the capacity design approach and is used for designing bridges in seismic regions.

In the capacity design approach, protected elements are designed for the largest possible force effects they might experience, considering overstrength that may exist because of higher actual material strength than that specified in design. The capacities of the bridge elements in the desired damage location (plastic hinge locations) are controlled through design. The plastic hinge regions are also detailed so that they can provide the desired capacities while deforming beyond elastic limits during a seismic event (ductility through adequate detailing).

In seismic areas, the use of an SDCL steel bridge system will demand the incorporation of a detail that can resist cyclic loading, which will require that the bottom portion of the recommended connection detail be designed for both tension and compression forces. Further, in seismic applications, the entire concrete diaphragm region, including the girder ends and connection elements, needs to remain completely elastic (protected elements) during the entire seismic event. An additional requirement is that the predefined damage areas (plastic hinge locations) must be forced to be at some distance away from the concrete diaphragm region, allowing repair and inspection after a major seismic event. These objectives could be achieved by making the concrete diaphragm and substructure elements integral, as depicted in Figure 27.

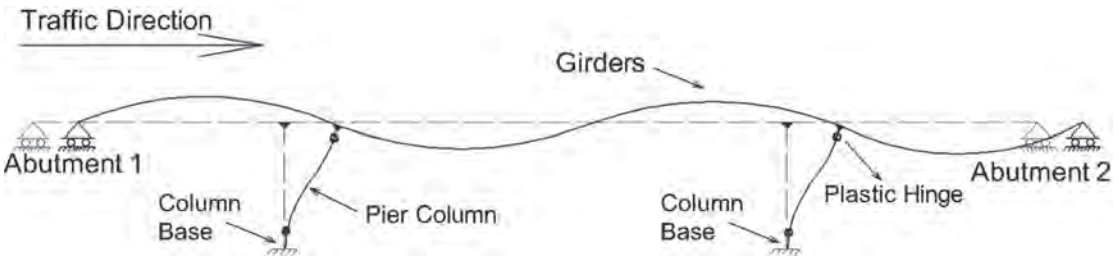

Fig. 25. Deflected shape of a three-span bridge in the longitudinal (parallel to traffic) direction.

The concrete diaphragm will be the protected element and must remain elastic; therefore, it must be designed for maximum credible torsion and remain elastic. The torsional moment to which the concrete diaphragm will be subjected is the negative moment at the girder ends, developed by various load combinations.

Several approaches can be used to ensure that the concrete diaphragm remains elastic under maximum credible torsion. Post-tensioning the concrete diaphragm (Patty, Seible and Uang 2001) is one possibility. Further, the plastic hinge at the column end must form at some distance away from column ends. The final configuration of the suitable detail should create a frame action between the superstructure and substructure (integral pier cap). The integral pier cap detail is also desirable for aesthetic considerations. A combination of experimental, numerical and analytical investigations will need to be carried out to develop a modified version of the recommended detail for seismic applications.

SUMMARY AND CONCLUSIONS

This paper and its related papers present the results of more than 10 years of experience gained from conducting research and performing field applications of the new steel bridge system for straight and minimally skewed bridges in which the skew angle is less than 10°, referred to as simple for dead load and continuous for live loads (SDCL). These papers provide a complete summary of the observations and recommendations related to the design, fabrication and construction of the SDCL steel bridge system. A major aspect of the system is the connection that should be used to join the girders over the interior supports. A recommended detail that was developed by conducting a combination of full-scale experimental tests and analytical and numerical studies is provided along with design provisions (Lampe et al., 2014; Farimani et al., 2014). The recommended detail has been applied successfully to several in-service bridges. Performance of several of these bridges has been monitored during construction, and for more than five years under ambient traffic and environmental loadings. Results of these monitoring programs, some of which have lasted more than five years, indicate excellent performance of the recommended detail (Yakel and Azizinamini, 2014). The recommended detail embodies the main philosophy that should be used in developing a suitable and economical connection detail for interior supports, namely, preventing the crushing of the

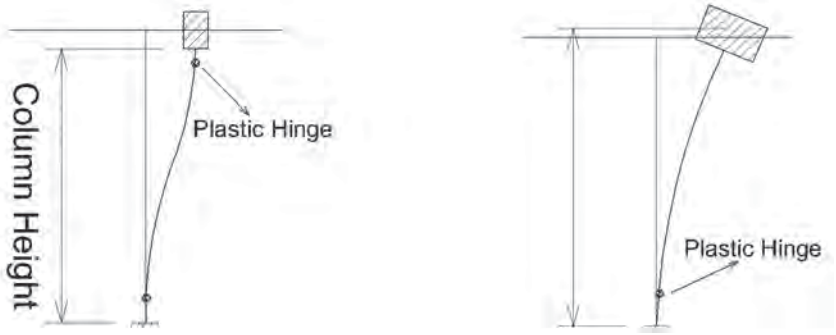

Fig. 26. Deflected shape of the pier column in the (a) longitudinal and (b) transverse directions.

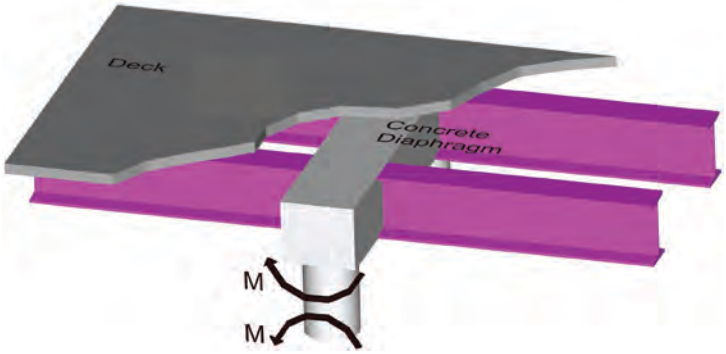

Fig. 27. Transfer column moment to the concrete diaphragm through an integral connection.

concrete within the concrete diaphragm. Using variations of the recommended detail is feasible, as long as they include characteristics described earlier in this paper.

An SDCL steel bridge system provides an excellent opportunity for accelerating the construction process. A variation of the recommended detail, suitable for ABC applications, was developed and full-scale tests were carried out to verify its behavior and develop design provisions. The same detail was also used in construction of a bridge that implemented the ABC philosophy and its behavior was monitored for about two years (Javidi, Yakel and Azizinamini, 2014). Results of the entire effort indicate that the recommended ABC detail provides an excellent connection detail for ABC application.

A few similar details comparable to the recommended detail are also used in practice by various DOTs. Known details are presented and their advantages and disadvantages are discussed.

An SDCL steel bridge system also potentially presents an attractive alternative for application in highly seismic areas but requires further investigation. Preliminary ideas on how to extend the SDCL steel bridge system to these areas are also presented.

In summary, the SDCL steel bridge system provides an economical bridge system for straight and minimally skewed bridges that also features the potential for enhanced service life. Eliminating bolted field splices and embedding the ends of the girder in concrete can result in a significant enhancement in service life. SDCL steel bridge systems reduce construction concerns such as stability and the sequence of deck casting. Less equipment is needed to erect SDCL bridge systems. SDCL system design is relatively simple, and field monitoring of several SDCL bridges already in service indicates excellent field performance. A suggestion for future research is the application of the SDCL concept to curved steel bridges.

ACKNOWLEDGMENTS

This investigation was directed by Atorod Azizinamini, Professor and Chair at Florida International University, and was made possible by contributions from many current and former graduate students and research associates, as well as input from many in the bridge community. In particular, the contributions of the following individuals are acknowledged.

Graduate students earning degrees from the project were Nick Lampe, Nazanin Mahasebi, Reza Farimani, Saeed Javidi, Derek Kowalski and Mark Otte. The research study was conducted at the University of Nebraska–Lincoln. Aaron Yakel was the research associate assisting the project. Laboratory technicians Jeff Boettcher, John Dageford, and Peter Hilsabeck assisted in conducting the experimental portion of the study. Graduate students who assisted with experimental testing include John Swendroski, J. Brian Hash, Patrick Mans, Luke Glaser and Nima Ala. The study was supported by the Federal Highway Administration and the Nebraska Department of Roads (NDOR). Several visionary engineers at NDOR were helpful to the successful completion of the project: Lyman Freeman, Moe Jamshdi and Hussam "Sam" Fallaha. Steel fabrication and assistance during specimen preparation were provided by Capitol Contractors of Lincoln, Nebraska.

The opinions and conclusions presented in this paper are those of the author and do not necessarily represent the viewpoints of the project sponsors.

REFERENCES

AASHTO (2012), *LRFD Bridge Design Specifications*, American Association of State Highway and Transportation Officials, Washington, DC.

Astaneh-Asl, A., Bolt, B., McMullin, K.M., Donikian, R.R., Modjtahedi, D. and Cho, S. (1994), *Seismic Performance of Steel Bridges During the 1994 Northridge Earthquake,* Report UCB/CE-STEEL-94-01, Department of Civil and Environmental Engineering, University of California, Berkeley, CA, 1994.

Azizinamini, A. and Ghosh, S.K. (1997), "Steel Reinforced Concrete Structures in 1995 Hyogoken Nanbu Earthquake." *Journal of Structural Engineering*, ASCE, Vol. 123, No. 8, pp. 986–992.

Azizinamini, A., Lampe, N.J. and Yakel, A.J. (2003), *Toward Development of a Steel Bridge System — Simple for Dead Load and Continuous for Live Load*, A Final Report Submitted to the Nebraska Department of Roads, National Bridge Research Organization: www.nlc.state.ne.us/epubs/r6000/b016.0088-2003.pdf.

Azizinamini, A., Yakel, A.J. and Farimani, M.R. (2005), *Development of a Steel Bridge System—Simple for Dead Load and Continuous for Live Load, Volume 1: Analysis and Recommendations*, Final Report NDOR 542, Nebraska Department of Roads, Lincoln, NE.

Azizinamini, A., Yakel, A.J., Lampe N.J., Mossahebi, N. and Otte, M. (2005), *Development of a Steel Bridge System—Simple for Dead Load and Continuous for Live Load, Volume 2: Experimental Results*, Final Report NDOR P542, Nebraska Department of Roads, Lincoln, NE.

Azizinamini, A., Yakel, A.J. and Swendroski J. (2003), *Development of a Design Guideline for Phase Construction of Steel Girder Bridges*, Final Report, Nebraska Department of Roads, Lincoln, NE.

Bruneau, M., Wilson, J.W., and Tremblay, R. (1996), "Performance of Steel Bridge during the 1995 Hyogoken-Nanbu (Kobe, Japan) Earthquake," *Canadian Journal of Civil Engineering,* Vol. 23, No. 3, pp. 678–713.

Chung, R., ed., (1996), "The January 17, 1995 Hyogken-Nanbu (Kobe) Earthquake Performance of Structures, Lifelines, and Fire Protection Systems," *NIST Special Publication 901*, Building and Fire Research Laboratory, National Institute of Standards and Technology, Gaithersburg, MD.

Dunker, K.F. and Rabbat, B.G. (1992), "Performance of Prestressed Concrete Highway Bridges in the United States—The First 40 Years," *PCI Journal,* Vol. 37, No. 3, May–June, pp. 487–464.

Farimani, M.R. (2006), *Resistance Mechanism of Simple-Made-Continuous Connections in Steel Girder Bridges*, Ph.D. Dissertation, University of Nebraska–Lincoln, Lincoln, NE.

Farimani, M.R., Javidi, S.N., Kowalski, D.T. and Azizinamini, A. (2014), "Numerical Analysis and Design Provision Development for the Simple for Dead Load–Continuous for Live Load Steel Bridge System," AISC, *Engineering Journal*, Second Quarter.

Freyermuth, C.L. (1969), "Design of Continuous Highway Bridges with Precast, Prestressed Concrete Girders," *PCI Journal,* Vol. 14, No. 2, April, pp. 14–39.

Javidi, S.N. (2009), *Resistance Mechanism of Simple-Made-Continuous Connections in Skew and Non-Skew Steel Girder Bridges Using Conventional and Accelerated Types of Construction*, Ph.D. dissertation, University of Nebraska–Lincoln, Lincoln, NE.

Javidi, S.N., Yakel, A.J. and Azizinamini, A. (2014), "Experimental Investigation, Application and Monitoring of a Simple for Dead Load–Continuous for Live Load Connection for Accelerated Modular Steel Bridge Construction," AISC, *Engineering Journal*, Third Quarter (in press).

Kowalski, D.T. (2007), *Development and Evaluation of Design Equations for the Simple-Made-Continuous Steel Bridge System*, M.S. Thesis, University of Nebraska–Lincoln, Lincoln, NE.

Lampe, N.J. (2001), *Steel Girder Bridges Enhancing the Economy*, M.S. Thesis, University of Nebraska–Lincoln, Lincoln, NE.

Lampe, N.J., Mossahebi, N., Yakel, A.J., Farimani, M.R. and Azizinamini, A. (2014), "Development and Experimental Testing of Connections for the Simple for Dead Load–Continuous for Live Load Steel Bridge System," AISC, *Engineering Journal*, Second Quarter.

Morales, D. (2004), "Feasibility Study of Continuous for Live Load Steel Bridges," M.S. Thesis, Oklahoma State University, 2004

Mossahebi, N. (2004), *New Steel Bridge System: Simple for Dead Load, Continuous for Live Loads*, M.S. Thesis, University of Nebraska–Lincoln, Lincoln, NE.

Otte, M.W. (2006), *Field monitoring of steel bridges-simple for dead, continuous for live*, M.S. Thesis, University of Nebraska–Lincoln, Lincoln, NE.

Patty, J., Seible, F. and Uang, C.M. (2001), *Seismic Response of Integral Bridge Connections: Structural Systems Research Project*, Final Report No. SSRP-2000/16, Department of Structural Engineering, University of California, San Diego, La Jolla, CA.

Shinozuka, M. (ed.), Ballantyne, D., Borcherdt, R., Buckle, I., O'Rourke, T. and Schiff, A. (1995), "The Hanshin-Awaji Earthquake of January 17, 1995, Performance of Lifelines," *Technical Report NCEER-95-0015*, National Center for Earthquake Engineering Research, Buffalo, NY.

Stone, A., Lindt, J. and Chen, S. (2011), *Development of Steel Design Details and Selection Criteria for Cost Effective and Innovative Steel Bridges in Colorado,* Final Report (CDOT Study No. 85-00) submitted to Colorado DOT, July.

Talbot, J. (2005), "Simple Made Continuous," *NSBA Steel Bridge News*, National Steel Bridge Alliance, Chicago, IL.

Wasserman, E. (2005), "Simplified Continuity Details for Short- and Medium-Span Composite Steel Girder Bridges," *Proceedings of TRB 6th International Bridge Engineering Conference Committee*, July.

Yakel, A. J. and Azizinamini, A. (2014), "Field Application Case Studies and Long Term Monitoring of Bridges Utilizing the Simple for Dead–Continuous for Live Bridge System," *Engineering Journal*, AISC, Third Quarter (in press).

Development and Experimental Testing of Connections for the Simple for Dead Load–Continuous for Live Load Steel Bridge System

NICK LAMPE, NAZANIN MOSSAHEBI, AARON YAKEL, REZA FARIMANI and ATOROD AZIZINAMINI

ABSTRACT

The most critical aspect of the simple for dead load and continuous for live load (SDCL) bridge system is identifying a detail capable of connecting the girders over the interior supports. An experimental program was set up to identify and study the fundamental characteristics of an interior connection for the SDCL bridge system. Three full-scale test specimens were constructed and tested, each using different connection details for possible use in the SDCL bridge system. Each specimen was subjected to two types of loading: cyclic testing to simulate long-term truck traffic loads and an ultimate load test to determine the ultimate capacity of the system. Results of the tests indicated that connection details meeting the design provisions could consist of embedding the girder ends in the concrete diaphragm and would provide a good service life. The main objective in using a concrete diaphragm to join the girder ends over the interior support is to prevent crushing of the concrete adjacent to the compression flanges of the girder and embedded in the concrete diaphragm. Two of the primary conclusions are that deck reinforcement is sufficient to develop continuity and the top flange need not be continuous over the interior support.

Keywords: steel bridges, steel girders, SDCL, simple for dead load–continuous for live load.

INTRODUCTION

The simple for dead load and continuous for live load (SDCL) bridge system utilizes a joint detail at the interior supports that does not become continuous until after the dead loads have been applied. Prior to attaining final continuity, the girders within the individual spans are simply supported. General information regarding the behavior and design of the SDCL system can be found in Azizinamini (2014).

To study potential details that could be used over interior supports of SDCL bridge systems, three full-scale specimens were tested. The design and construction of each specimen was completed according to the second edition of the American Association of State Highway and Transportation Officials (AASHTO) *Load and Resistance Factor Design Specifications* (AASHTO, 1998). Specimen 1 was intended to be a proof-of-concept specimen utilizing a connection detail that had a high probability of success. The purpose of specimen 2 was to explore the failure mechanisms that developed utilizing a minimalist connection detail. This provided a baseline and indicated what modes of failure needed to be addressed. Specimen 3 utilized a modified detail similar to that used in specimen 1 but simpler to construct and implement. In order to represent the loads that the structure would encounter, each specimen was subjected to two types of loading: cyclic testing to simulate long-term truck traffic loads and an ultimate load test to determine the ultimate capacity of the system.

DESIGN OF SPECIMENS

The prototype for the test specimens consisted of an existing in-service bridge. The prototype bridge is a two-span continuous structure, with each span 95 ft long and designed based on AASHTO LRFD specifications (1998). Detailed design of the prototype bridge is provided in Lampe (2001).

The test specimens represent the interior pier region of the two-span bridge, approximately from point of inflection to point of inflection centered about interior pier, as shown in Figure 1. Loads applied at the ends of the cantilevers allowed simulation of the type of loading the structure would be subjected to in the field and result in similar shear and moment profiles.

Nick Lampe, P.E., Bridge Engineer, HDR Engineering, Inc., Omaha, NE. E-mail: nick.lampe@hdrinc.com

Nazanin Mossahebi, Project Manager, Bureau Veritas North America, Inc., Los Angeles, CA. E-mail: nmossahebi@dpw.lacounty.gov

Aaron Yakel, Ph.D., Research Associate, Civil and Environmental Engineering Department, Florida International University, Miami, FL. E-mail: ayakel@fiu.edu

Reza Farimani, Ph.D, P.E., LEED AP, Associate, Thornton Tomasetti, New York, NY. E-mail: rfarimani@thorntontomasetti.com

Atorod Azizinamini, Ph.D., P.E., Professor and Chair, Civil and Environmental Engineering Department, Florida International University, Miami, FL (corresponding). E-mail: aazizina@fiu.edu

SPECIMEN DETAILS

The basic geometry and reinforcing are similar for all test specimens and are presented first. The specific differences in the connection details for each specimen are then presented. Figure 1 shows the basic geometry of the test specimens.

Concrete Diaphragm

The detailing of the diaphragm was similar to standard details used by many state departments of transportation. Reinforcement of the diaphragm consisted of closed #5 hoops spaced at 12 in. and #5 bars along the transverse faces. Holes were provided in the webs of the steel girders to allow the transverse reinforcement to pass through. A schematic of the diaphragm is shown in Figure 2.

Deck Reinforcement

The reinforcement of the 7½-in.-thick deck was based on the empirical deck design provisions given in the AASHTO LRFD specifications (AASHTO, 1998). The longitudinal steel includes #5 bars at 12 in. on center in the top layer and #4 bars at 12 in. on center in the bottom layer. The transverse reinforcement consists of #5 bars at 12 in. on center in the bottom layer and #4 bars at 12 in. on center in the top layer.

The negative moment produced by the live loads and superimposed dead loads are resisted by additional slab reinforcement at the interior pier location. One purpose of the larger research project was to determine any special requirements for this additional continuity reinforcement. Therefore, as a starting point, design of longitudinal rebar for the experimental program utilized classical concrete design theory. The details of calculations can be found in Lampe (2001). Based on this method, the additional reinforcement required in the top layer is comprised of two #8 bars centered between adjacent #5 bars. Similarly, one #7 bar is centered between adjacent #4 bars in the bottom longitudinal layer. This follows the AASHTO section 6.10.1.7 requirement of having ⅔ of the reinforcing steel in the top layer and ⅓ of the total area in the bottom layer. The details of the final slab reinforcement are shown in Figure 3.

Girder Connection Details

Three specimens were tested, each having different beam end connection details. This section provides description of different beam end details tested. The objective of test 1 was to examine a girder end detail with high probability of acceptable performance. In specimen 1, an end bearing plate is welded to the end of the girder (see Figure 4a). Two triangular plates are added to stiffen the end bearing plate above the bottom flange. The main characteristic of this specimen is the continuity of the bottom flanges over the pier. This continuity ensures that the specimen is capable of transferring the compressive stress of the bottom flange without substantial crushing of the diaphragm concrete. The connection of the two girders was done by extending the bottom flange plates and welding them together with complete-joint-penetration groove welds. This particular detail

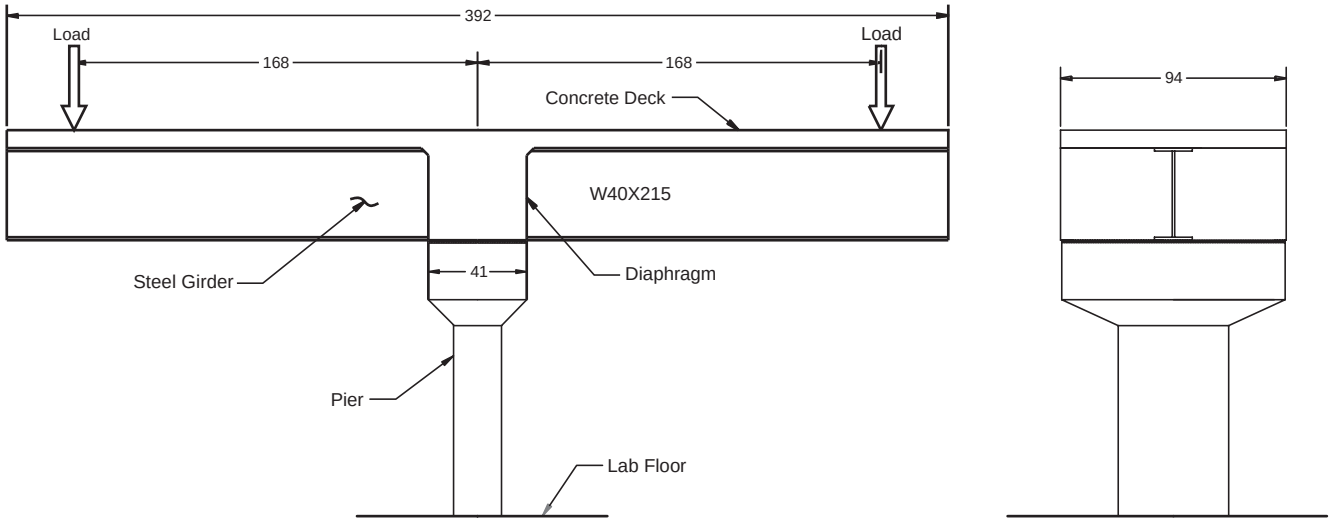

Fig. 1. Conceptual test specimen, dimensions in inches.

is certainly not considered cost effective, especially when conducted in the field. However, the goal of test 1 was to provide proof of concept. Later specimens then began to address cost effectiveness of the detailing.

The objective of test 2 was to establish the baseline and determine if special details at the girder ends are required. In specimen 2, the two girders simply sit on the pier, and the concrete diaphragm confines them (see Figure 4b). The two girders are completely separated, and there is no connection between bottom flanges. The negative moment is transferred through composite action of concrete and steel in the diaphragm. More complete information about specimen 2 can be found in Mossahebi (2004).

Test 3 was developed after completion of tests 1 and 2. The detail used in specimen 1 was judged to be acceptable, while the detail used in specimen 2 was judged to be unacceptable. The objective of specimen 3 was to explore the possibility of using a simpler form of the details used in specimen 1. Specimen 3 utilized bearing plates (without triangular stiffener plates) welded to the ends of the girders similar to specimen 1, but the bottom flanges were not connected (see Figure 4c). There was an 8-in. gap between the two girders.

CONSTRUCTION AND ERECTION

Construction of each test specimen was completed in the structures laboratory at the University of Nebraska–Lincoln. A reinforced concrete pier was built to support the cantilever system for all three specimens. The girders for the specimens were cut from the same stock (W40×215 rolled I-girders). A 15.75-in.-wide by 36-in.-long by 1-in.-thick 80-durometer elastomeric bearing was placed on the pier for the girders to bear on. Polystyrene 1 in. thick was placed at the base of the diaphragm to prevent bonding between the pier and concrete diaphragm and allow the girder rotation. Dowel bars were also provided as shown in Figure 5.

The combined details used allow rotation of the girders about the pier centerline while preventing the horizontal translation of the girders.

After the girders were set, diaphragm-reinforcing steel was placed and embedment gages were set. Formwork for the deck and diaphragm was added after the diaphragm-reinforcing steel was placed. Once the deck formwork was completed, the diaphragm was partially cast to approximately ¾ the height of the web to stabilize the specimens prior to casting of the deck. Once the diaphragm was poured, deck reinforcement was placed. The concrete deck was cast three days after the diaphragm was cast.

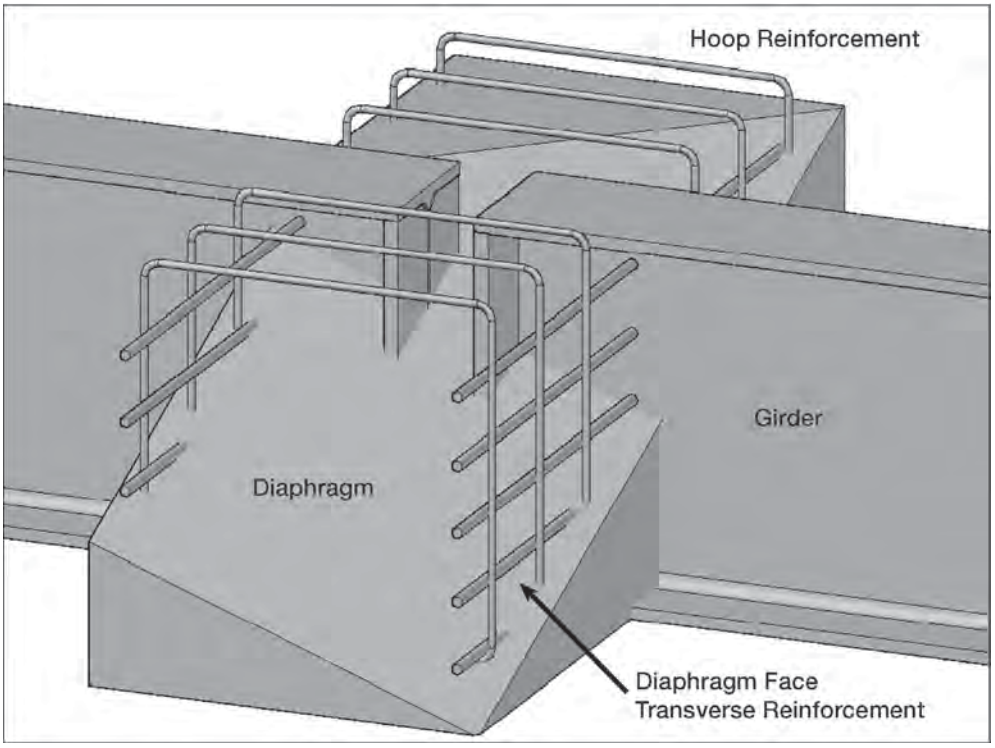

Fig. 2. Concrete diaphragm detail (cutaway).

INSTRUMENTATION

Several types of instrumentation were used to monitor performance of the test specimens under applied loads. Instruments included electrical strain gages, vibrating wire embedment gages and potentiometers. The strain gages were mounted on the steel girders and reinforcing bars. The embedment gages were placed inside the concrete diaphragm and deck. The potentiometers were used to measure the displacement of the end of the cantilevers. The horizontal movement of the bottom flanges into the diaphragm was measured by a potentiometer in specimen 3. To apply load on the specimens, displacement was applied at the end of each cantilever by hydraulic rams. The pressure of hydraulic oil inside the rams was measured by pressure meters built into the rams. Complete details of the instrumentation can be found in the experimentation report (Azizinamini et al., 2005).

MATERIAL PROPERTIES

The laboratory test specimens were constructed using materials representative of those utilized in typical bridge construction. Several component tests were performed in order to ensure that the bridge components possessed the specified material properties. The deck slab and diaphragm concrete had a specified minimum compressive strength of 4000 psi and were reinforced with grade 60 reinforcing bars. The bridge girders were fabricated from W40×215 rolled I-girders conforming to ASTM A709-50W specifications. The material testing procedure and results for each specimen are presented in the following sections.

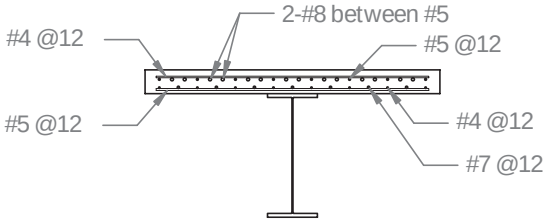

Fig. 3. Concrete slab section.

Concrete

For concrete, several 6-in.-diameter by 12-in.-long concrete cylinder samples were taken during the casting of both the diaphragm and the deck. The average compressive strength of cylinder specimens, tested in accordance with ASTM C39, is shown in Table 1.

Reinforcement Steel

For the steel reinforcing materials, samples of each deck-reinforcing-bar size were tested. Each sample was tested as a full section according to ASTM A370 specifications. Results of the tensile test are given in Table 2. The average reinforcing-bar yield stress was approximately 65 ksi for test 1, 73 ksi for test 2 and 69 ksi for test 3.

Girder Steel

Four material samples were taken from specimen 1, two each from the web and flange. The samples were taken from regions that were subjected to low flexural stresses during the testing sequence. The samples were tested as full sections according to the ASTM A370 specifications. The average yield strength of the girder steel was determined to be

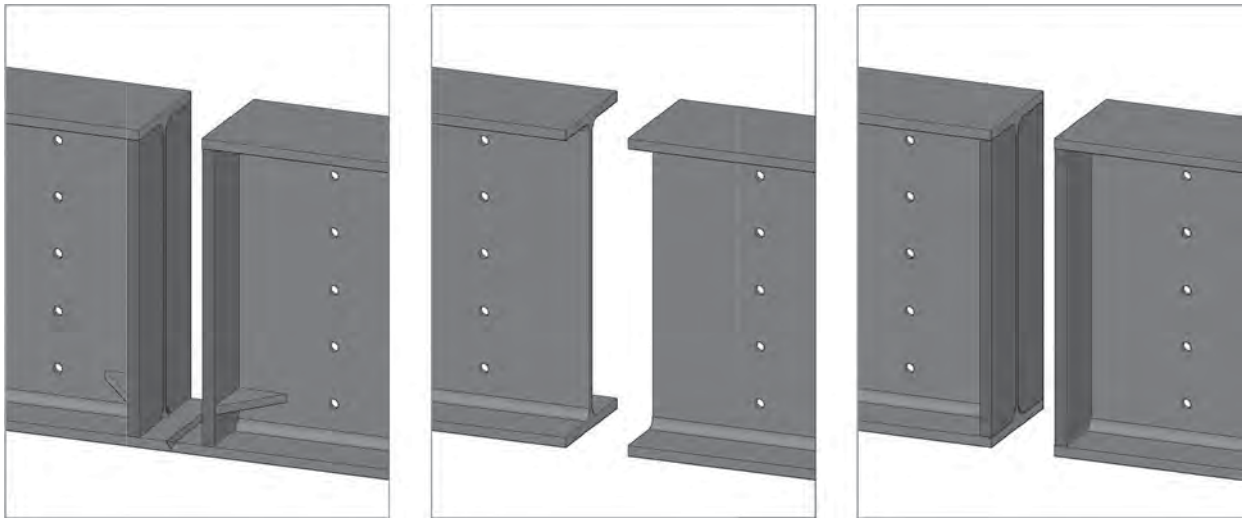

Fig. 4. Details of test specimens inside the diaphragm: (a) specimen 1; (b) specimen 2; (c) specimen 3.

Table 1. Average Concrete Compressive Strength, f'_c		
	f'_c (ksi)	
Test	Slab	Diaphragm
1	4.98	6.26
2	5.45	7.14
3	7.24	5.89

Table 2. Reinforcement Tensile Test Results							
	Yield Strength, f_y (ksi)			Ultimate Strength, v_u (ksi)			
Bar Size	Test 1	Test 2	Test 3	Test 1	Test 2	Test 3	f_u/f_y
#4	64.2	71.5	70.3	101.0	114.2	113.4	1.57
#5	63.8	76.5	68.9	101.0	122.8	108.7	1.58
#7	68.2	67.5	64.3	101.0	109.5	104.6	1.48
#8	65.5	75.5	73.2	105.4	110.6	107.8	1.61

Fig. 5. Photo of the two girders during construction.

57 ksi, and the average ultimate stress was 72 ksi. The material from all three specimens came from the same stock and separate material tests were not performed on specimens 2 and 3.

CYCLIC TESTING

The bridge structure is expected to endure millions of cycles of repeated axle loads from vehicles during the design life. The available data show that the number of trucks on a bridge can reach more than 180 million vehicle load cycles during the lifetime of 100 years (Szerszen and Nowak, 2000). The proposed connection should be able to operate and survive when subjected to cyclic loading generated by truck traffic. The specific goal of the cyclic testing performed was not intended to determine the fatigue strength or limit of the details, but rather as a proof loading to investigate whether the proposed details are capable of surviving a loading regimen equivalent to the cyclic loading anticipated over the design life of the bridge.

Cyclic Testing Procedures

The fatigue limit state load combination was used to calculate the shear and moment envelope to which the prototype bridge would be subjected to. According to AASHTO LRFD specifications (1998), during its 75-year design life, the prototype bridge (and, consequently, the connection of the two girders at the pier location) will experience 135,000,000 cycles of truck loadings. The simulation of this number of cycles in the laboratory would have taken a prohibitively long time. Therefore, there was a need to develop a procedure that could simulate 75 years of traffic in a reasonable time frame. Following is a discussion of the procedure that was used during the cyclic loading tests that allowed for a reduction in the number of cycles by increasing the magnitude of the applied load.

The connection detail is composed of steel and concrete elements in a complex arrangement, and there is no single fatigue life model that applies to situation. Therefore, at the outset, it was assumed that the steel elements within the detail would control the fatigue life of the detail; consequently, the fatigue model for steel, given by Equation 1, was used to determine the amplified load. In this expression, A is a constant dependent upon the geometry and the detail under consideration, while the exponent ⅓ is characteristic for the material and is the slope (negative) of the stress versus number of cycles curve when plotted on log-log scales. Regardless of the value of A, which is unknown for the detail under consideration, the fatigue model can be used to determine the amplified loading value.

$$\Delta F\left(\frac{A}{N}\right)^{1/3} \tag{1}$$

where:

N = number of cycles to failure
A = a constant representing the detail category of the connection
ΔF = load increment

Equation 1 may be rewritten for two conditions. Equation 2a represents the loading and number of cycles applied during the service life of the real structure as assumed for design. Equation 2b represents the structure under amplified loading.

$$M_1\left(\frac{A}{N_1}\right)^{1/3} \tag{2a}$$

$$M_2\left(\frac{A}{N_2}\right)^{1/3} \tag{2b}$$

where

M_1 = actual load
N_1 = cycles for actual structure corresponding to load of M_1
M_2 = amplified load (desired quantity)
N_2 = number of test cycles at load of M_2

Dividing M_1 by M_2 causes the constant A to cancel and results in Equation 3, which can be used to determine the amplified load M_2 that must be applied corresponding to a desired number of cycles. For the testing performed, the resulting amplified load was approximately four times nominal value.

$$\frac{M_1}{M_2} = \left(\frac{N_2}{N_1}\right)^{1/3} \tag{3}$$

If the specimen is subjected to the specified cycles at the amplified load level and does not experience a fatigue failure, the conclusion is that a fatigue failure due to the actual truck loading would occur beyond the service life of the bridge. In cases where the load intensity varied throughout the testing, Miner's rule was used to assess the cumulative damage.

The test setup had the same configuration for all three specimens. The cyclic load was applied using 220-kip hydraulic actuators placed at the ends of each cantilever as shown in Figure 6. The cyclic loading frequency was set at two cycles per second. At the beginning of each day, prior to the start of applying fatigue loads, the specimen was subjected to five cycles at a lower frequency. On the first of the

five slow cycles, the specimen was held at the peak end load and data were collected from all instruments, including the embedment gages. During the application of the five slow cycles, data from all instruments except embedment gages were collected.

Displacement control was used throughout the course of the cyclic investigation. Once the stiffness was obtained, the displacement required for a desired load was calculated and then applied. In all cases, a small positive bias was imposed to prevent load reversal in the test apparatus. In test 1, the load applied at each end cycled between 2 and 106 kips. This load was applied successfully to the specimen for 2,000,000 cycles.

The same initial process was used for specimen 2, and due to a slightly different initial stiffness, the target end load was found to be 104 kips rather than 106 kips. However, after applying a few cycles, it became apparent that the specimen could not resist the desired end load of 104 kips. The maximum load achieved from the calculated displacement, based on initial stiffness, had decreased to approximately 74 kips. As a result, the number of applied loading cycles had to be increased to compensate for the lower load level. The intent of specimen 2, which was to observe the failure modes in absence of any special detailing, made it perform poorly during the cyclic testing at the amplified load levels. Recall that the load level was amplified to allow application of a lower number of cycles. The applied displacement had to be adjusted three times during the cycling load test because the load achieved at the set displacement decreased over time. The cyclic testing was terminated after applying approximately 2,780,000 cycles because the load-carrying capacity continued to deteriorate.

Based on the experience of specimen 2, it was decided to initially apply a smaller amount of load and observe the behavior of specimen 3. Therefore, the end load was set to approximately 70 kips and 2,000,000 cycles were run with this configuration. Once completed, the load was increased to 85 kips for an additional 3,515,516 cycles. The number of cycles and load range in each test are summarized in Table 3.

Fig. 6. Specimen 1 cycling test setup and fixtures.

Table 3. Number of Cycles and Load Range for the Three Specimens		
Test	**Cycles**	**Load Range (kips)**
1	2,000,000	104
2	2,780,000	74
3	5,515,516	70 and 85

Cyclic Test Results

The following is a summary of observations made during the cyclic testing and the results obtained from the instrumentation. Additional information can be found in the full reports (Azizinamini, Lampe and Yakel, 2003; Azizinamini et al., 2005).

Cracking Patterns

For all three specimens, cracks on the surface of the deck slab were documented prior to application of fatigue cycles and then again at various times during the testing. The loads applied during the cyclic test were magnified by a factor of approximately 4 to shorten the length of time required for testing. As a result of the magnification, cracking of the concrete was exacerbated, and the degree of the observed cracking is not an indication of the performance under service load.

In test 1, mapping of deck cracks was done at 1 million, 1.5 million and 2 million cycles of load. The largest crack widths were observed to occur at the face of the diaphragm, near the edge of the slab. This can be attributed to the abrupt change in rigidity due to the presence of the concrete diaphragm at the pier. Additional cracks were observed but diminished in size and frequency as one moved away from the diaphragm. A crack map for 1.5 million loading cycles is shown in Figure 7. A comparison of the crack widths at 1.5 million compared to 1 million load cycles shows that there was virtually no change in crack widths over this interval. There were a few additional short cracks propagating inward from the edge of the deck, but the measured widths of existing cracks were unchanged. The fact that the crack widths were stable was an indication that no progressive damage occurred during the course of cycling. The cracking patterns and behavior of specimen 3 was nearly identical to that of specimen 1.

In specimen 2 cracks formed through the depth of the deck over the pier and close to the edge of the diaphragm during the cyclic testing similar to specimens 1 and 3. The initial cracks were observed near the diaphragm edge. As

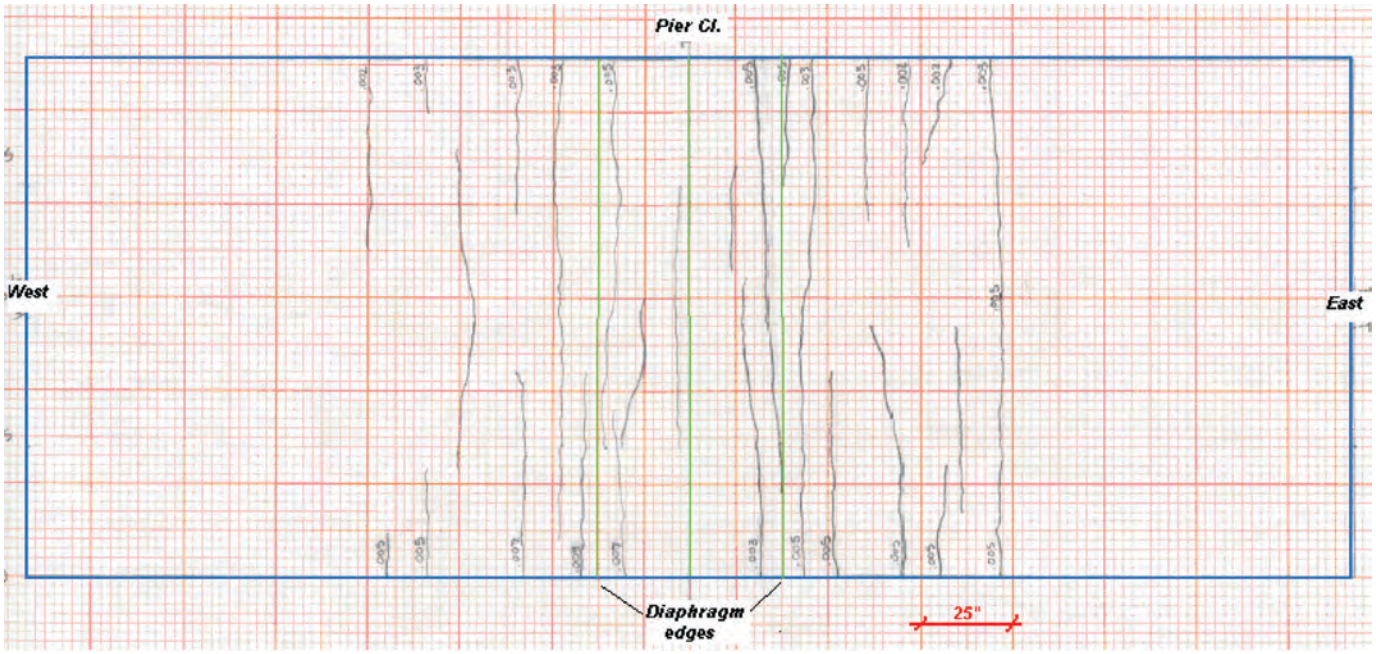

Fig. 7. Cracks mapped from the test 1 slab after 1.5 million cycles.

cyclic loading continued, the bottom flanges, subject to compression, were observed to actually penetrate into the diaphragm. This observation led to the discontinuation of testing as it had become apparent that the model was experiencing an ultimate strength failure.

Load-Deflection

The load-deflection plots shown in Figure 8 were generated from data collected from several cycles at the start of the test and then again at the end of the test. For specimen 1 (test 1), little change in stiffness was observed over the complete interval. In specimen 2 (test 2), the maximum load continued to decrease over the duration of the test. In specimen 3 (test 3), during the first 2,000,000 cycles, each day the cycling loads resulting from the applied displacement would experience a downward shift downward of nearly 10 kips by the end of the day's cycling. Note that both endpoint loads experienced the same drop so that the cycling range remained unchanged. The following day, the loads had recovered to the previous day's starting values. The effect stabilized within several hours, and on occasions when cycling was continued overnight for a period of days, there was no progressive decrease. Although no instrumentation was present to quantify the observation, the temperature of the concrete in the vicinity of the bottom flange was noticeably higher after cycling. Observation of the system stiffness, discussed in the next section, further supports the contention that the effect was due to benign causes and not fundamental structural changes.

Stiffness Softening

In specimen 1 (test 1), the experimental displacement required to attain the 106-kip load was 0.3083 in., based on the finite element analysis of the specimen under this load (Lampe, 2001). Only once was the applied displacement adjusted to maintain the 106-kip load during the cycling test. After 7400 cycles, the applied displacement was increased from 0.3083 in. to 0.3115 in. to compensate for the stiffness reduction. The amount of adjustment was about 0.5% of the initial applied displacement. The stiffness

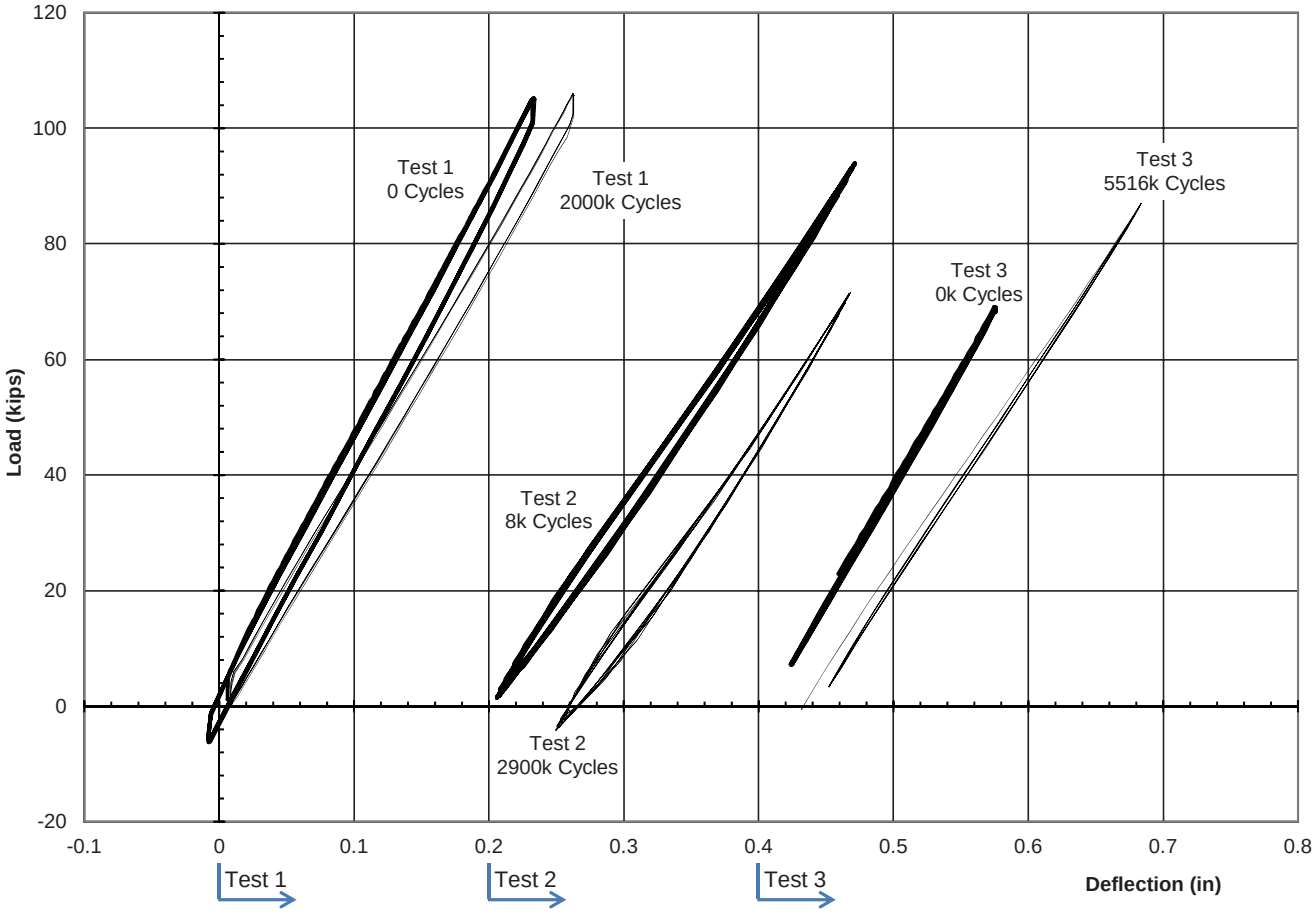

Fig. 8. Load-deflection plots of cyclic tests. The points of zero deflection for specimens 2 and 3 are shifted to the right to improve clarity.

softening in the load-deflection response of specimen 1 can be seen in Figure 9. The slope of the load-deflection curves at the zero cycle is about 437 kip/in. This slope decreased to about 394 kip/in. after 2,000,000 cycles. Figure 9 plots the resulting specimen stiffness over time. Because the adjustment was only needed once at 7400 cycles and there was virtually no change in specimen response throughout the remaining cycles, it is likely that the slight stiffness change was due to initial concrete damage, such as tensile cracking of the concrete deck. The loss of stiffness in test 1 was about 10% through the entire cycling test. The behavior of specimen 3 was very similar to that of specimen 1 and gave a similar stiffness value during the initial portion of loading. Several small adjustments were made at the outset of cycling to accommodate a small reduction in stiffness similar to that observed in specimen 1. After the load was increased, at 2,000,000 cycles, the stiffness did decrease slightly. Again, it is likely this decrease in stiffness was due to an initial finite amount of damage in the concrete, such as tensile cracking. Once the initial damage had taken place, the stiffness then stabilized and remained constant through the remainder of the test. The adjustments appear as permanent set in Figure 9.

The behavior of specimen 2 (test 2) was somewhat different than that observed in specimens 1 and 3. The actual initial stiffness of the structure is not accurately illustrated in Figure 9 due to the fact that the specimen was unable to support cyclic loading at the load level that was first applied. During the first portion of the testing, approximately 8000 cycles, the applied displacement had to be adjusted until the resulting load stabilized. The adjustments appear as permanent set in Figure 9. Note that the stiffness shown in Figure 9 is after 8000 cycles, when the specimen already had experienced a loss in stiffness; an elastic estimate of initial stiffness for specimen 2 would predict a value close to that of specimen 3 (test 3).

Vertical Strain Distribution

The vertical strain profiles through the depth of the diaphragm at the centerline of the pier are shown in Figure 10. These strains were measured by embedment gages inside the concrete diaphragm during the cycling tests. The strain distribution from both the specimens 1 and 3 (tests 1 and 3) exhibited only slight variations over the duration of the test. As evident in Figure 10, the strain distribution through the concrete diaphragm at the centerline is not linear, particularly in the case of specimen 3, in which the concrete must transfer the concentrated compressive load from the bottom flanges through the diaphragm. The magnitude of strains observed in both specimens 1 and 3 are similar, yet the load applied to specimen 1 was 25% greater.

The maximum observed compressive stress due to cyclic loading at the bottom of the diaphragm during test 3 was 2.2 ksi, which is 37% of the compressive strength of the material. The AASHTO LRFD specifications do not explicitly address the fatigue of concrete in compression; however,

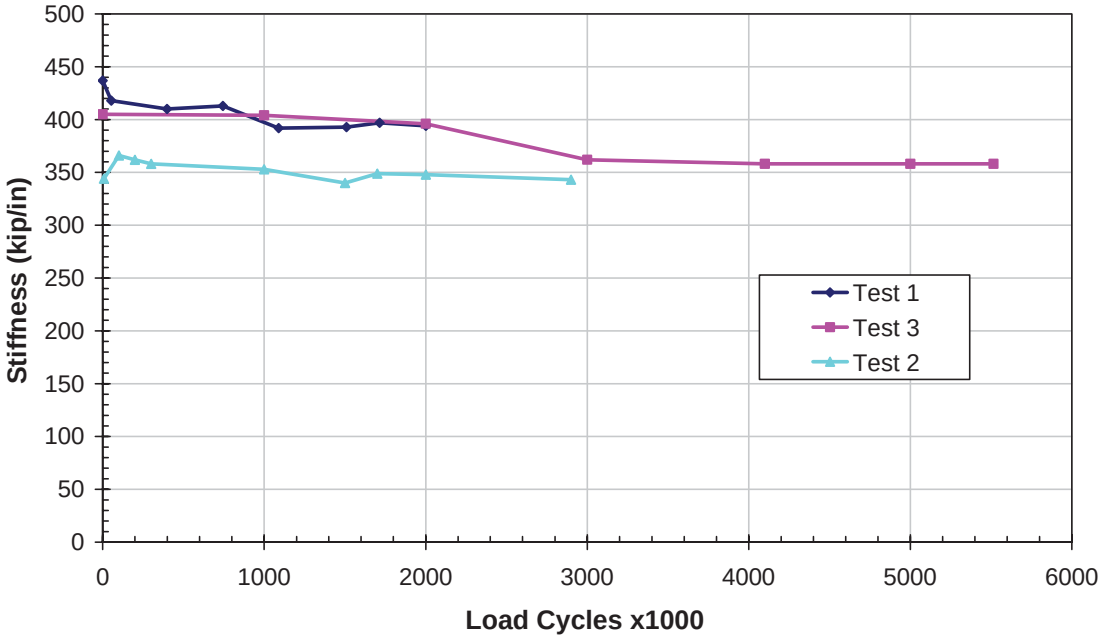

Fig. 9. Stiffness variation during cycling tests.

the observed stress level would satisfy the Eurocode provisions, which only require detailed investigation if the stress level is greater than 50% of the compressive strength (Milenkovic and Pluis, 2000).

Figure 11 shows a similar vertical strain profile for a section just outside of the diaphragm. As seen in Figure 11, the specimen 1 (test 1) strain profile remained virtually unchanged over the course of 2 million cycles. Although the profile obtained from specimen 3 (test 3) appears changed at the end of loading, recall that specimen 3 had an increase in the applied load after 2 million cycles. This increase in load would have the effect of scaling the strain values, resulting in a rotation of the strain profile, which is essentially what can be seen in Figure 11. Again, specimen 2 (test 2) is the exception, with a marked decrease in strains within the bottom flange by the end of the test.

The vertical distribution of the strain through the depth of the girder is not linear inside the concrete diaphragm (see Figure 11). This violates the assumption that plane sections remain plane in the classical beam theory, even though the concrete strain is within the elastic limit in the compression zone. However, the trend of the strain distribution outside of diaphragm is close to a linear fit. The one exception is specimen 2 (test 2), for which the bottom flange was observed moving relative to the concrete diaphragm. The nonlinearity of the strain profile for test 2 is additional evidence that the compression flange moved into the diaphragm. This movement was visible during the cyclic loading.

Strain in Deck Reinforcement

The strain in the deck reinforcement was also monitored during the fatigue loading for all three specimens. Figure 12 shows strain plots for the reinforcing bar located near the centerline of the deck in the top rebar layer (shown by an arrow in Figure 12). The longitudinal location of the gages was near the pier centerline. Care was taken in placing the reinforcement to ensure the single gage per bar was oriented toward the side of the bar to avoid localized bending effects. Additionally, longitudinal locations were chosen to avoid areas of large curvature to minimize local bending of the reinforcement, which can cause difficulties in strain measurements obtained with a single gage. During testing of specimen 1 (test 1), the tensile strain in the reinforcing steel varied only slightly over the 2 million cycles. In specimen 2 (test 2), there was a constant and significant increase of strain throughout the test, with the final value being nearly three times the initial value. In specimen 3 (test 3), there is an increase in the strain plot that coincides to the increase in applied load from 70 kips to 85 kips after 2 million cycles. Otherwise, there was little change. Note that the strains obtained for each specimen were in response to different load levels. The intent of Figure 12 is to show the change in strain over time of each individual specimen, not compare the absolute magnitude in the different specimens. For all specimens, the stress levels in the reinforcement remained below the threshold value required for infinite life according to the AASHTO LRFD specifications.

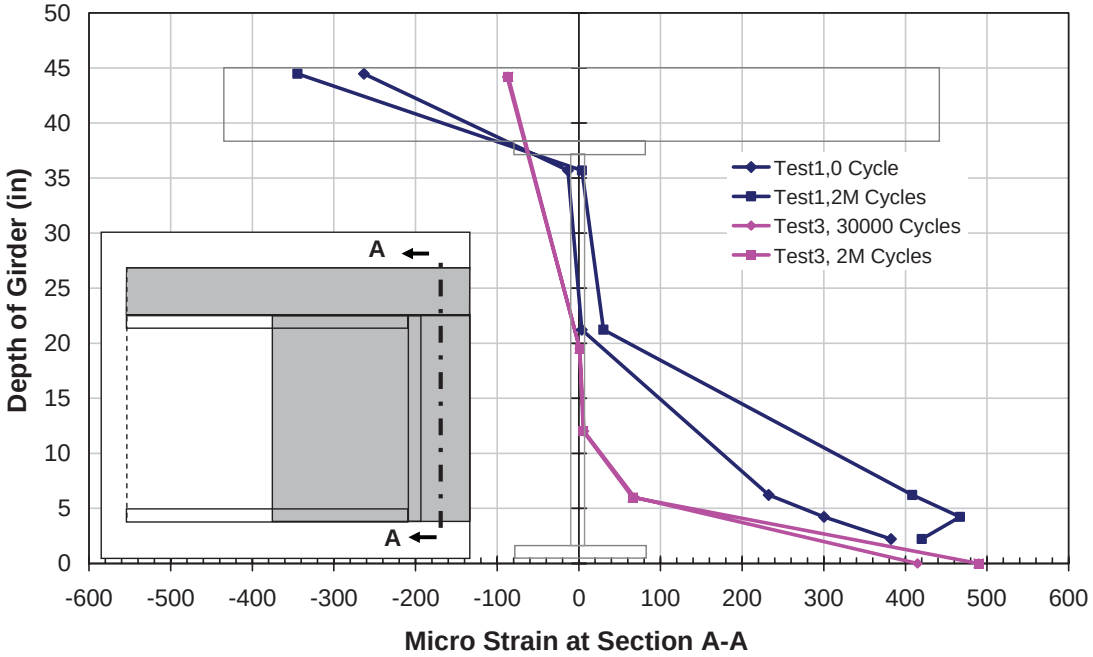

Fig. 10. Vertical profile of longitudinal strain at center of diaphragm.

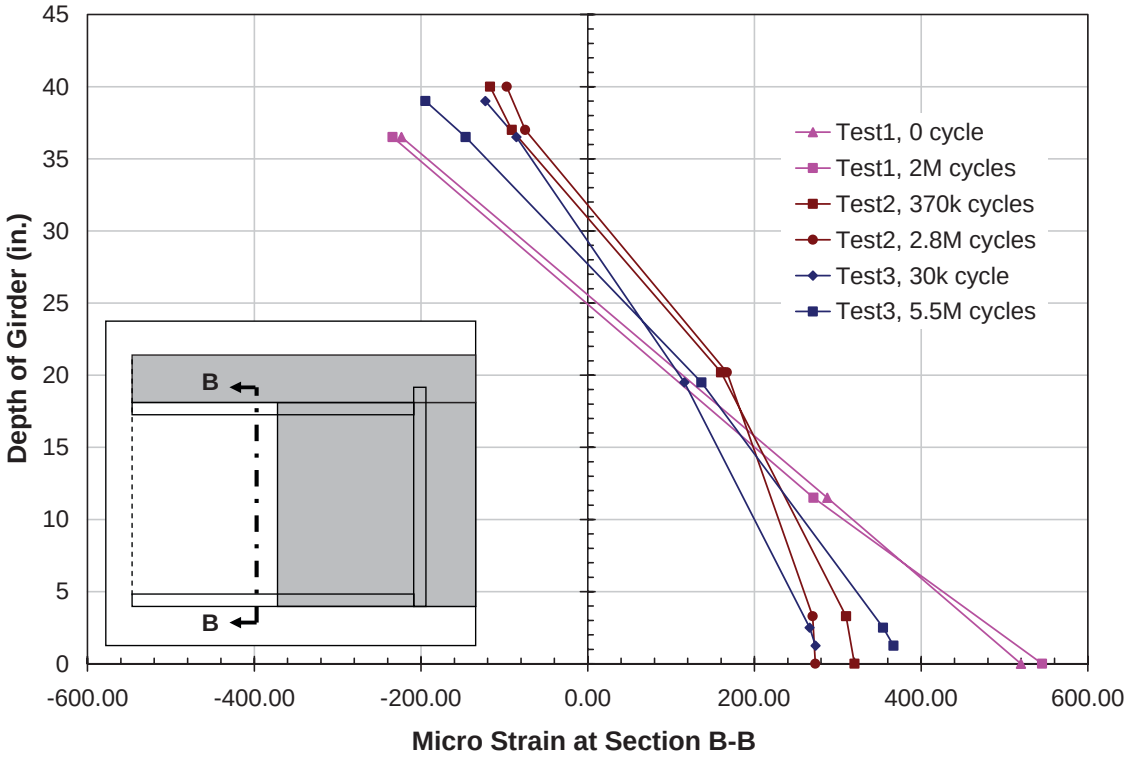

Fig. 11. Vertical profile of longitudinal strain outside of diaphragm.

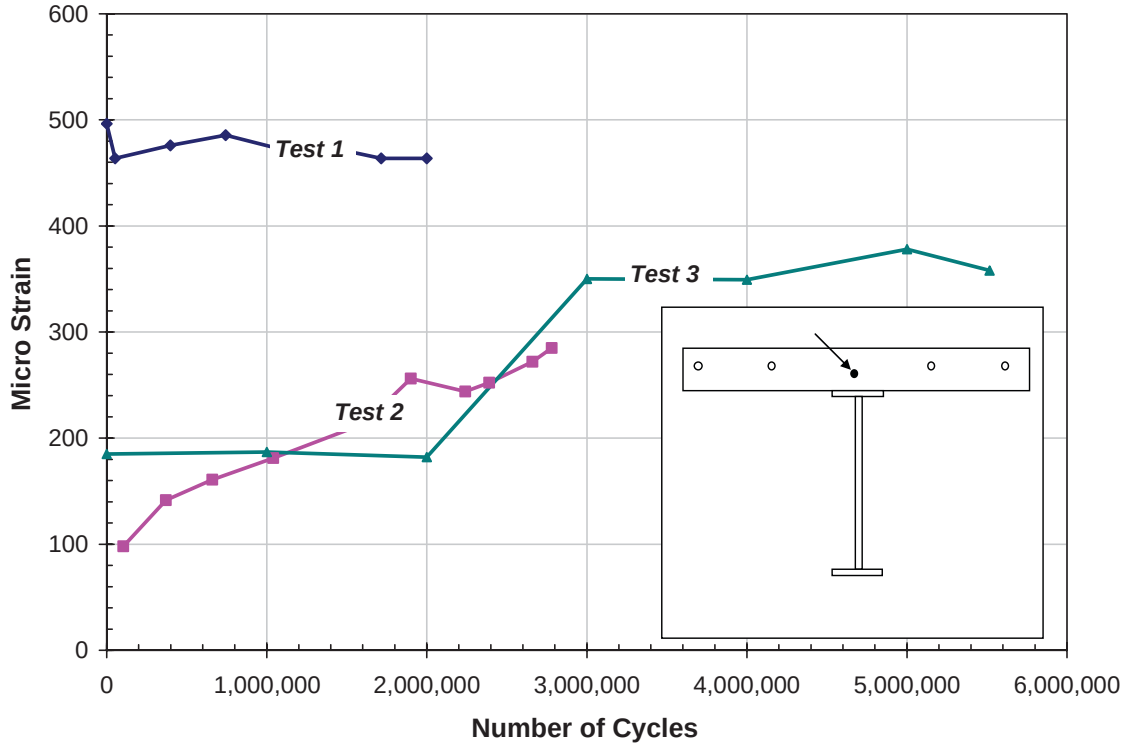

Fig. 12. Strain in top reinforcing bar.

ULTIMATE LOAD TESTING

The ultimate load tests were carried out to investigate the behavior of the specimen under ultimate load and evaluate the strength and ductility of the system. Loading of the specimen was applied through spreader beams placed on the deck at each end of the specimens. Threaded rods extended from the spreader to the basement of the structures laboratory. The loading system for the ultimate load test is shown in Figure 13. The distance from the spreader beam center to the centerline of the pier was 12 ft for specimen 1 and 15 ft for specimens 2 and 3. The change was necessitated by equipment constraints. During testing, displacement was applied in small increments with pauses for observations and data acquisition.

Results

The ultimate load tests were performed to obtain the ultimate load capacity of the various connections details and provide information regarding the associated failure mechanisms.

Load-Deflection

Load versus deflection plots were generated for both the west- and east-side cantilevers for each specimen. Because the location of applied load differed between the specimens, the loading data are expressed as moment and the deflection is normalized against the distance between pier centerline and load position. The responses from all three specimens have been combined in Figure 14. The saw-tooth appearance of the curve was caused by pauses for data collection, in which relaxation of the specimen occurs due to the onset of plastic flow. The maximum observed load, moment and deflection of the specimens are listed in Table 4. The values shown in the table refer to the maximum from either the west or east cantilever in each specimen. Notice that the moment capacities of the specimens 1 and 3 are approximately 1.5 times that of specimen 2.

From the data plot for test 1 (specimen 1), shown in Figure 14, it can be seen that the initially linear behavior ends near a moment of 3800 kip-ft. Further investigation into the experimental data revealed that the reinforcement near the girder centerline had just reached yield at this load. In

Fig. 13. Specimen 2 ultimate test setup.

Table 4. Displacement, Load and Moment at Maximum Observed Load			
Test	**Displacement (in.)**	**Load (kip)**	**Moment (kip-ft)**
1	2.59	516	6192
2	4.12	263	3945
3	4.50	391	5865

test 2 (specimen 2), the system response was linear up to a moment level of about 1800 kip-ft. At a moment magnitude of 3900 kip-ft, the system was unloaded due to a problem in the loading system. As a result of the initial loading, the system displayed a permanent set of approximately 0.75 in. Upon subsequent reloading, the system responded linearly until intersecting the original load-deflection curve. Despite substantial incurred damages, the initial stiffness during reloading was nearly equal to the original stiffness. The moment deflection behavior of test 3 (specimen 3) was quite similar to that of specimen 1. The initial elastic region ended at a lower load level of 1900 kip-ft. The loading rolled off smoothly until a load level of 5050 kip-ft, where a small break in the curve can be seen. The load level was still increasing slightly when the test was terminated due to the extreme deflection levels that were resulting in unsafe conditions in the load apparatus.

Cracking Observations

All specimens exhibited cracking of the concrete over the pier. As an example, cracking of specimen 3 is shown in Figure 15, which is representative of the general pattern of cracking displayed by all specimens. The results presented are for the ultimate loading. The cracking patterns are being used to interpret the failure modes. As such, the extent and magnitude of cracking are not indicative of what would be found at service levels. The following describes observations specific to each specimen.

Many of the cracks that initiated during the cyclic testing were simply widened in the ultimate test. At the end of the ultimate load test, cracks were observed penetrating through the depth of the slab at the edge of the diaphragm. There were both transverse and longitudinal cracks in the slab. The longitudinal cracks were found directly over the steel girder.

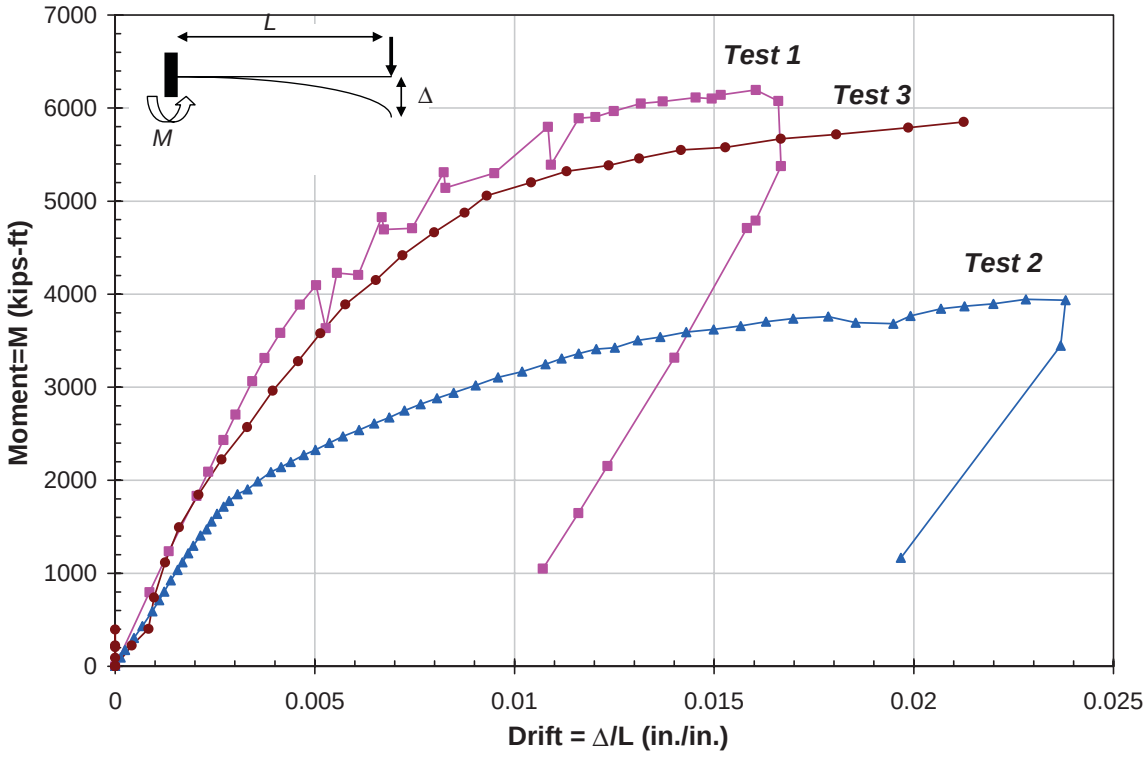

Fig. 14. Moment–drift plots of three experiments.

A 45° crack was observed at the diaphragm lateral face, indicating that cracking existed through the width of the diaphragm and had reached the outer face. This implies that the entire concrete diaphragm was participating in the resistance mechanism. No major cracks were observed around the bottom flange and the web.

From the outset of the ultimate load test for specimen 2, cracks in the concrete slab began to increase in width. Most of the cracks had formed during fatigue cycling, and these further increased in width during the ultimate load test. The majority of cracking occurred near the edge of the diaphragm. However, there were several large cracks at the centerline of the pier that were wider than those near the edge of the diaphragm. There were additional cracks through the depth of the slab. These cracks propagated further during the ultimate load test.

As was noticed in the previous specimens, the major cracks on specimen 3 were transverse and parallel to each other. These cracks penetrated through the depth of the slab. The 45° cracking at the lateral face of diaphragm was observed in this test as well. Cracks were also observed at the transverse face of the diaphragm initiating from the bottom flange toward the slab in approximately a 45° angle. As was noted for specimen 1, the inclined cracks on the lateral diaphragm face indicate that the failure of diaphragm concrete in these two specimens is not localized. This implies that the concrete diaphragm outside the width of the end plates (or outside the core concrete) participates in the ultimate strength of the connection.

Yielding of Longitudinal Reinforcement

Examination of strain values from specimen 1 indicate that the first yielding occurred in the top reinforcing layer near the girder centerline. This observation is a confirmation of one design goal during the initial specimen design, which was to achieve yielding of the tensile reinforcement prior to crushing of the bottom concrete (Lampe 2001).

Figure 16 shows the moment at the pier centerline when yield initiated in the top layer reinforcement for specimen 1. As can be seen, the middle bars yielded first or at a lower applied load than the outer bars. Load was then shed to adjacent bars as the loading continued. This is an illustration of the shear lag phenomenon in the concrete slab and the concept of effective width.

A similar result was observed in specimen 3. Unfortunately, strain data prior to load stage 24, which was beyond the initial yield point, were lost so the moment value at which initial yielding of the reinforcement occurred cannot be determined. However, the overall trend was observed in the available data, where strains in the middle bars were above yield and significantly higher than the strains in the gages near the edges.

Behavior of specimen 2 was different in that only two of the reinforcing bars were observed to yield prior to failure of specimen. However, similar to the pattern observed in tests 1 and 2, both of these bars were located near the centerline of the deck. The outer bars remained in the elastic region throughout the loading of specimen 2.

Observed Ductility of Connections

The observed ductility of the connections is defined as the displacement at the maximum applied load, or displacement at completion of the test if load is still increasing, divided by the deflection of the first yield in the system. Based on this definition, the observed ductility ratios of the three specimens are given in Table 5. In this table, the first yield load

(a) *(b)*

Fig. 15. Specimen 3 crack patterns at completion of ultimate test: (a) concrete slab, plan view; (b) face of diaphragm.

Table 5. Yield Load, Displacements and Ductility Ratios				
Specimen	First Yield Load (kips)	Yield Displacement (in.)	Displacement at Maximum Load (in.)	Observed Ductility Ratio
1	320	0.66	2.59	3.92
2	191	1.54	4.12	2.67
3	290	1.45	4.50	3.10

of specimen 3 was interpolated based on the first yield load of specimen 1 and the yield load obtained from the only strain gage functional in the top layer of specimen 3. Note that specimen 1 has the maximum observed ductility while specimen 2 has the minimum.

Behavior of Concrete in Compression Zone

Strains from specimen 1, recorded by embedment gages placed inside the diaphragm between the two girders, are shown in Figure 17. The elevations given are measured from the top of the bottom flange to the gage. Also shown in the figure are strain values obtained from a gage attached to the top of the bottom flange. Note that the embedment gages are not capable of measuring strains above 1800 micro-strain, which is less than the typical failure strain of the concrete (3000 micro-strain). As shown in Figure 17, the bottom plate strain gages passed the 3000 micro-strain at load level of 450 kips.

In specimen 2, crushing of the concrete was evident during the cycling test, and by the end of the ultimate test, the gap between the bottom flanges had reduced from the initial separation of 8 in. to 5 in. (see Figure 18).

Although the embedment gages directly in line with the girders were compromised, those only a short distance away measured relatively small strains during the ultimate test. This indicates that the concrete damage was highly localized around the interface of the bottom flange and the diaphragm. Essentially, the web and bottom flange of the steel girder acted like the edge of a knife that cut through the concrete diaphragm.

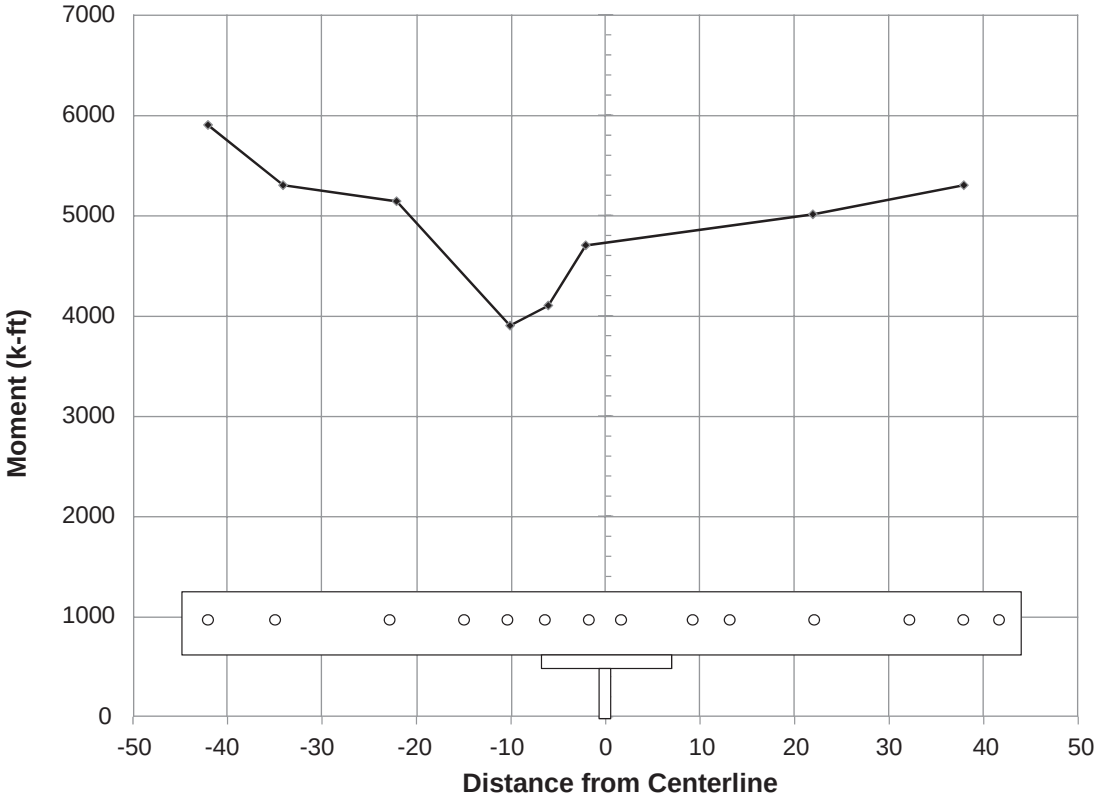

Fig. 16. Moment at which yield initiated in the top layer rebar—specimen 1.

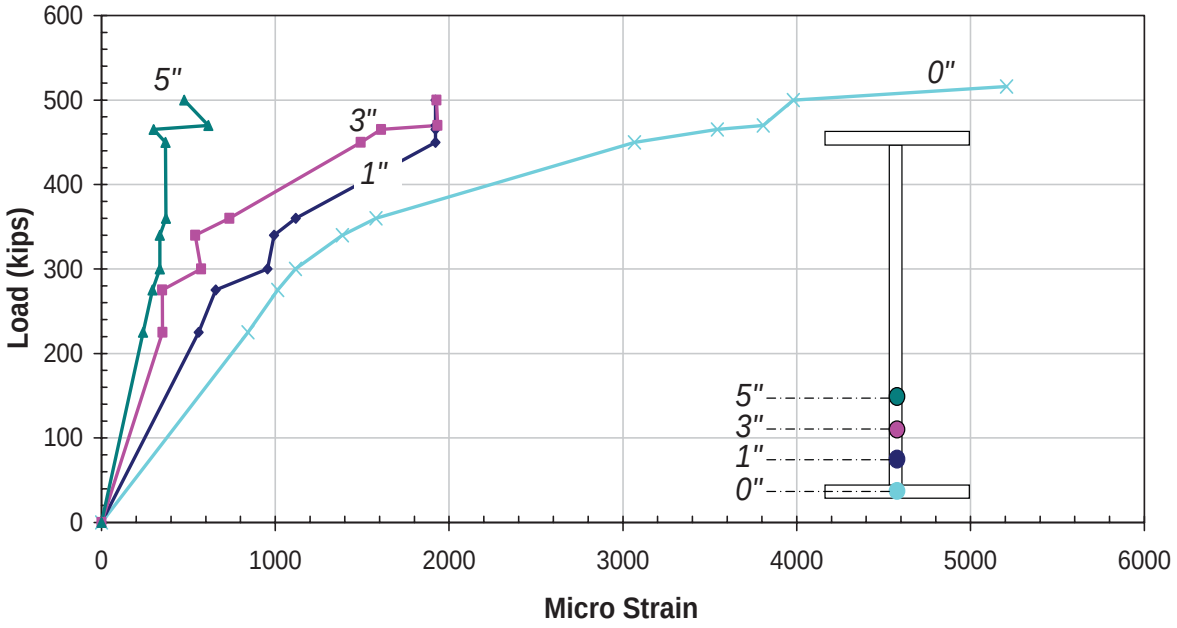

Fig. 17. Strain in concrete diaphragm between girders—specimen 1.

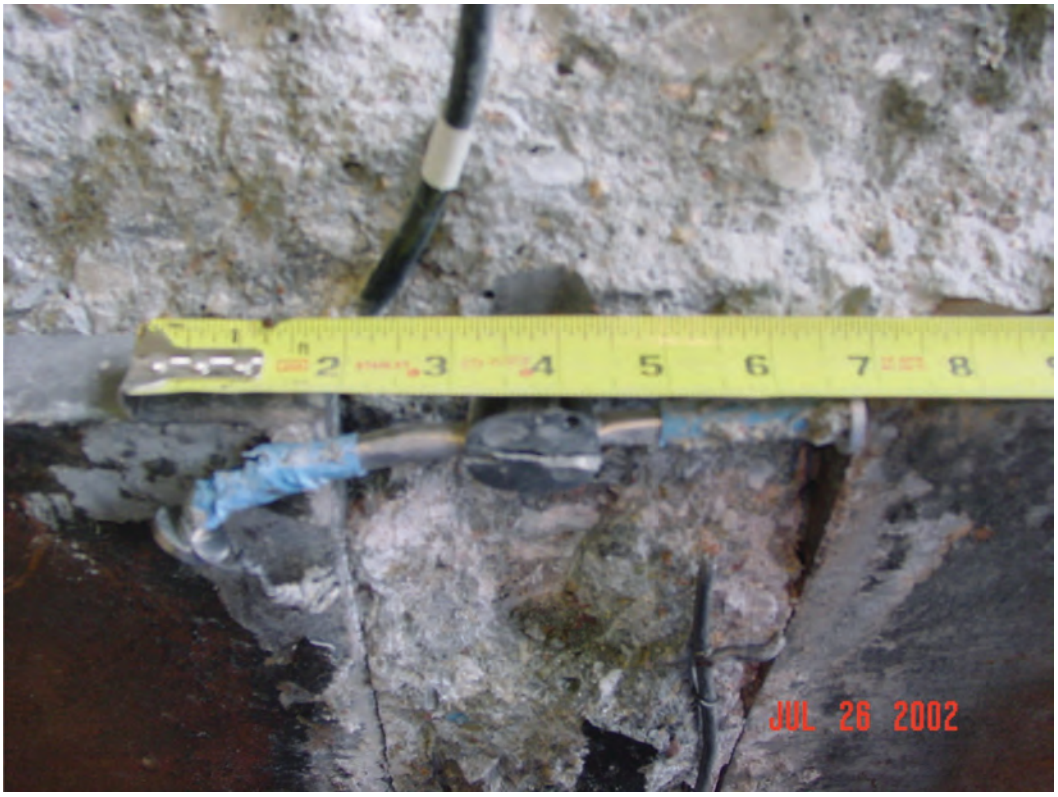

Fig. 18. Gap between bottom flanges.

In specimen 3, many of the embedment gages between the two bottom flanges were no longer functioning by the start of the ultimate test. It is unclear if this was due to damage of the gages as a result of excessive strains or damage to the wiring, either of which could have been sustained during cyclic loading. A few gages located farther from the bottom flange survived and measured the concrete strain throughout the test. The load-strain plots of two embedment gages placed at the centerline of the pier are shown in Figure 19. The strain reading of EG-10 exceeded the typical crushing strain of concrete (3000 micro-strain). Note that this was a different gage type than was used on specimen 1, which could only read up to 1800 micro-strain. Therefore, the concrete in vicinity of this gage and at the lower depths would be expected to have crushed. Instrumentation monitoring movement of the steel girder relative to the face of the diaphragm indicates that the steel pushed into diaphragm 0.35 in. on each side, which would also support the conclusion that the concrete had crushed by the end of the test.

Strain Distribution through the Depth

The strain distribution through the depth of the section has a crucial role in determining the resistance mechanism of the system. Figure 20 shows the strain profile at three different locations within and near the diaphragm. The values reported are from a time when the applied load was near the maximum observed value. Values for each section were not available for all specimens. The strain distribution inside the concrete diaphragm and at the centerline of the pier for specimen 1 is shown in Figure 20a. Due to high compressive stress in this region, most of the embedment gages placed inside the diaphragm of specimens 2 and 3 failed during the ultimate tests. As seen in Figure 20a, the strain distribution at the centerline of the pier inside the diaphragm is not linear but rather exhibits deep beam behavior where plane sections do not remain plane during loading. A plot of the vertical strain profile has been repeated in Figure 20b for a section that is still inside the diaphragm but away from the pier centerline. Here, data are available both from embedment gages indicating strains in the concrete and gages on the steel girder indicating the strains in the steel section. Again, some degree of nonlinearity is observed in the strain profile. Specifically, note the embedment gages near the bottom of the profile.

Finally, the strain distribution obtained from all three tests at a section outside of the diaphragm is depicted in Figure 20c. In this case, the strain profile is much closer to a linear pattern than the previous cases. In both Figures 20b and 20c, the large strains in the steel at the top of the section are due to yielding of the steel. The variation of strain along the

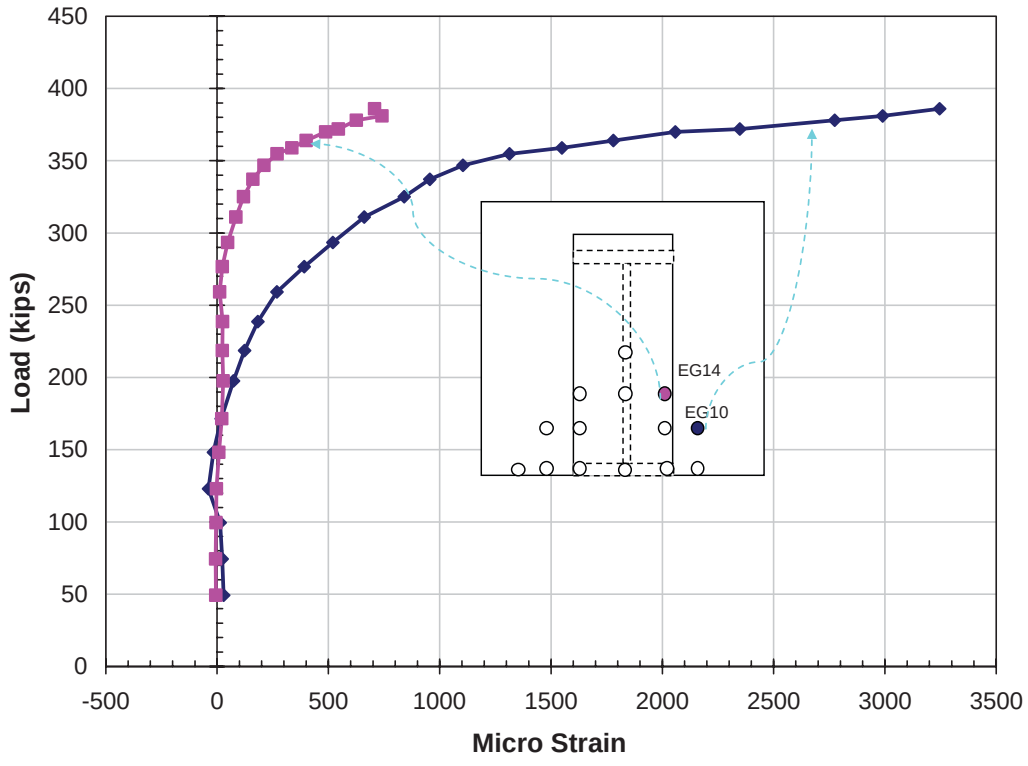

Fig. 19. Strain in concrete diaphragm between girders—specimen 3.

depth of specimen 3 is very close to specimen 1 behavior. It is noted that the applied moment at this section is approximately equal for specimen 1 and specimen 3. These plots indicate that the assumption that the plane sections remain plane can be justified for the steel girder strain profile but not within the concrete diaphragm.

Strain Distribution along the Length of the Flanges

The strain responses along the length of the flanges for the three specimens are shown in in Figure 21. The strain values shown are for when the loading was near the maximum observed value. The strain in the bottom flange, inside the core, of specimen 1 (test 1) exceeded the yield limit of the steel. Yielding was not observed in the other two specimens (test 2 and test 3) at the bottom flange. As seen in this figure, the strain reached a maximum value near the intersection of the bottom flange and the end bearing plate in test 1. The reduction of the strain within the core diaphragm could be due to the compressive resistance of the concrete sharing a portion of the compressive force with the bottom flange. This contribution from the concrete can also be seen in the strain profile from specimen 3. The decrease in bottom flange strain within the diaphragm compared to outside of the diaphragm can be attributed to composite action of the concrete diaphragm and steel girder. Bottom flange strain data from inside the diaphragm for specimen 2 were not available.

Next consider the top flange strain profile shown in Figure 21. Note that the strain values drop substantially near the end of the top flange. These low values are expected because the concrete that is immediately beyond the tip of the top flange cannot transfer the tension force. The spikes in the top flange strain at the face of the diaphragm seen in specimens 2 and 3 are likely due to concentrated rotation (kink) at the face of the diaphragm (the gage is on the top of the top flange). Further evidence of the concentrated rotation is the degree of cracking observed in the deck at this location, as discussed previously.

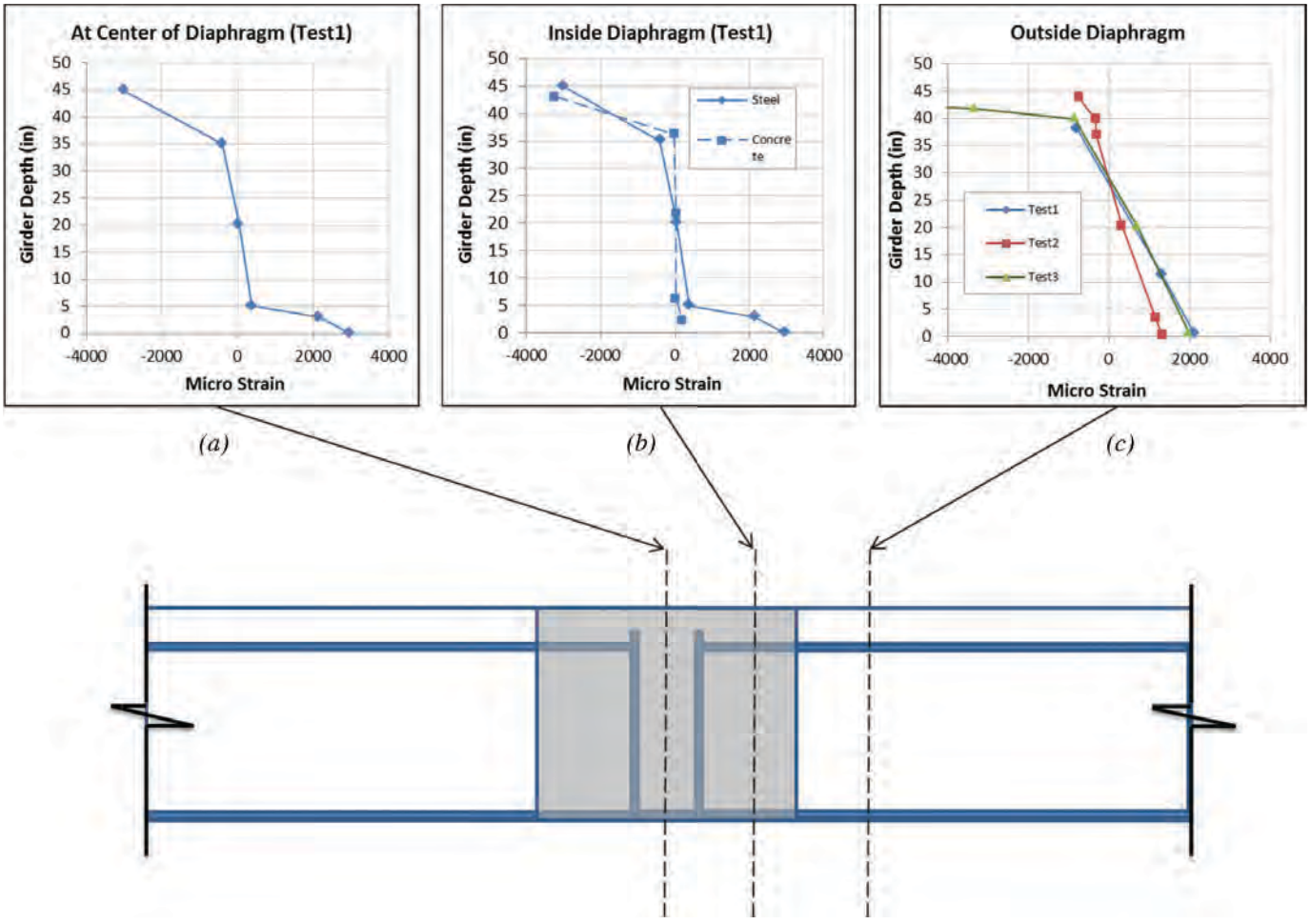

Fig. 20. Vertical strain profiles at maximum load condition.

Interface Behavior between Steel Girder and Concrete Diaphragm

The girder end detail used in specimen 1 was intended to divert compressive force away from the diaphragm concrete. Specimen 3 utilized end plates to distribute the compressive force over an increased concrete area. Specimen 2 allowed the concentrated compressive force from the steel to be applied over the steel girder area only. In addition to direct bearing, the compressive force was also transferred by bond between the portion of the girder that was embedded in the diaphragm and by transverse steel bars within the diaphragm that passed through holes in the girder web.

In specimen 2, penetration of the bottom flange into the diaphragm, along with the formation of large cracks (see Figure 22) indicates that bonding between the steel girder and concrete diaphragm failed during testing of specimen 2. After conclusion of the ultimate test, the dissection of specimen 2 revealed that the transverse bars placed through holes in the web had been sheared through, as shown in Figure 23. Recall this specimen was deliberately intended to illustrate the failure mechanisms of simplistic detail and the shearing of reinforcement was not observed in specimens 1 and 3.

The connectivity of the top flange and the concrete slab was ensured by designing and providing an adequate number of shear studs on the top flange. The visual observation of the studs after conclusion of the ultimate tests and dissections of the specimens did not show failure of the studs.

Summary of Observed Behavior

The test results presented in the preceding sections are summarized to give a general picture of the behavior of the test specimens. For each specimen, the load corresponding to the theoretical plastic moment is given. This calculation is

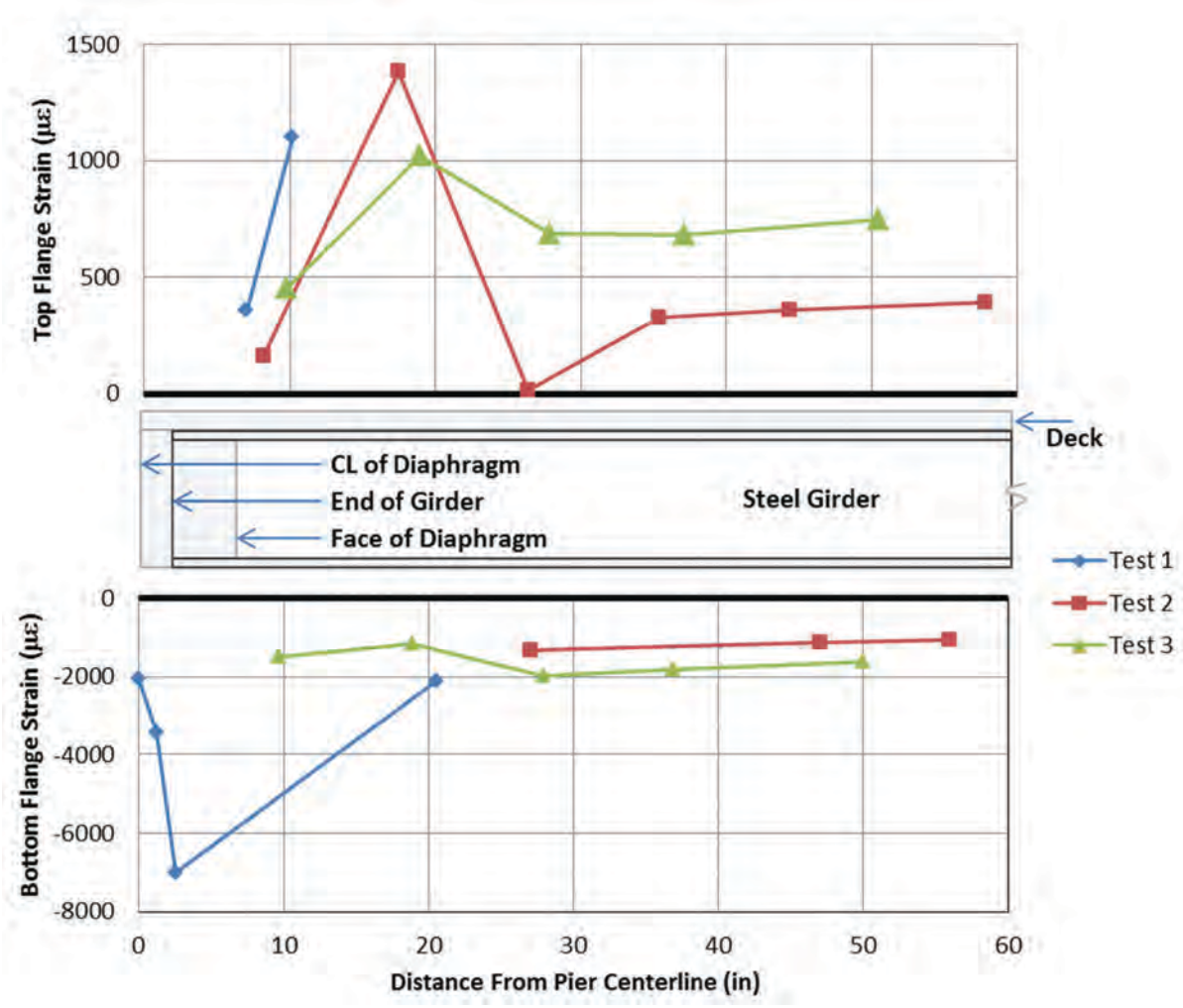

Fig. 21. Strain profile along the longitudinal axis of both flanges.

based on the actual material properties and assumes complete participation of the full steel section and reinforcement. The assumption provides a value for reference and is not necessarily a basis for strength calculation, which is discussed in more detail elsewhere (Farimani et al., 2013). The arm distance for calculating the applied moment is taken to the center of the diaphragm and was 12 ft for test 1 and 15 ft for tests 2 and 3.

Specimen (Test) 1

Behavior of specimen 1 during ultimate load test is shown in Figure 24. The load corresponding to the theoretical plastic moment calculated at the face of the diaphragm is 510 kips. This figure identifies several important stages during ultimate load test. Each of the events identified in Figure 24 is described here:

1. The cracks remaining from the cycling test widened and propagated in the concrete slab from the early stage of loading (5% of the maximum observed load). These cracks started at the diaphragm edge and the centerline of the pier.
2. The yielding started at the top layer of reinforcements at 62% of the maximum observed load. The location of the first yield was around the girder axis and centerline of the pier.
3. After a further small increase in load to 65% of the maximum observed load, the bottom plate strain passed the yielding limit.
4. The concrete between the two end bearing plates at the bottom of the diaphragm experienced strain more than 0.003 in./in. at 87% of the maximum observed load.
5. The entire top layer rebar passed the yielding limit at 95% of the maximum observed load.
6. All of the slab rebar around the pier centerline yielded at 98% of the maximum observed load.

Specimen (Test) 2

The load-deflection response of specimen 2 is shown in Figure 25. The deflection values in the plot are average values obtained from the readings of the east and west girders. The load corresponding to the theoretical plastic moment calculated at the face of the diaphragm is 414 kips. The maximum applied load was well below this value. Due to damaged instrumentation, there were not adequate data to quantify the structural behavior of the system as were obtained for specimen 1. However, based on the visual observations along with the recorded data, the behavior of the system is predicted as follows:

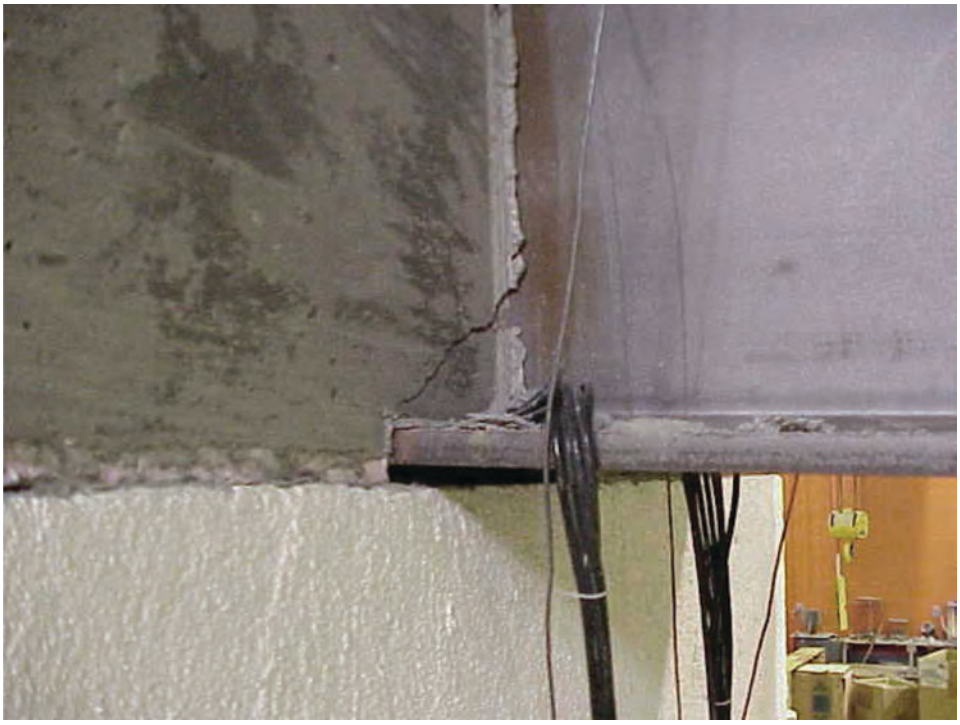

Fig. 22. Cracking of the concrete diaphragm around the bottom flange—specimen 2.

1. The cracks formed during the cycling loads grew from beginning of loading, especially on the surface of deck.
2. Local crushing of concrete occurred at the interface of the bottom flange and the concrete after cracking, but there are not enough data to locate more exact load level.
3. The large deformation and failure of the transverse reinforcement within concrete diaphragm occurred at 43% of the maximum observed load.
4. At 78% of the maximum observed load, the first bar at the middle of the top layer at the pier centerline yielded.
5. The slab concrete around the top flange and edge of diaphragm failed at about 97% of the maximum observed load.

It is noted that the bond between the steel girder and the concrete diaphragm failed during the cycling test and so has not been shown here. The failure of the specimen occurred following the failure of the concrete deck. Movement of the beam bottom flanges (compression flange) into the concrete diaphragm resulted in large rotation of the steel girder and pull out of beam top flange (tension flange) from the concrete diaphragm, as shown in Figure 26.

Specimen (Test) 3

The load-deflection response of specimen 3 is shown in Figure 27. This figure is the average of the east and west girders. The load corresponding to the theoretical plastic moment calculated at the face of the diaphragm is 412 kips. The exact location of the structural events for this test, similar to that described for test specimen 1, was not possible due to loss of instrumentation. However, test observations and results indicate that the resistance of the specimen is predicted as follows:

1. Concrete cracks formed during the cycling test propagated from the beginning of the ultimate test.
2. The first yield would be estimated at about 60% of the maximum observed load.
3. The top rebar layer yielded at 80% of the maximum observed load and caused the slope of the load-deflection plot to change around this point.
4. The failure of the specimen occurred as inclined cracks formed throughout the concrete diaphragm.

Fig. 23. Shear failure of the transverse bar inside the diaphragm after the conclusion of the ultimate test—specimen 2.

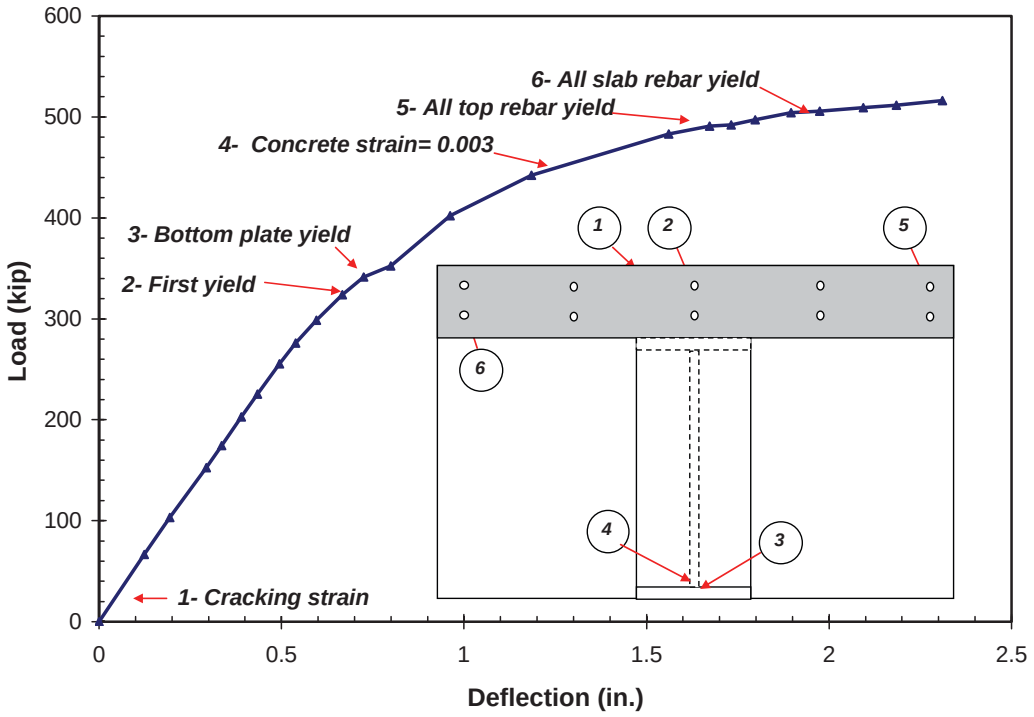

Fig. 24. Specimen 1 observations.

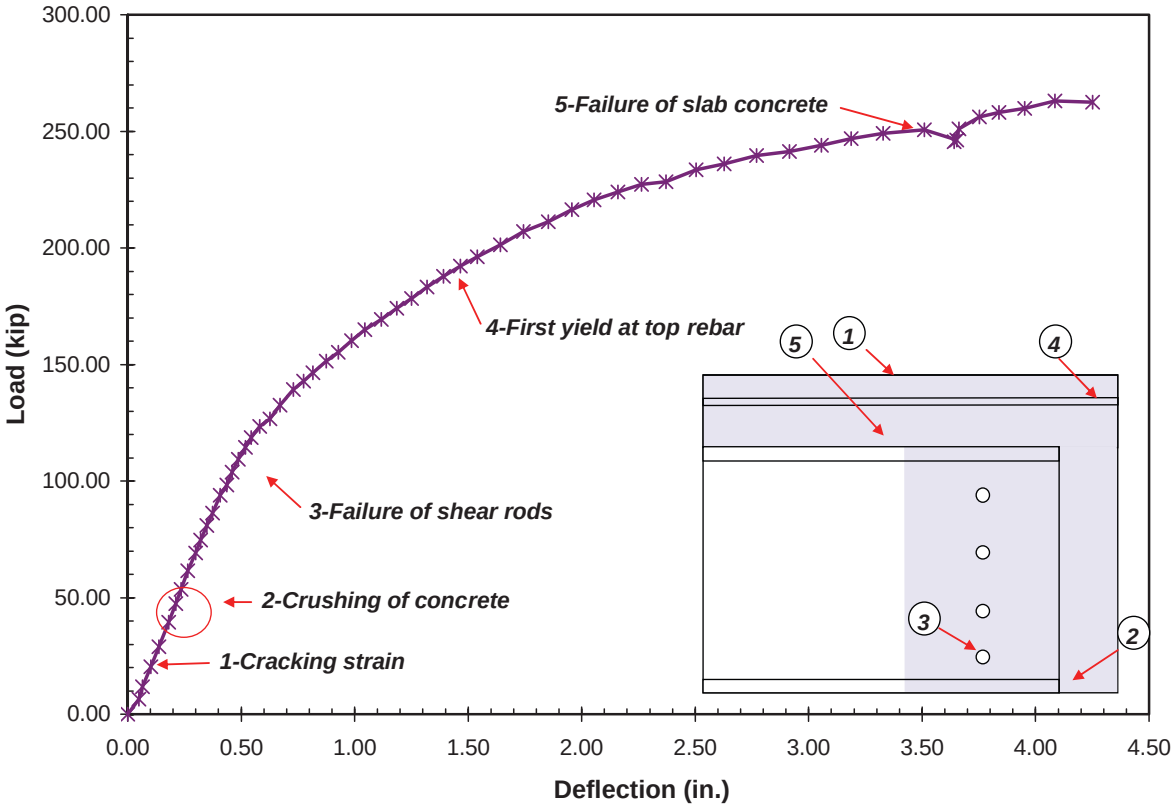

Fig. 25. Specimen 2 observations.

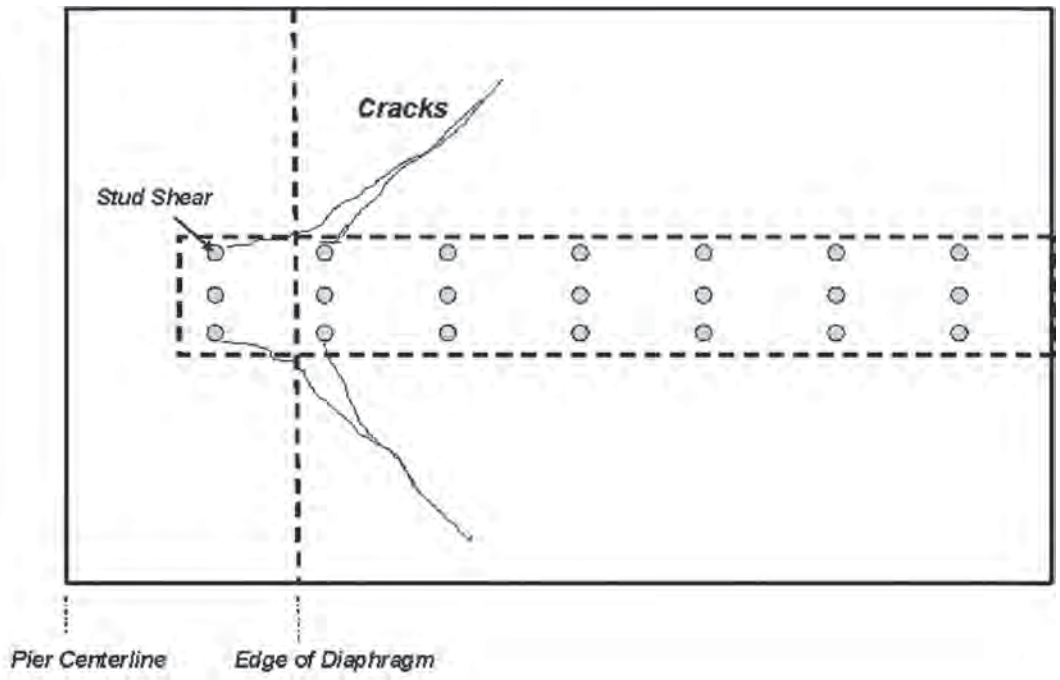

Fig. 26. Concrete failure of the specimen 2 deck.

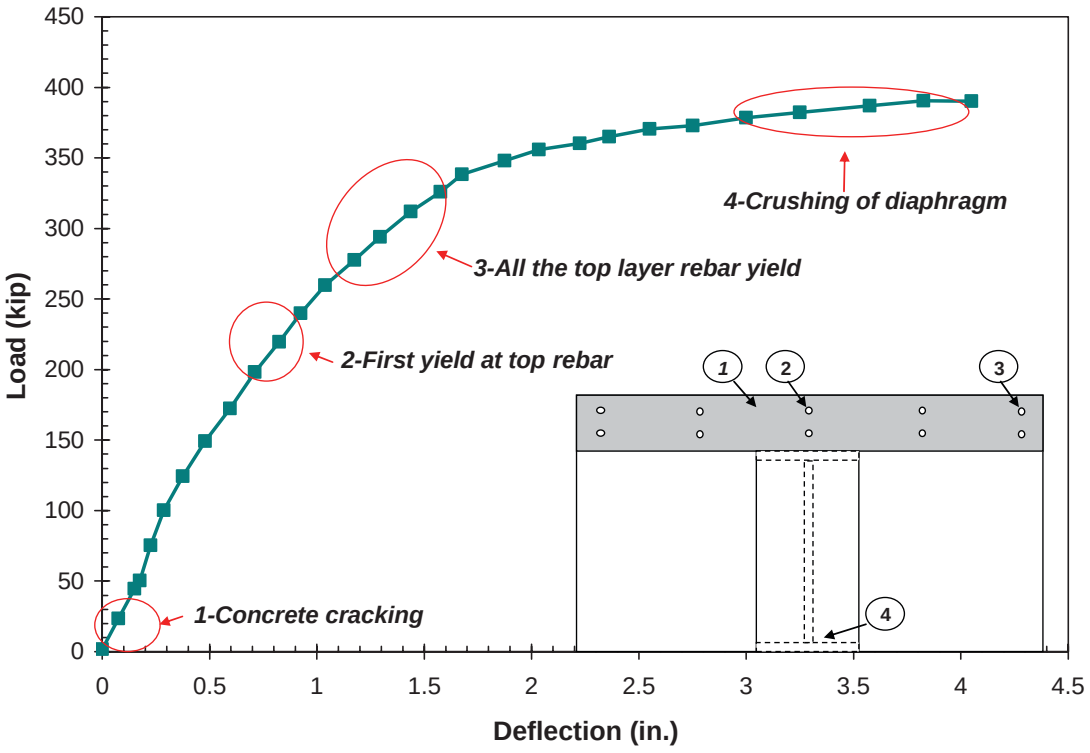

Fig. 27. Specimen 3 observations.

CONCLUSIONS

The compressive force component, carried by the bottom flange, should not be transferred directly to the concrete at the interior support. It is preferred that a continuous steel path be provided for the compressive force, such as that provided by the detail used in specimen 1. Note, however, that the detail in specimen 1 was intended to be proof-of-concept detail but is not necessarily practical for field implementation.

Test 2 showed that the compressive force is sufficiently concentrated and crushing of the concrete can occur, thus necessitating the force transfer through a steel path. The ultimate performance of specimen 3, which utilized an end plate to distribute the load, was comparable to that of specimen 1, with a continuous steel path. However, there were some differences in the observed data during the cyclic testing. For this reason, the end plate detail is not recommended at this time, though it may actually provide satisfactory performance. Instead, a mechanism should be provided to prevent transfer of compression force from the bottom flanges to the concrete diaphragm. One practical detail that provides a continuous steel path, but is simpler to construct than the detail used in specimen 1, is shown in Figure 28.

The specimens were designed following the concepts from reinforced concrete that prevent over-reinforcement of the system. This requires that sufficient compressive resistance should be developed to force initial yield to occur in continuity reinforcement within the slab. This was achieved in both the specimens 1 and 3. Specimen 2 did not possess sufficient compressive resistance to cause yield in the continuity reinforcement.

The maximum applied load for specimen 1 exceeded the load corresponding to the theoretical plastic moment capacity obtained, assuming full participation of the steel section. The maximum applied load for specimen 2 was well below the plastic capacity, and the maximum applied load for specimen 3 was just below the plastic capacity.

One of the primary conclusions is that experimental testing confirmed that reinforcement in the deck is sufficient to develop continuity. That is, the top flange does not need to be made continuous over the interior support. The extent of the cracking observed during the cyclic testing was minimal and comparable to what is expected in conventionally detailed construction, even at the amplified load levels that were used, such that no durability issues are expected.

The results of the three tests that were conducted provide good insight into the resistance mechanism at work in the system, but due to limited experimentation, a general mechanism cannot be derived from experimentation alone. Furthermore, the results from the three specimens do not provide enough data points to adequately quantify the ultimate capacity of the structure. To obtain more information regarding the behavior of system, a series of finite element analyses were completed to compliment the experimental studies. The numerical studies are presented in Farimani et al. (2014).

ACKNOWLEDGMENTS

The initiative was directed by Atorod Azizinamini, Professor and Chair at Florida International University, and was made possible by contributions from many current and former graduate students and research associates, as well as input from many in the bridge community. In particular, the contributions of the following individuals are acknowledged.

Graduate students earning degrees from the project were Nick Lampe, Nazanin Mahasebi, Reza Farimani, Saeed Javidi, Derek Kowalski and Mark Otte. The research study

Fig. 28. Bearing block detail.

was conducted at the University of Nebraska–Lincoln. Aaron Yakel was the research associate assisting the project. Laboratory technicians Jeff Boettcher, John Dageford, and Peter Hilsabeck assisted in conducting the experimental portion of the study. Graduate students who assisted with experimental testing include John Swendroski, J. Brian Hash, Patrick Mans, Luke Glaser and Nima Ala. The study was supported by the Federal Highway Administration and the Nebraska Department of Roads. Several visionary engineers at NDOR were critical to the successful completion of the project: Lyman Freeman, Moe Jamshdi and Hussam "Sam" Fallaha. Steel fabrication and assistance during specimen preparation were provided by Capitol Contractors of Lincoln, NE.

The opinions and conclusions presented in this paper are those of the authors and do not necessarily represent the viewpoints of the project sponsors.

REFERENCES

AASHTO (1998), *LRFD Bridge Design Specifications*, 2nd Ed., American Association of State Highway and Transportation Officials, Washington, DC.

Azizinamini, A. (2014), "Simple for Dead Load–Continuous for Live Load Steel Bridge Systems," AISC, *Engineering Journal*, Second Quarter.

Azizinamini, A., Lampe, N.J. and Yakel, A.J. (2003), *Toward Development of a Steel Bridge System—Simple for Dead Load and Continuous for Live Load*, A Final Report Submitted to the Nebraska Department of Roads, National Bridge Research Organization: www.nlc.state.ne.us/epubs/r6000/b016.0088-2003.pdf.

Azizinamini, A., Yakel, A.J., Lampe N.J., Mossahebi, N. and Otte, M. (2005), *Development of a Steel Bridge System—Simple for Dead Load and Continuous for Live Load, Volume 2: Experimental Results*, Final Report NDOR P542, Nebraska Department of Roads, Lincoln, NE.

Farimani, M.R., Javidi, S.N., Kowalski, D.T. and Azizinamini, A. (2014), "Numerical Analysis and Design Provision Development of the Simple for Dead Load–Continuous for Live Load Steel Bridge System," AISC, *Engineering Journal*, Second Quarter.

Milenkovic, A. and Pluis, M. (2000), "Fatigue of Normal Weight Concrete and Lightweight Concrete," European Union—Brite EuRam III, Document BE96-3942/R34.

Mossahebi, N. (2004), *New Steel Bridge System: Simple for Dead Load, Continuous for Live Loads*, M.S. Thesis, University of Nebraska–Lincoln, Lincoln, NE.

Lampe, N.J. (2001), *Steel Girder Bridges Enhancing the Economy*, M.S. Thesis, University of Nebraska–Lincoln, Lincoln, NE.

Szerszen, M.M. and Nowak, A. (2000), "Fatigue Evaluation of Steel and Concrete Bridges," *Transportation Research Record,* Vol. 1696.

Numerical Analysis and Design Provision Development for the Simple for Dead Load–Continuous for Live Load Steel Bridge System

REZA FARIMANI, SAEED JAVIDI, DEREK KOWALSKI and ATOROD AZIZINAMINI

ABSTRACT

The proposed connections of steel bridge girders at the pier for the simple for dead load and continuous for live load concept (SDCL) were investigated. Analytical models were developed for four connection types that previously were tested in the structural lab. For the numerical modeling of the tested specimens, nonlinear finite element was utilized. The behavior of the numerical models of each tested specimen was verified by the experimental results. The force resistance mechanism of each specimen was studied using the experimental and numerical data. In developing a resistance mechanism for the connections, the yielding of the rebar in the slab, the steel girder bottom plate and the crushing of the concrete diaphragm at pier were considered. A set of detailed equations was developed to conceptualize the connection behavior at the ultimate capacity under negative flexure. The developed equations show a good agreement with the finite element analysis results. For practical purposes, simplified equations were derived from the more detailed equations to calculate the negative ultimate flexure capacity, at the section through the pier, for two connection types. To verify the proposed design equations for a wider range of bridges, a parametric study was performed. The nonlinear finite element models of the bridges from the parametric study were used for verification of the proposed equations.

Keywords: steel bridges, steel girders, SDCL, simple for dead load–continuous for live load.

INTRODUCTION

This paper is part of series of publications describing the development and implementation of the simple for dead–continuous for live (SDCL) bridge system for steel girders. The SDCL bridge system utilizes a joint detail at the interior supports that does not become continuous until after the dead loads have been applied. Prior to attaining this final continuity, the girders within the individual spans are simply supported. General information regarding the behavior and design of the SDCL system can be found in the companion paper by Azizinamini (2014).

Four details for the connection of the girders over the pier were proposed based on preliminary studies. Full-scale specimens of these connections were tested in the lab for fatigue and ultimate loading, similar to what an actual bridge could experience. Additional details of the testing can be found in the companion paper by Lampe et al. (2014), and complete results are contained in the project reports by Azizinamini, Lampe and Yakel (2003) and Azizinamini et al. (2005) and graduate theses by Lampe (2001), Mossahebi (2004) and Javidi (2009).

In this paper, the results of nonlinear finite element modeling of the connection details are presented. Based on the experimental data and numerical analysis, the load resistance mechanism of each connection under ultimate design loads is discussed. Design equations are then derived based on the resistance mechanism. Finally, parametric study was carried out to comprehend the sensitivity of the proposed simplified design equations.

CONNECTION DETAILS

Figure 1 shows each of the three connection details investigated. The following sections provide description of each detail.

Type 1 Connection: Bottom Flange Continuous

This class of connection represents details where bottom flanges are made continuous. The continuity in the test specimen was achieved by welding the extension of bottom flanges, as shown in Figure 1a. This detail is to represent the continuity of the compression flange. A more practical detail is where steel blocks welded to bottom flanges similar to the

Reza Farimani, Ph.D, P.E., LEED AP, Associate, Thornton Tomasetti, New York, NY. E-mail: rfarimani@thorntontomasetti.com

Saeed Javidi, Ph.D., P.Eng., Structural Engineer, Associated Engineering Ltd., Burnaby, BC, Canada. E-mail: sjavidin@gmail.com

Derek Kowalski, P.E., Design Engineer, Nucor-Vulcraft Group, Norfolk, NE. E-mail: derek.kowalski@nucor.com

Atorod Azizinamini, Ph.D., P.E., Professor and Chair, Civil and Environmental Engineering Department, Florida International University, Miami, FL (corresponding). E-mail: aazizina@fiu.edu

type 4 connection described later. The top flanges were not connected, but a rebar cage was placed in the diaphragm to connect the two girders. The continuity of the bridge girders—specifically, the ability to resist tensile forces due to live load negative moment—was provided.

Type 2 Connection: Bare End

The conceptual detail of this type is seen in Figure 1b. The second detail was similar to the first test, except that the bottom flanges were not welded, and no end plate was added to the girders. Basically, two W-shape girders were simply placed on the pier and embedded in the concrete diaphragm. Again, the tension portion of the continuity for live load was provided by continuous longitudinal rebar in the slab.

Type 3 Connection: End Plate

The third detail was similar to the first detail, except that the bottom flanges were not extended and welded, as shown in Figure 1c. End plates were installed similar to the first detail. The continuity for live load was again provided by continuous longitudinal reinforcement in the slab.

Type 4 Connection: Modular

A final detail has been developed that can be used in conjunction with bridges constructed using conventional or accelerated construction philosophy. Figure 2 shows the connection detail over the pier. In this detail, a thick plate, which is referred to as a "block" in this paper, was welded to each girder bottom flange, as seen in Figure 3. The girders were placed on the pier such that the blocks came in contact with each other but were not welded together. The continuity for live load negative moment was provided by longitudinal slab rebar with 90° hooks in the concrete diaphragm. The development of this connection and additional details are discussed in the fifth paper of this series (Javidi, Yakel and Azizinamini, 2014).

NUMERICAL STUDY

The connections described in the previous sections were modeled by nonlinear finite element programs to study their behavior in more detail and develop information that could complement the experimental results. Two commercial finite element software packages (ANSYS 5.7 and ABAQUS 6.9) were used independently for the modeling of the test specimens. The following sections address the details of finite element analysis (FEA) using ABAQUS. Details of the numerical work conducted using ANSYS are provided elsewhere (Farimani, 2006).

Modeling

The finite element models consisted of the steel girder, concrete slab, concrete diaphragm, bearing pads and rebar and steel details such as stiffeners and shear studs. The sizes and dimensions of the elements were obtained from the specimen as-built drawings.

Material Properties for Steel

The steel material properties were acquired from coupon tests obtained from the girders, as well as rebar. The material test details and their results can be found in the research report by Azizinamini et al. (2005). In this study, a multilinear isotropic hardening material based on true stress-strain curve of the materials was considered in the modeling (Javidi, 2009).

(a) *(b)* *(c)*

Fig. 1. Details of specimens inside the diaphragm: (a) type 1; (b) type 2; (c) type 3.

Concrete Material Modeling

The reinforced concrete was modeled using the concrete damaged plasticity model in ABAQUS. In this technique, the rebar was modeled by truss elements with compatible displacement with the concrete element around the rebar. The inelastic behavior of concrete in the concrete-damaged plasticity model is based on a concept of combined isotropic-damaged elasticity and isotropic tensile (compressive) plasticity. Concrete in compression, based on the amount of strain, can have a linear-elastic, nonlinear-elastic and nonlinear-plastic behavior.

In tension, concrete behaves as linear-elastic to the maximum tensile strength and has nonlinear post-cracking behavior. In this study, tension stiffening is applied to the model by the post-failure stress-strain relationship. Exponential behavior was chosen to describe the tension-stiffening curve after maximum tension strength of the concrete (ABAQUS, 2009).

In compression, the Carreira-Chu model (ABAQUS, 2009) was adopted in the FEA modeling of this study. In this model, the uniaxial-compression stress-strain curve is assumed to be linear up to $0.3f'_c$, where f'_c is the 28-day compressive strength of the standard cylinder, followed by a nonlinear behavior up to failure.

In multi-axial stress states, the uniaxial behavior of concrete can be generalized through the failure surface and ultimate strength in stress space. For the failure criteria of concrete, the Drucker-Prager model (ABAQUS, 2009) was adopted.

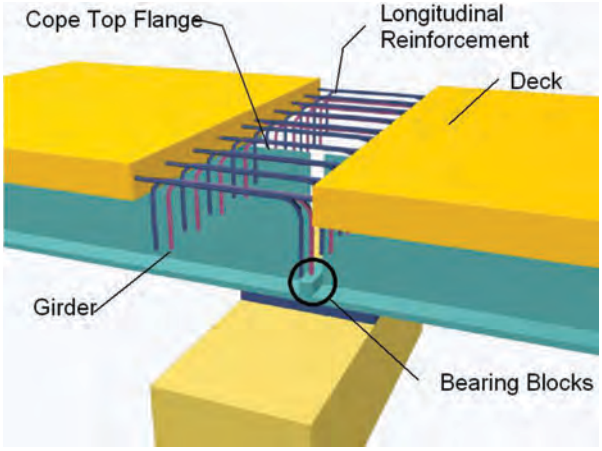

Fig. 2. Pier connection detail for modular system (type 4).

Element Type

In the finite element models, the girders, stiffener plates and end plates were modeled by a four-node, doubly curved, general-purpose, structural shell element. The shear studs, dowels and bolts were modeled using beam elements.

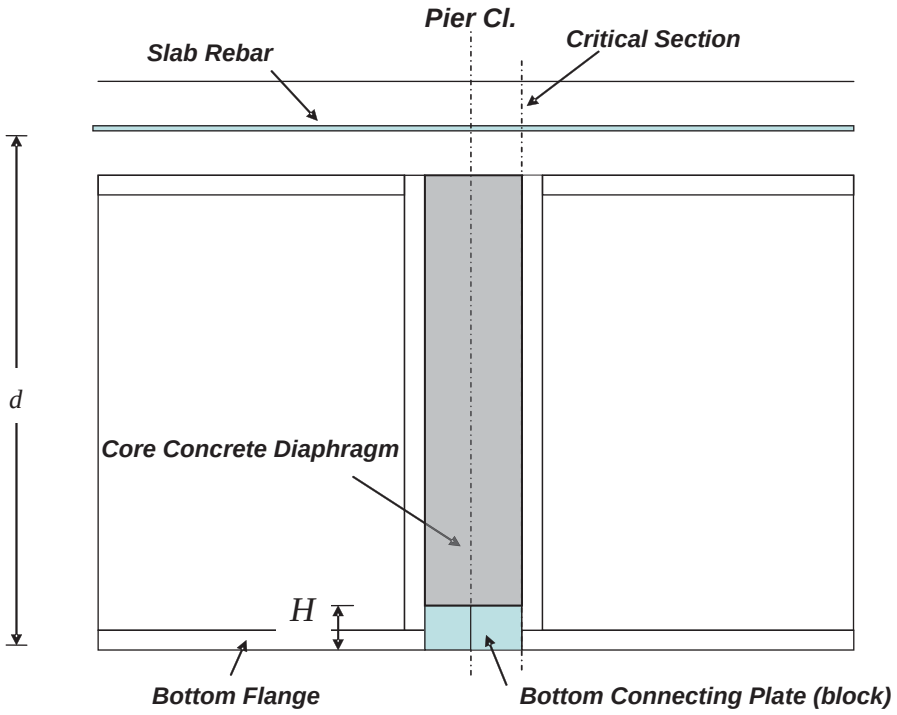

Fig. 3. Details of specimens inside the diaphragm.

All reinforcing bars were modeled using truss elements with only an axial degree of freedom.

Boundary Conditions and Connectivity

All reinforcing bars are embedded in concrete. The girders are connected to the deck by embedding the shear studs in the concrete deck. The elastomeric pad is constrained in all three translation directions. Two shear locks are restrained in only the transverse directions. Therefore, the bearing pad is the only element that can carry load in the vertical direction as a support.

Solution Strategy

Several sensitivity analyses were carried out to test the sensitivity of the different parameters of the model. To verify mesh size, different element sizes were employed, and the proper mesh size was selected for final analysis.

Different approaches were employed to observe the effect of the loading type. It was noticed that using a spreader beam, similar to the one used in the tests, was a better approach to model the loading. Load was applied to the specimen in a displacement-control fashion. Static analysis was chosen due to the low rate of monotonic loading applied in the tests.

Results

The following sections examine the results obtained from the finite element analyses and compare the results with those obtained from experimental testing.

Load-Displacement

Load-displacement results obtained from experimental testing and the corresponding numerical analysis of all described specimens are shown in Figures 4, 5 and 6. The notable events that a specimen experienced during loading are shown on the plots. These events consist of first cracking in the concrete, yielding of the steel and crushing of the concrete. These events were obtained from FEA results and were verified by the available experimental data.

Figure 4 shows the load displacement for the type 1 connection with a continuous bottom flange. In this specimen, the first yielding occurred in the top longitudinal reinforcement of the slab; subsequently, the bottom plate that connected the two girders yielded. In the next stage, the concrete between the two girder end bearing plates crushed. It should be noted that the crushing of the concrete was localized and in the vicinity of the compression flange. The yielding of all rebar occurred after the crushing of the concrete. The

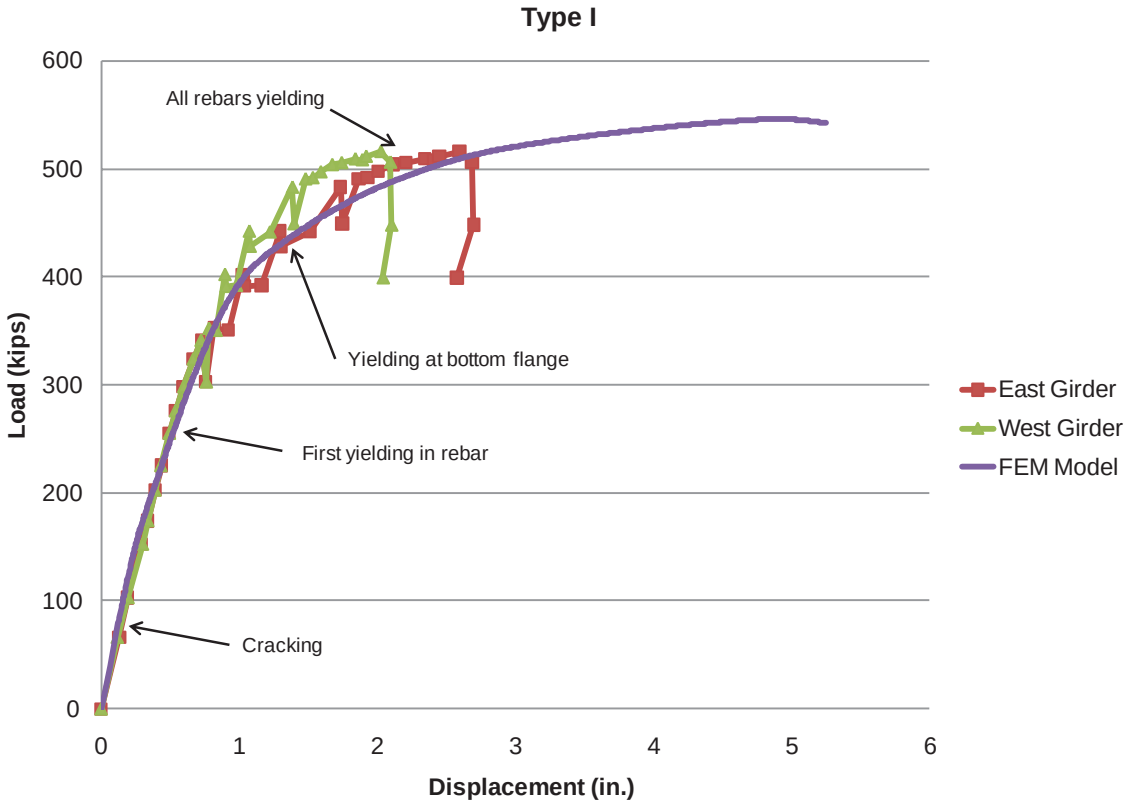

Fig. 4. Load displacement behavior— type 1 (continuous bottom flange).

mode of failure predicted using the numerical model was a flexural mode of failure, consistent with the test response, due to increasing plastic strains developed in the tension reinforcement.

The finite element analysis of the second specimen was not numerically stable because crushing of the concrete occurred in the early stages of loading. In the second specimen, crushing of the concrete occurred before yielding of the rebar. The bare-ended type 2 connection results are not addressed in this paper because of its poor performance during the fatigue and ultimate experimental tests.

Figure 5 shows the load-displacement curve of the finite element model (FEM) results versus experimental results for the type 3 connection with end plate. In the third specimen, the yielding was initiated in the top slab rebar, and crushing occurred after the partial yielding of the slab bars. The failure of the specimen occurred upon yielding of all slab reinforcements.

Figure 6 shows the load-displacement curve of the experimental test and FEM result for the modular type 4 connection. In this specimen, the top longitudinal bars yielded at the edges of the concrete diaphragm over the pier. At this location, the longitudinal rebar typically did not overlap. During the final stage of loading, all of the slab rebar yielded.

Based on the test results and the finite element studies, it was observed that there were three main modes of failure for the specimens:

1. All of the slab longitudinal rebar yielded under negative flexure. Failure of the specimen was due to the excessive plastic strain in the reinforcing bars.
2. The concrete crushed at the bottom part of the diaphragm under compression, preventing the yielding of all of the longitudinal reinforcement over the pier.
3. Some of the rebar yielded in the slab, but crushing of the concrete resulted in failure of the specimen.

Strain Distribution in Slab Longitudinal Rebar

It was observed in the tests and FEM results that the strain distribution in the top rebar across the width of the slab is not uniform. Figures 7, 8 and 9 show the strain distribution in various stages of loadings for each specimen.

The main reason for nonlinearity of strain—and, consequently stress in the slab—is the shear lag in the concrete slab.

In a vertical section along the depth of the girder, a linear distribution assumption—that is, plane sections remain

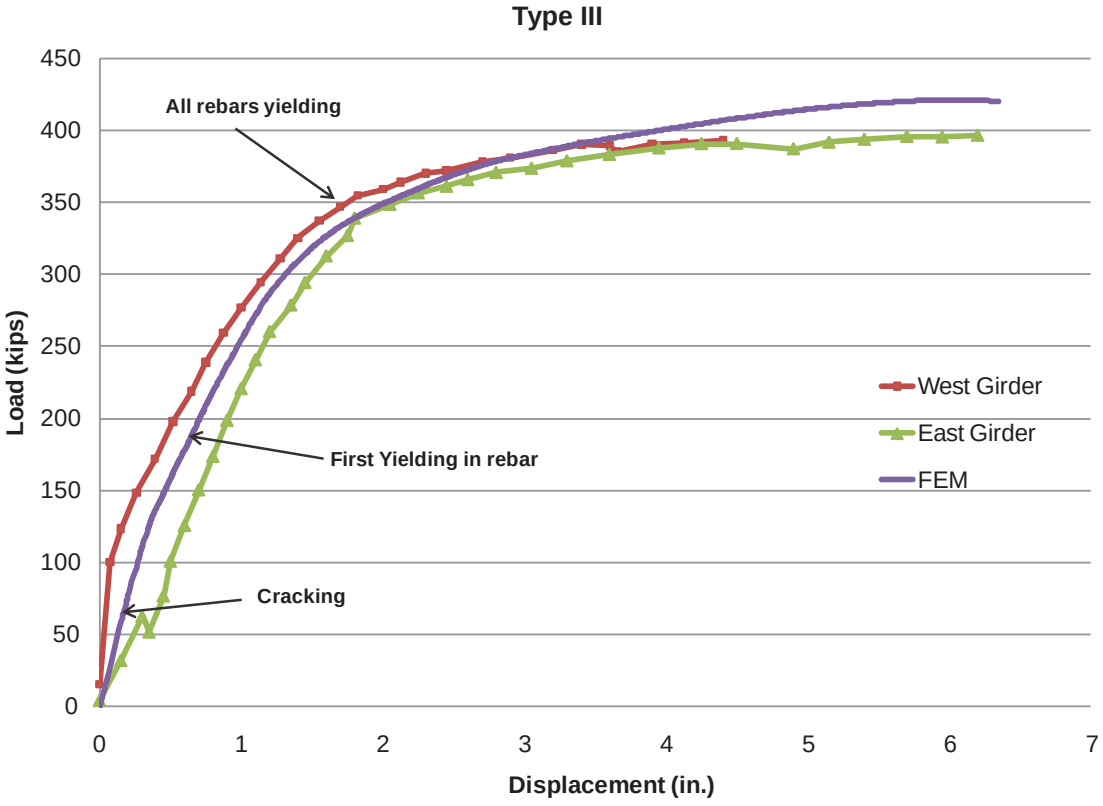

Fig. 5. Load vs. displacement—type 3 (end plate).

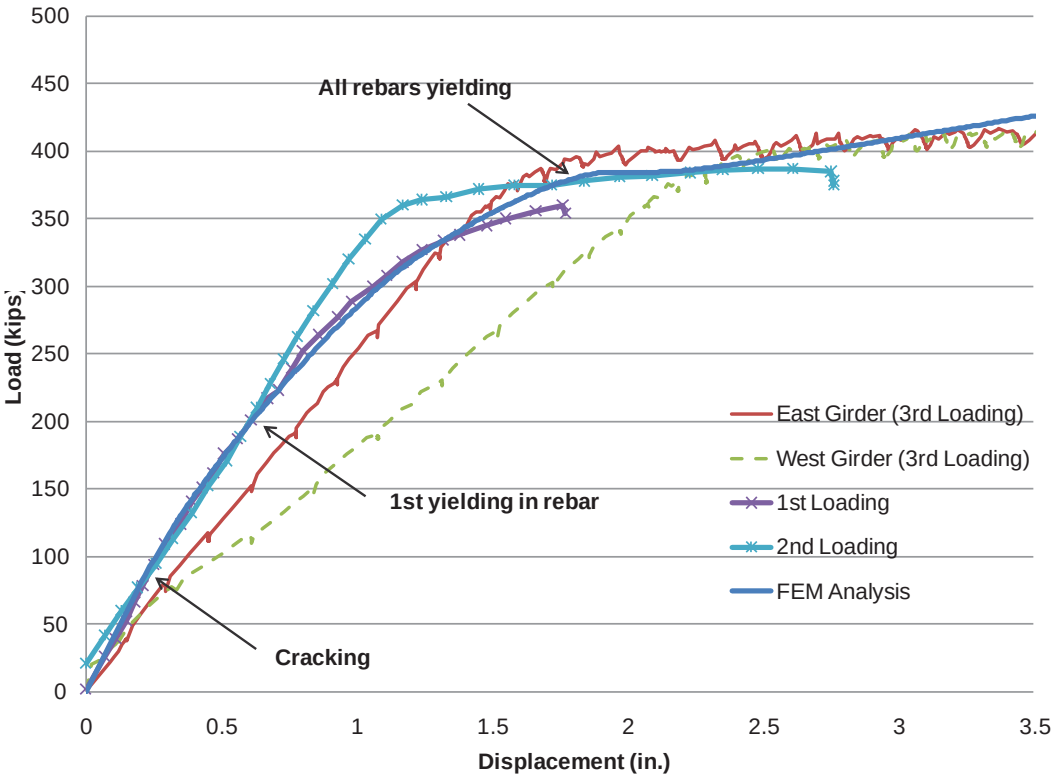

Fig. 6. Load vs. displacement—type 4 (modular).

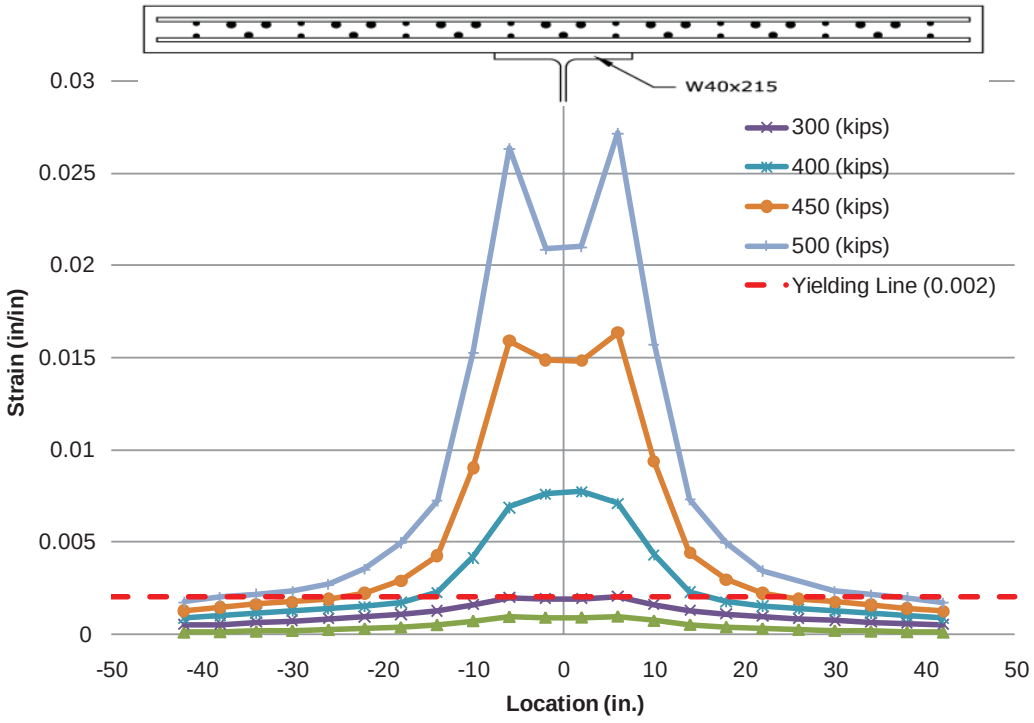

Fig. 7. Rebar strain distribution—type 1 (continuous bottom flange).

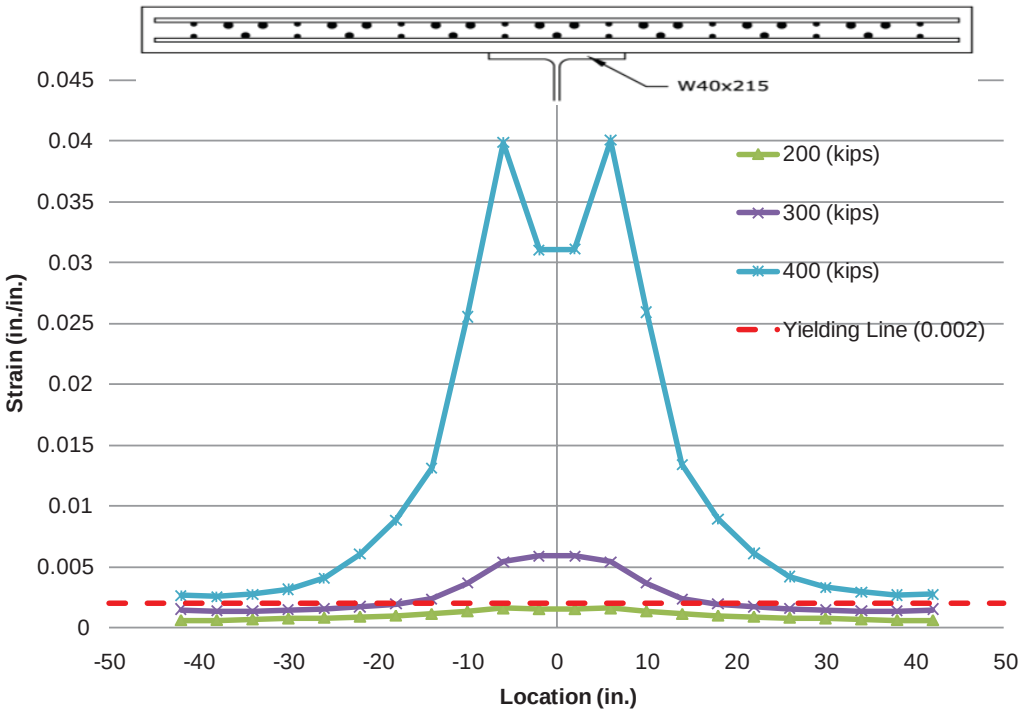

Fig. 8. Rebar strain distribution—type 3 (end plate).

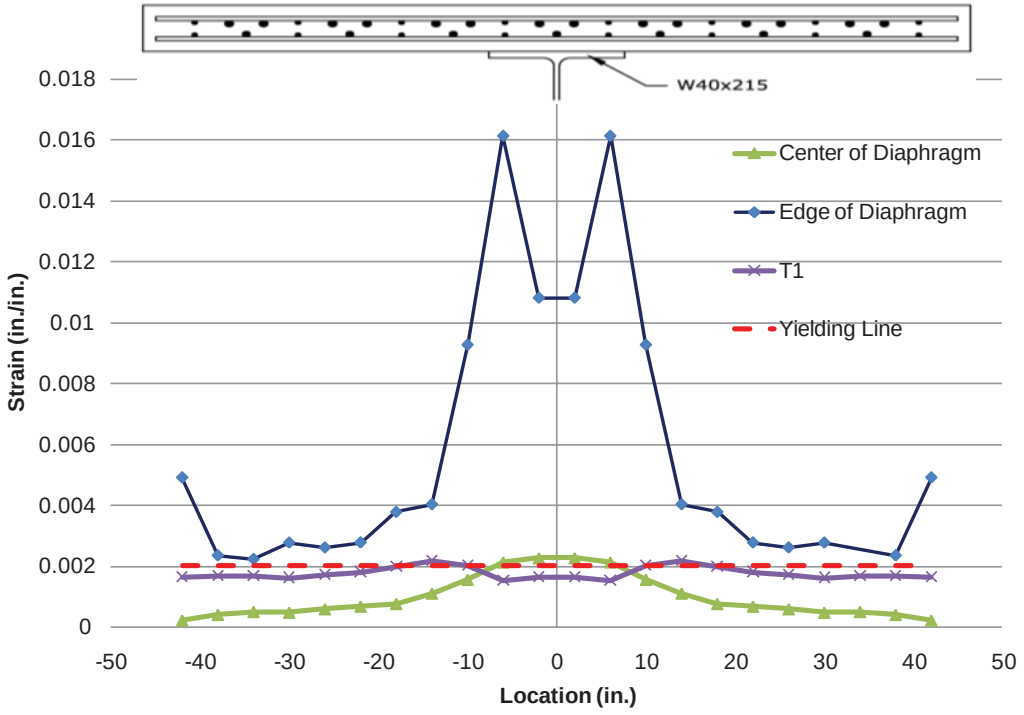

Fig. 9. Rebar strain distribution—type 4 (modular).

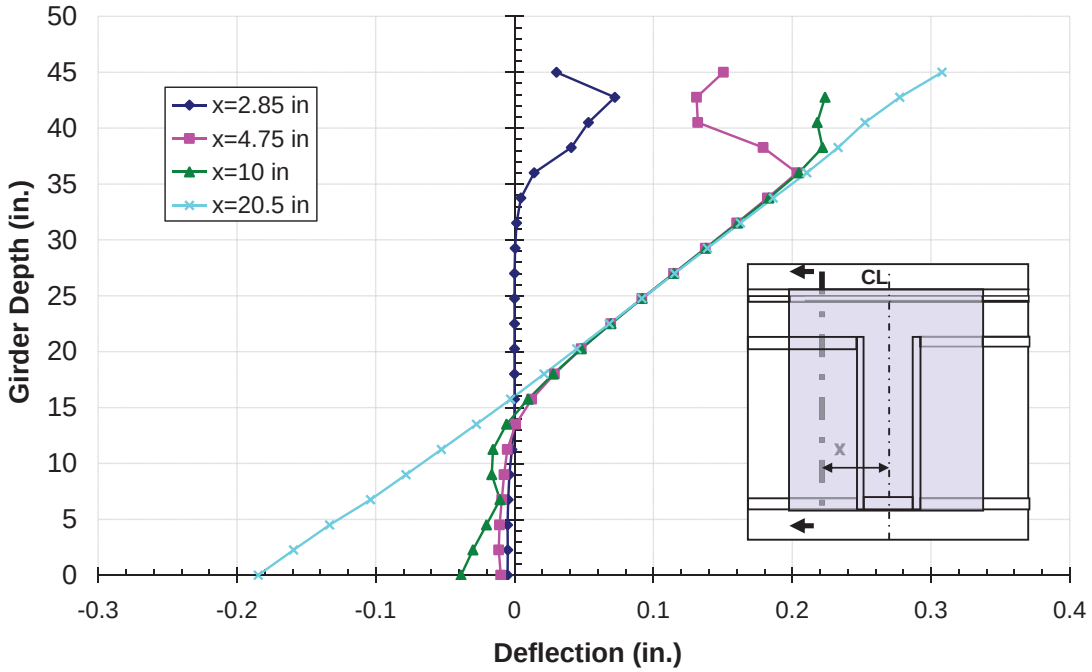

Fig. 10. Vertical strain distribution—type 1 (continuous bottom flange).

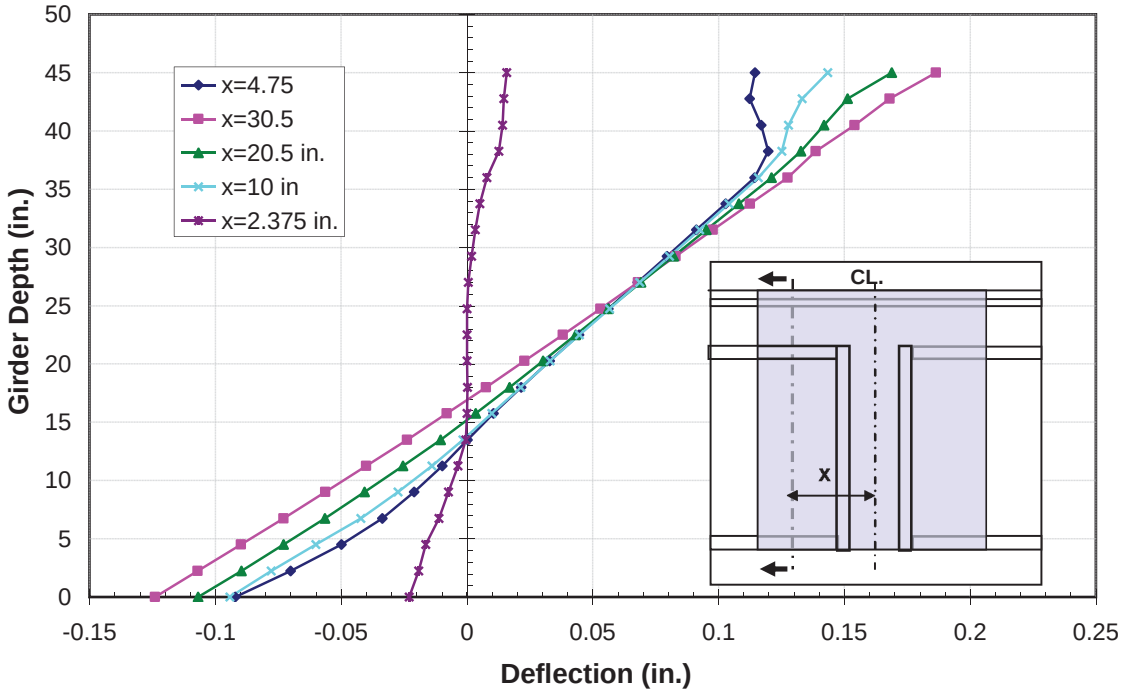

Fig. 11. Vertical strain distribution—type 3 (end plate).

plane (Bernoulli's principle)—is not valid based on the tests and finite element results. The profiles of the deflection of the sections inside the concrete diaphragms are shown in Figures 10 and 11 for the type 1 (continuous bottom flange) and type 3 (end plate) specimens, respectively. However, the strain distribution in sections farther from the pier centerline tends to be linear. This is also valid for the modular type 4 connection, as shown in Figure 12. In this figure, the strain distribution is depicted at the edge of the diaphragm. Note that for design purposes, a linear strain distribution was utilized, similar to traditional reinforced concrete design.

LOAD RESISTANCE MECHANISM BASED ON EXPERIMENTAL AND FINITE ELEMENT RESULTS

The elements that resist the applied negative moment in the concrete diaphragm are the top and bottom layers of longitudinal rebar in the slab, the concrete diaphragm in tension, the rebar hoops, the bottom plate or steel block and the concrete in compression. The results of finite element analyses indicate that the slab rebar, bottom connection plate or concrete core are the main elements contributing to the ultimate negative moment resistance of the tested connections. Other elements such as tension resistance in the concrete, diaphragm rebar hoops and the concrete diaphragm outside of the core have less effect, which can be neglected in calculations of the ultimate moment capacity.

Idealized Stress and Strain Distributions

For the purpose of design, based on the test and FEA results, idealized strain and stress distributions are proposed for the pier centerline section at the ultimate condition.

Longitudinal Reinforcement

It is evident from both test data and finite element analysis that the stress is not uniformly distributed in the slab rebar along the slab width. This phenomenon was also demonstrated by Timoshenko and Goodier (1970) using a stress function that satisfies the two-dimensional linear elasticity differential equation, along with the boundary conditions. The main reason for nonlinearity of strain—and, consequently, stress in the slab—is the shear lag phenomenon (Timoshenko and Goodier, 1970).

To derive a strain distribution, in the longitudinal reinforcement across the slab width and for the ultimate condition similar to what was observed in the tests and FEA, a simplified model was developed. In this model, as shown in Figure 13, the slab is assumed to act as a continuous beam supported by series of longitudinal reinforcement. The longitudinal reinforcements are modeled using one-dimensional

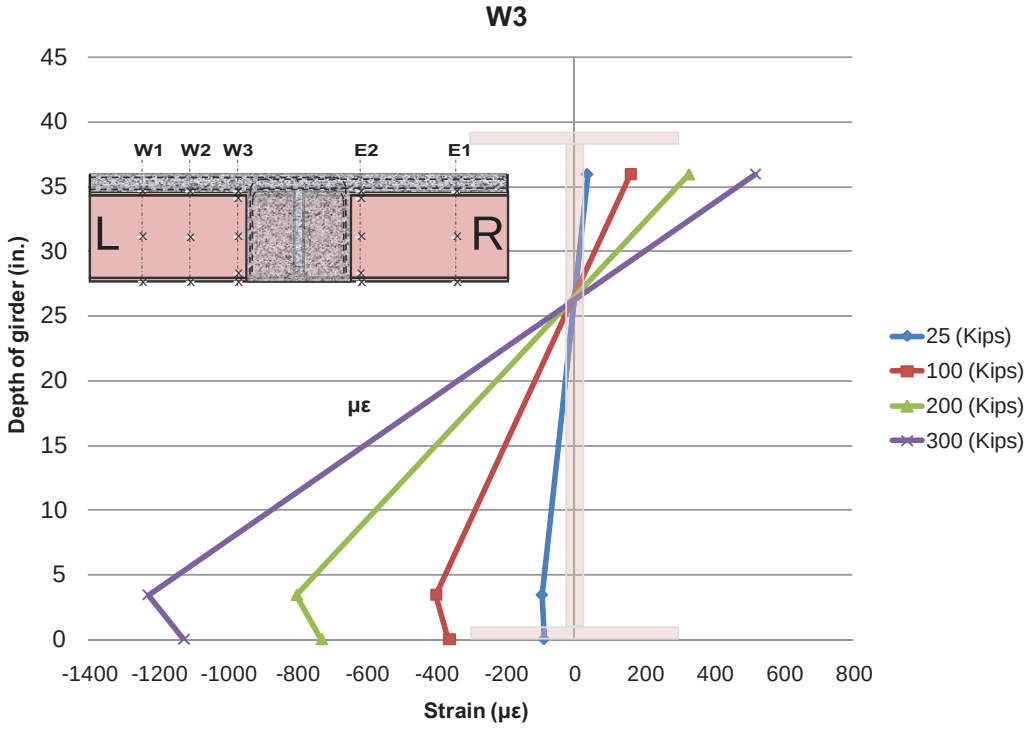

Fig. 12. Vertical strain distribution at edge of diaphragm—type 4 (modular).

springs, and the shear is transferred to the reinforcements through the concrete slab. The differential equation for a beam resting on springs is given by

$$\frac{d\delta}{dy} = -\frac{kv}{G_c A_c} \tag{1}$$

where

δ = deflection of the beam as a function of y
k = shear stress factor, which is about 1.5 for rectangular sections
v = shear force in any section of the beam
G_c = shear modulus
A_c = $t_s\Delta$
T_s = slab thickness
Δ = crack spacing

Solving the differential equation in Equation 1 results in:

$$\varepsilon = \frac{V\lambda}{2dk_r\left(1-e^{\frac{-\lambda b_s}{2}}\right)} e^{-\lambda y} \tag{2}$$

Or, in a simpler form,

$$\varepsilon = \varepsilon_s e^{-\lambda y} \tag{3}$$

where

$$\lambda = \sqrt{\frac{1.5k_r}{0.4G_c A_c}}$$

L = length of the cantilever girder
V = shear force
d = distance between the center of the slab reinforcements and the center of the compression force in the concrete diaphragm
k_r = slab rebar stiffness
k_s = stiffness of a strip of concrete slab
ε_s = constant
ε_y = strain of rebar at yielding

For design purposes, a uniform strain and stress distribution is assumed over the width of the top flange (b_f in Figure 14) with an exponential strain distribution everywhere else. The stress distribution follows the strain distribution in the linear region, which is exponential. It is uniform in the yielded areas (denoted by b_e in Figure 14).

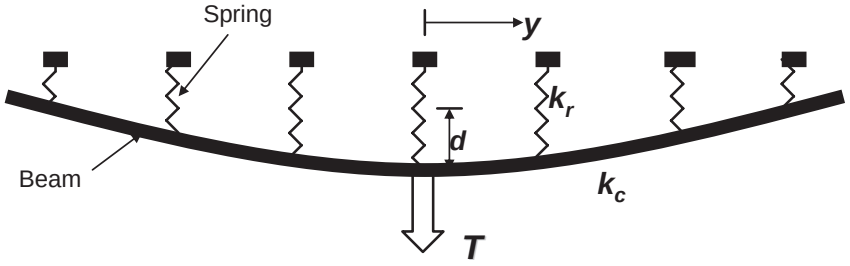

Fig. 13. Beam-spring model for a slice of the concrete slab and the rebar.

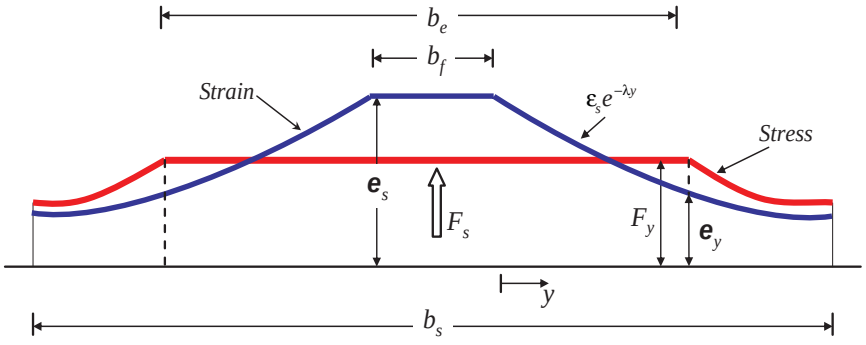

Fig. 14. Stress and strain distribution across the width of slab in reinforcement.

Diaphragm Concrete

Figure 15 shows the simplified stress and strain profiles in the concrete through the depth of the diaphragm in the middle of pier. The strain distribution is assumed to be linear, while the stress profile is nonlinear.

A uniform stress distribution is assumed for the core concrete region across the width of the end bearing plate as shown in Figure 16, and an exponential stress distribution is considered for the concrete diaphragm outside the core region.

Concrete Strength

Results of numerical studies indicate that the crushing of the concrete between the two end bearing plates (the core concrete) was the reason for failure of specimens 2 and 3 (more so for specimen 2). Based on the finite element results of the third specimen, most of the compressive force in the bottom flange of the steel girder is transferred through the core concrete. The finite element results also confirm that the compressive stress in this region is higher than the uniaxial compressive strength of the concrete due to the confinement of the core concrete by the surrounding concrete diaphragm and the end bearing plates. A simple model was implemented to achieve a closed-form solution for the concrete strength in the triaxial stress state for design purposes. This is shown in Figure 17. The applied pressure, q, is resisted by the direct concrete compressive strength, f_c, plus shear resistance denoted by s, in Figure 17.

$$qab_f = 2sat_c + f_c ab_f \tag{4}$$

where

a = depth of compression stress block in core region
b_f = width of the end bearing plate, which is equal to flange width in current study
t_c = thickness of concrete core

The concrete compressive strength due to the diaphragm confinement can be computed based on a linear approximation of a three-parameter method developed by Willam and Warnke (1975). For a linear approximation of the failure surface, the lateral stress, shown by p in Figure 17, is assumed to be less than 20% of the normal stress, which is a reasonable assumption based on the fact that concrete cracks in this direction and the cracking stress of concrete is less

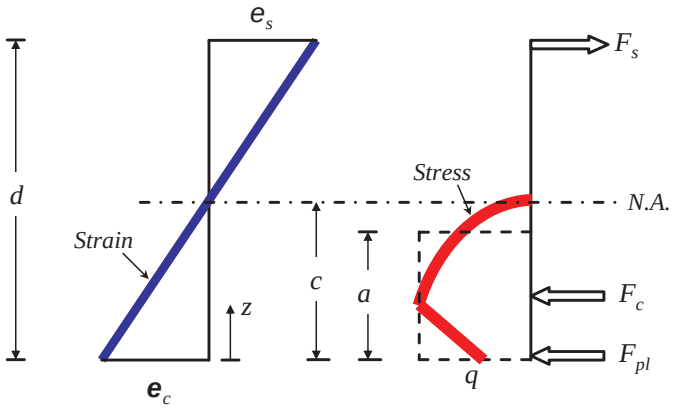

Fig. 15. Strain, stress and force diagrams in the vertical direction at the centerline of pier located in the plane of the web.

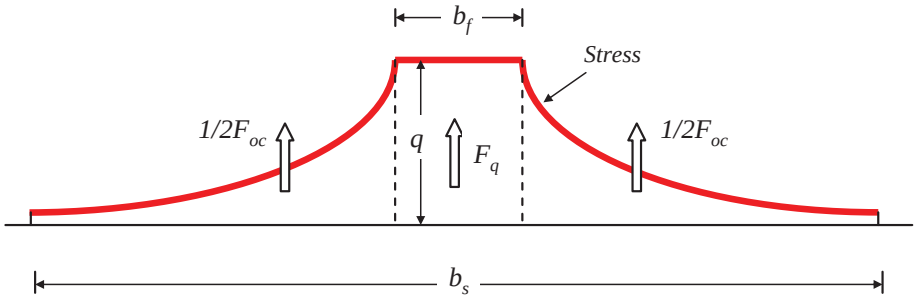

Fig. 16. Stress distribution of the compressive concrete across the width of diaphragm.

than 20% of the compressive stress. Based on a linear fit of the failure surface (Farimani, 2006), the relationship of normal stress, f_c, and lateral principal stress, p, can be described in the following formula:

$$f_c = 1.6p + f_c' \tag{5}$$

The finite element analysis of the tested specimens indicates that the first principal stress in the core concrete region is not more than the tensile strength of the concrete. The tensile strength is adopted from the AASHTO LRFD (2007) formula for the splitting tensile strength in ksi:

$$f_t' = 0.24\sqrt{f_c'} \tag{6}$$

Substituting from Equation 6 for p in Equation 5 gives

$$f_c = 0.38\sqrt{f_c'} + f_c' \tag{7}$$

Shear strength, s, is conservatively taken as zero.

$$s = 0 \tag{8}$$

Substituting Equations 8 and 7 into Equation 4, the following relationship is derived for the concrete strength in the core region:

$$q = 0.38\sqrt{f_c'} + f_c' \tag{9}$$

where

f'_c = uniaxial compressive strength of the concrete, ksi

The compressive strength of the core region, F_q, is computed using an equivalent rectangular stress block as shown in Figure 15:

$$F_q = qab_f \tag{10}$$

This load is assumed to be applied at a depth equal to half of the stress block depth, a. By neglecting concrete resistance outside the core, the total compressive resistance, F_c, provided by the concrete diaphragm at the ultimate condition at the pier centerline is:

$$F_c = F_q \tag{11}$$

Reinforcement Strength

When all of the slab rebar are in the elastic range, a linear strain-stress relationship is adopted, and the total tensile force in the slab rebar, F_s, can be computed according to the strain and stress distribution shown in Figure 14 as:

$$F_s = E_s\varepsilon_s A_s \frac{b_f}{b_s} + 2\int_0^{\left(\frac{b_s - b_f}{2}\right)} E_s\varepsilon_s e^{-\lambda y}\frac{A_s}{b_s}dy \tag{12}$$

In Equation 12, the origin of the y-coordinate axis has been shifted to the edge of the flange for the sake of simplicity, as seen in Figure 14. Simplifying Equation 12 gives:

$$F_s = \rho b_f + 2\frac{\rho}{\lambda}\left[1 - e^{\frac{-\lambda\left(b_s - b_f\right)}{2}}\right] \tag{13}$$

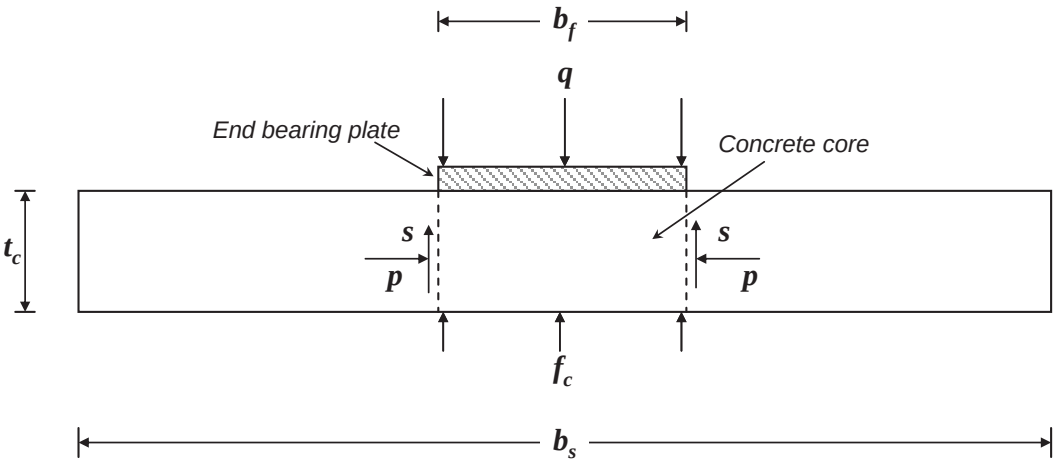

Fig. 17. End bearing plate resting on the core concrete.

Table 1. Comparison of Results of the FEA and Developed Equations					
		Specimen 1		Specimen 3	
Output	Units	Equations	FEA	Equations	FEA
F_{pl}	kips	924.30	913.0	0.00	0.00
q	ksi	7.2	6.97	6.81	7.49
F_s	kips	1474.40	1476.0	1416.20	1396.0
F_{st}*	kips	182.40	247.0	175.20	168.0
a	in.	3.8	7.06	12.2	9.79
b_e	in.	93.00	93.00	93.00	93.00
M_u	kip-in.	68061	68949	57528	61107
*F_{st} is the contribution of the stirrups in the diaphragm.					

where

$$\rho = \frac{E_s \varepsilon_s A_s}{b_s}$$

E_s = steel rebar elasticity modulus

Part of the rebar in the concrete slab might yield at the ultimate condition; in this case, the width of the yielded area (denoted by b_e as shown in Figure 14) is given by:

$$b_e = \frac{-2}{\lambda} \ln \frac{\varepsilon_y}{\varepsilon_s} + b_f \tag{14}$$

where ε_y is the yield strain of the rebar.

The total tensile force in the rebar is computed based on the following equation:

$$F_s = \frac{b_e}{b_s} A_s F_{yr} + \frac{2E_s \varepsilon_s A_s e^{\frac{\lambda b_f}{2}}}{\lambda b_s} \left(e^{\frac{-\lambda b_e}{2}} - e^{\frac{-\lambda b_s}{2}} \right) \tag{15}$$

where F_{yr} is the yield strength of the slab rebar.

Connecting Plate Strength

In connections similar to the first test specimen, a plate that connects two girders' bottom plates participates in transferring the compression along with the concrete. The experimental data and finite element simulations both indicate this plate yielded almost uniformly across its width. Therefore, its resistance, F_{pl} (see Figure 15), can be easily computed as follows:

$$F_{pl} = A_{pl} E_s \varepsilon_c \quad \text{if} \quad \varepsilon_c \le \varepsilon_y \tag{16}$$

$$F_{pl} = A_{pl} F_{yp} \quad \text{if} \quad \varepsilon_c \ge \varepsilon_y \tag{17}$$

where

A_{pl} = the cross-section area of the connecting plate
F_{yp} = yield strength of the plate
ε_c = concrete strain at the plate elevation

Verification of Proposed Mechanistic Model

The derived equations were implemented for the first and third tests to find their ultimate moment capacity at the pier. For this purpose, the depth of the concrete rectangular block, a (see Figure 15), is computed based on the force equilibrium in the section:

$$F_s - F_c - F_{pl} = 0 \tag{18}$$

Substituting from Equations 10 and 11,

$$a = \frac{F_s - F_{pl}}{q b_f} \tag{19}$$

The moment capacity of the section is computed based on the moment equilibrium about the center of the concrete compression block using the following equation:

$$M_u = F_s \left(d - \frac{a}{2} \right) + F_{pl} \left(\frac{a}{2} \right) \tag{20}$$

The results are compared to the finite element analysis in the next step. It should be noted that the yield stress of the rebar was calculated based on the average stress obtained from the finite element analysis at the ultimate condition and included strain hardening effects.

The final results are listed in Table 1. The comparison of the results with the finite element analysis of the first and the third tests indicates that there is good agreement for the moment strength of these two sections.

It should be noted that the tensile strength of the stirrups was calculated in the same manner as slab rebar tensile force and added to the total force equilibrium. This was done to ensure an accurate comparison with the finite element results as listed in Table 1. Also, the tensile strength of the concrete was ignored in the design calculation listed in Table 1, but it has only a slight effect on the total flexural capacity.

SIMPLIFIED DESIGN PROVISION FOR NEGATIVE FLEXURE

In this section, the development of simplified design equations for connection types 1, 3 and 4 are addressed. These represent two classes of connections: the first class in which a bottom plate or steel block transfers the compression forces (types 1 and 4) and the second class without the bottom plate that relies on concrete to carry compressive force (type 3).

In the previous section, a detailed force transfer mechanism was developed. This detailed approach was intended to understand and comprehend the contribution of various connection elements to the load-carrying capacity. This result was used to select the important elements and develop a simplified approach that is suitable for design yet captures the essential connection behavior described in the previous section. The following assumptions were made, while developing the simplified design provisions:

- The stirrups were shown in the previous section to have a minor contribution to the strength of the connection in comparison to the other elements. Thus, they will not be considered in this section.
- Contribution of concrete in tension to moment capacity is ignored.
- The critical section for moment capacity calculation purposes is assumed to be inside the concrete diaphragm at the end of the steel girder. The composite girder outside of the diaphragm can be designed using AASHTO LRFD design provisions.
- Moment reversal such as that which could exist in seismic design is not considered.
- It is assumed that the bottom flange is predominantly subjected to compression. Type 1 and 4 connection details can be modified for application in cases where bottom flanges are subjected to significant tension, a scenario that could exist when the number of bridge spans exceeds or equals three and when uneven span length are used. More detailed discussion of this scenario is provided in Azizinamini (2014). Type 3 connection detail is not applicable when bottom flanges are subjected to significant tension.

Continuous Bottom Flange (Type 1) and Modular (Type 4)

In this type of connection, for the case of negative flexure, the tension force is mainly resisted by longitudinal reinforcement in the slab. The compression force is resisted, predominately by bottom plate or steel block. The failure of the connection can be initiated by yielding of the bottom plate, yielding of the top rebar or crushing of the diaphragm concrete. To avoid crushing the concrete in the vicinity of the bottom plate, this plate (block) is sized to stay elastic when all reinforcement in the slab reaches its ultimate capacity, which is larger than yield capacity.

If the plate is to remain elastic until all slab reinforcement reaches its ultimate capacity, then it can be assumed that the core concrete will not crush. The net result is that the failure of the connection will coincide with slab reinforcement reaching its ultimate capacity. It should be noted that the ultimate capacity of the slab reinforcement is equal to total area of slab reinforcement multiplied by the ultimate strength of reinforcement.

Predicting the ultimate strength of the slab reinforcement could be achieved by examining the available information on material properties of the reinforcement used. For the sake of developing design provisions, it is assumed that ultimate strength of reinforcement is related to yield stress, using following relationship:

$$F_u = \alpha f_y \tag{21}$$

where

α = ductility ratio of rebar
F_y = yield stress of deck rebar

Thus, for the compression plate to remain elastic under ultimate load, the desired height of the compression plate conservatively is

$$H > \frac{\alpha A_s f_y}{b_f F_{pl}} \tag{22}$$

where

A_s = total area of deck reinforcement
F_{pl} = yield stress of compression plate or block

Because a large majority of the compressive force is resisted by the stiff compression plate, as evidenced by the low neutral axis, the resultant of the compressive force will be located within the compression plate. Also, because it has been assumed that the deck reinforcement is the only portion of the cross-section that can resist any tensile stress, an estimate of the moment arm, which is the distance between center of tension and compression resultant forces, is easily obtained. Under these assumptions, the moment arm

is simply distance between center of reinforcement in the top and center of steel block in the bottom. The moment capacity of the connection is then estimated using following equation:

$$M_n = A_s f_y \left(d - H/2\right) \tag{23}$$

For comparison purposes, the nominal capacity of the first test specimen was calculated, using the measures yield strength of reinforcing bars (65.4 ksi):

$$M_n = (19.4)(65.4)(43 - 1.2/2)$$
$$= 53{,}795 \text{ kip-in.}$$

The nominal capacity just calculated is approximately 72% of the moment obtained from the experimental test (74,304 kip-in.).

For the fourth tested specimen, the capacity is:

$$M_n = (19.4)(66.5)(43.2 - 4/2)$$
$$= 53{,}152 \text{ kip-in.}$$

The nominal capacity is approximately 79% of the ultimate moment obtained from the test (67,500 kip-in.).

End Plate (Type 3)

This detail is not recommended for new design. However, it may have applicability to cases where existing bridges are retrofitted and simple spans are made continuous.

The geometry of the third specimen type bears a strong resemblance to that of simple-made-continuous prestressed concrete connections. Due to the similarity of these connections, the same method used for prestressed concrete connection as recommended by the PCI *Bridge Design Manual* (PCI, 1997) may be sufficient for the design of this connection in steel girder bridges as well. However, the additional aspect that is added to the design method pertains to the confinement of the core concrete, which increases the capacity of the connection.

In order to obtain an appropriate design method for this detail, it is clear that the confinement needs be taken into consideration. The enhanced concrete compressive strength because of confinement can be estimated using Equation 9. Using the magnified strength, it is proposed that standard reinforced concrete design methods be used.

To ensure the ductility of section, it is recommended to use AASHTO LRFD requirements, as stated by Equation 24:

$$\frac{c}{d} = 0.42 \tag{24}$$

The objective of the preceding limitation is to prevent use of sections with very large compression block. For type 3 connection details, Kowalski (2007) indicates that the c/d ratio can be as large as 0.62 when confinement effects are considered.

To demonstrate the simple design procedure, the moment capacity of the third test specimen is calculated based on Equation 9:

$$q = 0.38\sqrt{5.9} + 5.9$$
$$= 6.82 \text{ ksi}$$

$$a = f_y A_s / (0.85 q b_f)$$
$$= (69.2)(19.4) / [0.85(6.82)(15.8)]$$
$$= 14.7 \text{ in.}$$

$$c = a/\beta$$
$$= 14.7/0.85 = 17.2 \text{ in.}$$

$$c/d = 17.2/43$$
$$= 0.4 < 0.42 \textbf{ ok}$$

$$M_n = A_s f_y (d - a/2)$$
$$= 19.4(69.2)(43 - 14.7/2)$$
$$= 47{,}859 \text{ kip-in.}$$

The nominal moment capacity is approximately 68% of the capacity of the tested specimen (70,380 kip-in.). One main reason for the conservative prediction of the moment capacity by the simplified equation is the overstrength of the top longitudinal rebar, which was ignored in the simplified equations. Kowalski (2007) showed that this level of conservative design is in line with current practice of cast-in-place concrete beam flexure design.

PARAMETRIC STUDIES

Two different studies were carried out to investigate the efficacy of the simplified design equations. The first study focused on the connection types 1 and 4, which rely on steel to provide continuity of the compressive force at the bottom flange. The second study considered the type 3 connections, which utilize concrete to transmit the compressive force.

Continuous Bottom Flange (Type 1) and Modular (Type 4)

To verify the validity of the proposed method, a typical 100-ft span bridge was designed according to AASHTO LRFD bridge specifications. The bridge was designed to act as a simple span for the dead loads and continuous for the live loads. The bottom plate, which connects the bottom flanges of the girders in the core region as shown in Figure 1, was considered to have five different heights, *H*.

A finite element model was constructed and analyzed to obtain the ultimate capacity of the specimen for each plate height, as listed in column 4 of Table 2. The ultimate moment capacity of the connection at the pier centerline was calculated using the detailed method described earlier and

Table 2. Ultimate Moment Capacity Comparison of Simplified and Detailed Prediction Methods versus Finite Element Results			
	M_u (kip-in.)		
H (in.)	Simplified	Detailed	FEA
0.5	45,408	53,319	57,523
1.0	45,078	57,063	61,638
1.73	44,596	63,785	69,667
2.16	44,312	61,419	72,539
4.0	43,098	62,266	74,318

Table 3. Parametric Study Variables						
		Span of Each Bridge				
Input	Units	50 ft	75 ft	100 ft	125 ft	150 ft
Steel girder flange width	in.	10.4	11.5	12.215	16.51	16.87
Concrete core thickness	in.	2	4	5	6	8
f'_c	ksi	4	4.5	5.5	6	6.5
Diaphragm thickness	in.	10	15	20	25	30
Width of the slab/diaphragm	in.	96	108	120	132	144
Slab thickness	in.	7	7	7.5	7.5	8
Total area of the slab rebar in longitudinal direction	$in.^2$	7	15	22	30	35
Yield strength of steel rebar	ksi	60	60	60	60	60

listed in the third column of Table 2. The capacity was also computed using the simplified method developed earlier and listed in the second column of Table 2.

End Plate (Type 3)

Two-span I-girder bridges were designed according to AASHTO-LRFD bridge specifications to examine the proposed design method for the type 3 connection. The bridge dimensions were selected in order to cover a practical range. The bridge properties are summarized in Table 3. The bridges consist of four equally spaced I-girders. The interior girder for each bridge is designed for the applied dead loads and HL-93 live load according to AASHTO LRFD provisions. The bridges were analyzed acting as two simple spans for the dead weight and as continuous for the superimposed dead loads and live loads. The bridges were designed for several load combinations, including constructability, strength limit state I, and service limit state II. The proposed design methods were used to evaluate the required longitudinal tensile reinforcement at the pier location in the slab. In the design of steel girders and slab rebar, several iterations were made to find an optimum section.

The designed bridges were analyzed using nonlinear finite element analysis. The ultimate strengths of the bridges at the pier centerline were compared with what were predicted by the design methods developed in previous sections of this paper (see Table 4).

It is observed that the predicted capacity, in general, is in good agreement with FEA results. However, for the longer span, the simplified equations result in slightly higher ultimate moment capacity. In calculations presented earlier, the effective width was assumed to equal to tributary width.

CONCLUSIONS

The SDCL concept for steel bridges requires a connection between the girders over the bridge piers. In this paper, the structural behavior of four proposed connections was investigated through numerical and analytical methods. The comparison of the finite element models of the four connections exhibit good agreement with the results obtained from the full-scale tests. Based on numerical, analytical and experimental results, the force-resistance mechanisms of the connections are described in the form of mathematical equations. Good comparisons were obtained between results of nonlinear finite element analysis and a detailed approach to

Table 4. Ultimate Moment Capacity Comparison of Simplified and Detailed Prediction Methods versus Finite Element Results					
	Span of Each Bridge				
Method	**50 ft**	**75 ft**	**100 ft**	**125 ft**	**150 ft**
Simplified	13,247	28,930	46,179	73,056	102,409
Detailed	13,783	30,520	48,240	74,272	103,477
FEA	17,294	33,054	49,542	72,276	101,298

calculate moment capacity of all connection detail types. For practical purposes, a set of simplified equations were derived from the more detailed approach mentioned earlier for two connection types to calculate the ultimate negative moment capacity at the critical sections. The simplified approach is recommended for use in the design process.

ACKNOWLEDGMENTS

This paper presents details of a major undertaking to develop an economical steel bridge system. The investigation was directed by Atorod Azizinamini, Professor and Chair at Florida International University, and was made possible by contributions from many current and former graduate students and research associates, as well as input from many in the bridge community. In particular, the contributions of the following individuals are acknowledged.

Graduate students earning degrees from the project were Nick Lampe, Nazanin Mahasebi, Reza Farimani, Saeed Javidi, Derek Kowalski and Mark Otte. The research study was conducted at the University of Nebraska–Lincoln. Aaron Yakel was the research associate assisting the project. Laboratory technicians Jeff Boettcher, John Dageford and Peter Hilsabeck assisted in conducting the experimental portion of the study. Graduate students who assisted with experimental testing include John Swendroski, J. Brian Hash, Patrick Mans, Luke Glaser and Nima Ala. The study was supported by the Federal Highway Administration and the Nebraska Department of Roads (NDOR). Several visionary engineers at NDOR were critical to the successful completion of the project: Lyman Freeman, Moe Jamshdi and Hussam "Sam" Fallaha. Steel fabrication and assistance during specimen preparation were provided by Capitol Contractors of Lincoln, Nebraska.

The opinions and conclusions presented in this paper are those of the authors and do not necessarily represent the viewpoints of the project sponsors.

REFERENCES

AASHTO (2007), *LRFD Bridge Design Specifications*, 4th ed., American Association of State Highway and Transportation Officials, Washington, DC.

ABAQUS (2009), *ABAQUS Theory Manual,* SIMULIA, Providence, RI.

Azizinamini, A. (2014), "Simple for Dead Load–Continuous for Live Load Steel Bridge Systems," AISC, *Engineering Journal*, Second Quarter.

Azizinamini, A., Lampe, N.J. and Yakel, A.J. (2003), *Toward Development of a Steel Bridge System—Simple for Dead Load and Continuous for Live Load*, Final Report for Nebraska Department of Roads Research Project Number SPRL-PL-1(035) P515, University of Nebraska–Lincoln, Lincoln, NE.

Azizinamini, A., Yakel, A.J., Lampe N.J., Mossahebi, N. and Otte, M. (2005), *Development of a Steel Bridge System—Simple for Dead Load and Continuous for Live Load, Volume 2: Experimental Results*, Final Report NDOR P542, Nebraska Department of Roads, Lincoln, NE.

Farimani, M.R. (2006), *Resistance Mechanism of Simple-Made-Continuous Connections in Steel Girder Bridges*, Ph.D. Dissertation, University of Nebraska–Lincoln, Lincoln, NE.

Javidi, S.N. (2009), *Resistance Mechanism of Simple-Made-Continuous Connections in Skew and Non-Skew Steel Girder Bridges Using Conventional and Accelerated Types of Construction*, Ph.D. Dissertation, University of Nebraska–Lincoln, Lincoln, NE.

Javidi, S.N., Yakel, A.J. and Azizinamini, A. (2014), "Experimental Investigation, Application and Monitoring of a Simple for Dead Load–Continuous for Live Load Connection for Accelerated Modular Steel Bridge Construction," AISC, *Engineering Journal*, Third Quarter (in press).

Kowalski, D.T. (2007), *Development and Evaluation of Design Equations for the Simple-Made-Continuous Steel Bridge System*, M.S. Thesis, University of Nebraska–Lincoln, Lincoln, NE.

Lampe, N.J. (2001), *Steel Girder Bridges Enhancing the Economy*, M.S. Thesis, University of Nebraska–Lincoln, Lincoln, NE.

Lampe, N.J., Mossahebi, N., Yakel, A.J., Farimani, M.R. and Azizinamini, A. (2014), "Development and Experimental Testing of Connections for the Simple for Dead Load–Continuous for Live Load Steel Bridge System," AISC, *Engineering Journal*, Second Quarter.

Mossahebi, N. (2004), *New Steel Bridge System: Simple for Dead Load, Continuous for Live Loads*, M.S. Thesis, University of Nebraska–Lincoln, Lincoln, NE.

PCI (1997), *Precast Prestressed Concrete Bridge Design Manual*, 2nd ed., Precast/Prestressed Concrete Institute, Chicago, IL.

Timoshenko, S. and Goodier, J. (1970), *Theory of Elasticity*, 3rd ed., McGraw-Hill, New York, NY.

William, K.J., and Warnke, E.P. (1975), "Constitutive Model for the Triaxial Behavior of Concrete," *Proc. International Association for Bridge and Structural Engineering 19*, ISMES, Bergamo, Italy.

Continuous for Live Load Steel Girder Construction in the Northern Panhandle of West Virginia

ANTHONY REAM and WILLIAM BEINING

ABSTRACT

This paper presents two recently constructed steel girder bridges in the northern panhandle of West Virginia featuring simple for dead load–continuous for live load (SDCL) construction. The design, fabrication, construction and maintenance of this structure type are explored in addition to positive impacts on traffic control.

Keywords: steel bridges, steel girders, SDCL, simple for dead load–continuous for live load.

INTRODUCTION

The West Virginia Department of Transportation recently investigated the benefits of simple for dead load–continuous for live load (SDCL) bridges through the construction of the Three Springs Drive Bridge and the Washington Avenue Bridge in the northern panhandle of West Virginia. SDCL structures minimize or eliminate flange transitions for steel girders, provide the simplicity of simple span structures for fabrication and erection and eliminate problematic deck joints, as in typical continuous structures. These factors reduce costs, improve performance, reduce maintenance and accelerate construction.

STRUCTURE

These projects involve the replacement of the Three Springs Drive Bridge over U.S. Route 22 in Weirton, West Virigina, and the Washington Avenue Bridge over Interstate 70 in Wheeling, West Virginia. Both projects consist of replacing existing four-span bridges originally built in the 1960s with two-span steel SDCL structures. The existing Three Springs Drive Bridge was a prestressed concrete I-beam structure. The existing Washington Avenue Bridge consisted of rolled steel beams.

The final deck geometry of both replacement structures was very similar, with five 12-ft traffic lanes and two 3-ft-wide shoulders on an 8-in.-thick concrete deck at each location. A 5-ft-wide raised sidewalk is also present on one side of each structure, as shown in Figure 1. The only difference in deck width results from a slightly wider sidewalk barrier at the Washington Avenue location. The new Three Springs Drive Bridge was opened to traffic in 2007. The bridge at Washington Avenue was completed in 2008.

For Three Springs Drive, as shown in Figure 2, the deck is supported by seven 54-in.-deep weathering steel plate girders spaced at 11 ft 2 in. with spans of 125 ft 6 in. and 95 ft. Span lengths were dictated by the configuration of U.S. Route 22, and the 54-in. girder depth was based on preliminary depth studies. K-type cross frames are provided at intermediate locations.

The Washington Avenue Bridge, as shown in Figure 3, is supported by seven 45-in.-deep weathering steel plate girders spaced at 11 ft 2 in. with spans of 96 ft and 112 ft. Span lengths were dictated by the configuration of Interstate 70, and the 45-in. girder depth was limited by vertical clearance requirements. Bent plate diaphragms are provided at intermediate locations.

The steel girders were placed as simple spans to resist noncomposite forces. After placement of the deck in both spans, flange splices were connected over the pier to provide continuity for composite dead and live loads, and an integral concrete diaphragm was cast in place concurrent with the deck closure pour. Both structures are supported at the ends by jointless, integral abutments founded on steel H-piles. Mechanically stabilized earth (MSE) walls surround the integral abutments at the Washington Avenue location.

It was desirable to maintain traffic throughout construction at both locations; therefore, partial-width staged construction was used to allow on-alignment replacement of each bridge.

Girder Design

The steel continuity splice over the pier allows for simple span girder construction, which is then made continuous for

Anthony Ream, P.E., Senior Structural Engineer, HDR Engineering, Inc., Pittsburgh, PA (corresponding). E-mail: tony.ream@hdrinc.com

William Beining, P.E., Senior Structural Engineer, HDR Engineering, Inc., Pittsburgh, PA. E-mail: bill.beining@hdrinc.com

composite loads. SDCL construction shifts negative moment from the interior support (typically higher for conventional girder structures) to the positive moment regions, as shown in Figure 4.

By shifting a portion of the load to positive moment regions that can develop resistances above yield and have compression flanges that are continuously braced by the deck, the mid-span and interior support cross-sections are similar. This reduces the number of flange transitions. For structures with smaller, more balanced span arrangements, transitions can be entirely eliminated, and the use of rolled sections becomes more economical.

At these West Virginia locations, span lengths dictated the use of plate girders rather than rolled beams. However, at the Washington Avenue Bridge, with a maximum span of 112 ft, flange transitions were completely eliminated, with 20-in.-wide plates of constant thickness used for both the top and bottom flange.

The maximum span length at the Three Springs Drive Bridge is 125 ft 6 in. The positive moment in this span dictated two flange transitions for economy. The bottom flange remains a constant 20 in. wide, while its thickness varies from 1 to 1½ in. The top flange remains a constant 1 in. thick, while varying in width only for each span.

Steel Continuity Splice

SDCL construction was accomplished by splicing the top and bottom flanges of the simple span girders at the interior support location after placement and curing of the deck, which was poured to within 5 ft of the centerline of bearing at the abutments and pier (pouring the deck as near as possible to the supports minimized noncomposite forces on the continuity splice). The girders were placed on elastomeric bearings with preformed joint filler between the remaining

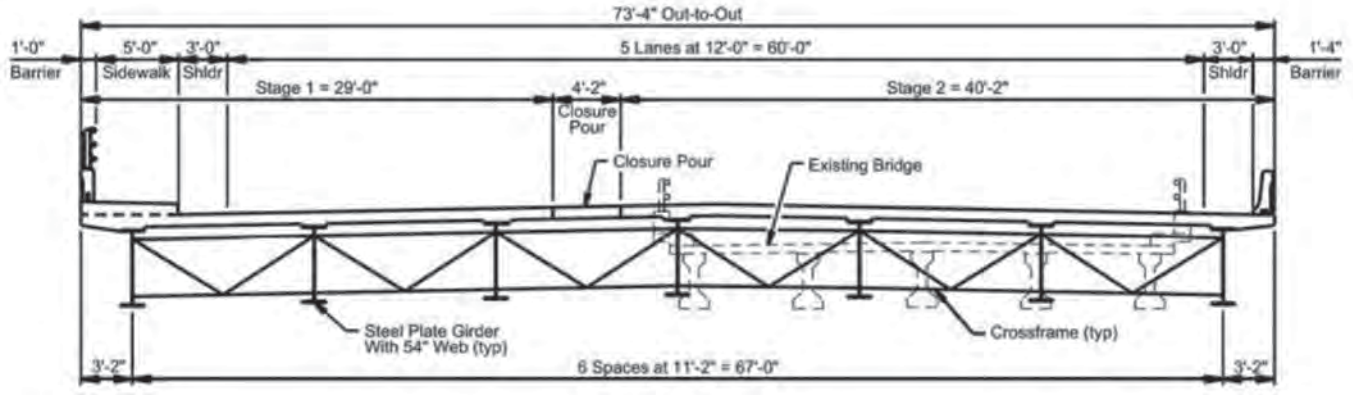

Fig. 1. Three Springs Drive typical section. Washington Avenue is similar with 45-in.-deep girders and bent plate diaphragms.

Fig. 2. Three Springs Drive.

Fig. 3. Washington Avenue.

portions of the girder bottom flange and top of pier cap. The remainder of the pier cap was covered with a ½-in. layer of preformed joint filler to allow rotation of the concrete diaphragm under live loads after completion of the structure, as shown in Figure 5.

Design of the steel continuity splice was accomplished by resolving the factored moment at the pier into a force couple. Flange to web welds in the vicinity of the splice were sized to allow the portion of the moment resisted by the web to be transferred into the top and bottom flanges. An outside bolted splice plate in single shear was used to transmit the top flange tension force of the composite section. The connection was considered slip-critical. The contribution of deck reinforcement was not included in the tension capacity of the splice, providing redundancy in the system. To transmit the compression force of the bottom flange, steel-bearing plates were placed between the bottom portion of the girder webs and flanges. At the Three Springs Bridge, this was achieved through the use of steel end plates welded to the girder web, with bearing plates and shims filling the void between the end plates, as shown in Figure 6. A slightly simpler detail was used at the Washington Avenue location, with the bearing plates welded directly to the web without a steel end plate. At both locations, steel shims were placed between the bearing plates after placement of the deck, with the majority of dead load rotations realized.

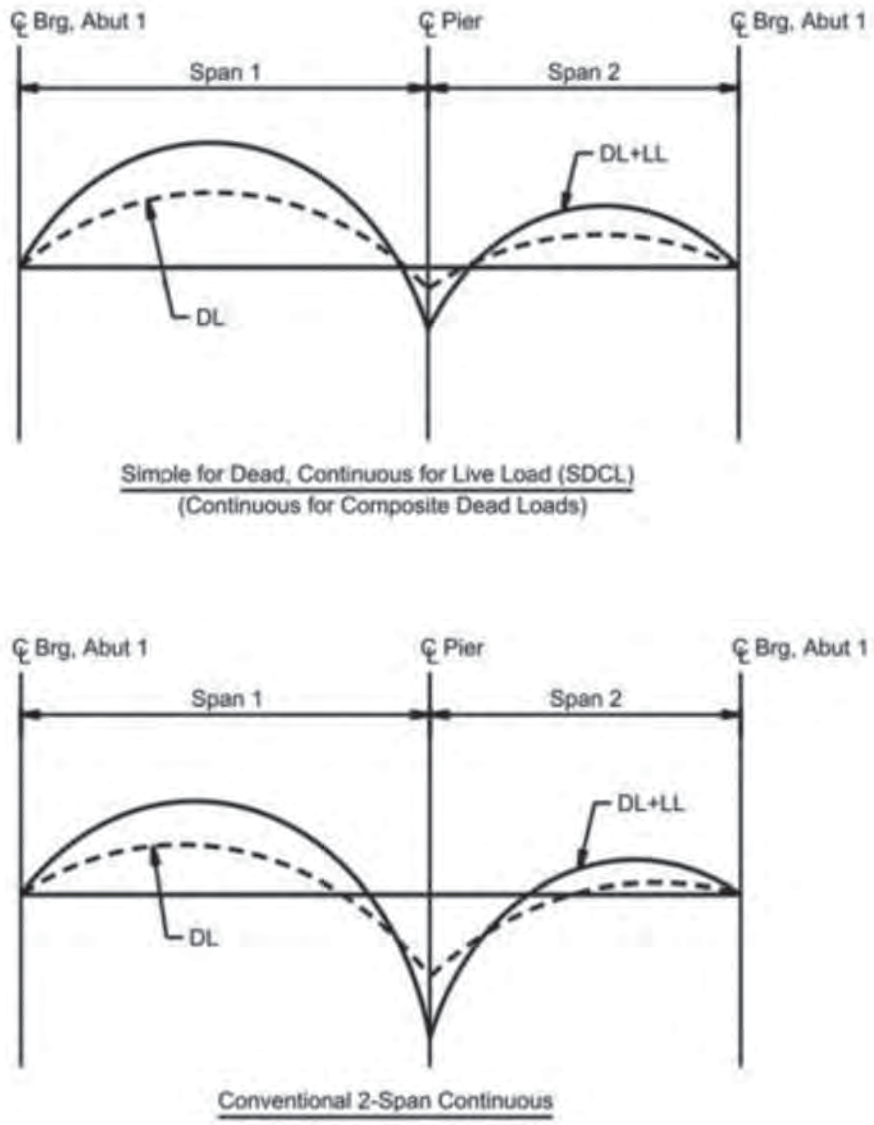

Fig. 4. SDCL and continuous-span moment diagrams.

To anchor the superstructure at the pier, reinforcement bars were used as dowels extending from the pier cap into the concrete diaphragm. Transverse bars were placed through holes in the girder webs, and shear stirrups were used to form a cage extending from above the pier cap into the deck. After completing the reinforcement, the diaphragms, including the deck within 5 ft of the centerline of pier and abutments, were placed. The completed diaphragm is shown in Figure 7.

To provide stability at the supports during placement of the deck, temporary cross frames, as shown in Figure 8, and consisting of threaded bars with turnbuckles for the diagonals were used. After the deck was cured, these temporary cross frames were removed to allow space for completion of the steel continuity splice and minimize the possibility of corrosion and voids within the concrete diaphragm.

FABRICATION BENEFITS

SDCL girder designs provide potential cost and time benefits during fabrication. Based on preliminary design studies, it is believed that balanced span lengths less than 100 ft provide the optimal situation for efficiency by reducing steel weight and eliminating full-penetration welds in the flanges. As the span lengths increase or become unbalanced, evaluating the construction, traffic and maintenance benefits of SDCL structures plays a greater importance in determining their efficiency.

Because of its increased and unbalanced span lengths (125 ft 6 in. and 95 ft), the Three Springs Drive structure required welded plate girders with two bottom flange transitions in the longer span. The structure's steel weight of 24 lb/ft^2 was comparable to conventional continuous girders. However, the number of plate thickness transitions was reduced.

The Washington Avenue structure's steel weight of 25 lb/ft^2 was comparable and also in line with conventional continuous girders. However, with a more favorable span balance (96 and 112 ft), flange transitions were completely eliminated from the design.

Thus, while the steel weight for each of these structures was in line with conventional continuous steel girders, the elimination of welds associated with flange transitions did offer some advantage.

In addition to advantages in girder fabrication, the use of concrete diaphragms at the piers eliminates the need for larger, more complex steel cross frames at the supports to transmit lateral loads. The use of concrete diaphragms also leads to simplified bearing pads, which don't require steel sole plates welded to the girder flanges.

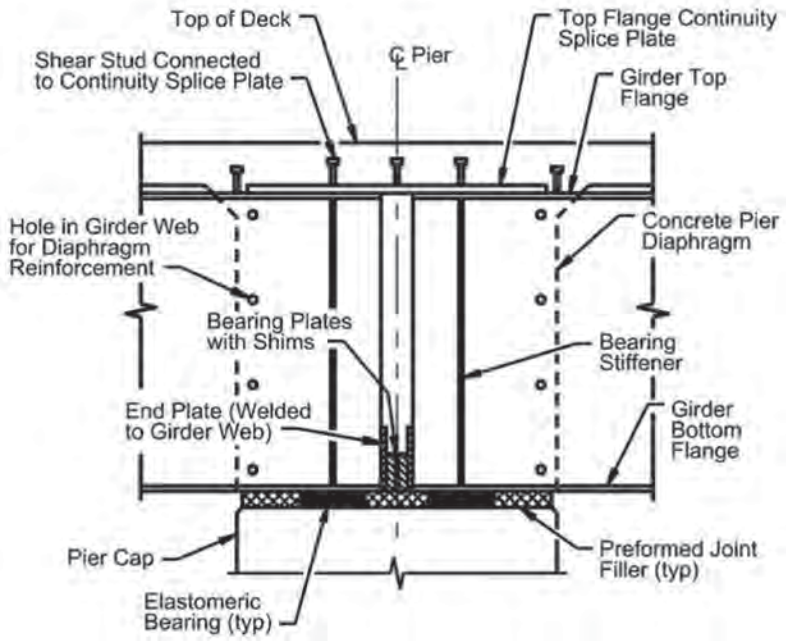

Fig. 5. Steel continuity splice details.

CONSTRUCTION BENEFITS

SDCL girders accelerate construction by eliminating in-span field splices and reducing complex steel details. Moving the splice from a typical inflection point for continuous girders to the pier location eliminates the need for temporary supports and working over traffic, which leads to increased worker safety. The type of splice used for SDCL girders is also less complex, reducing labor and skill-level requirements.

The continuity splice also reduces crane requirements. Because the splice is made at the interior supports, cranes do not have to hold pieces while connections are being made, reducing crane hold times.

Because the structure does not rely on the splice to provide stability for the bridge, the splice is removed from the critical path. Therefore, the construction of the splice can be performed when convenient, possibly when barrier formwork is being installed.

These projects also show SDCL construction's compatibility with partial-width staged construction. Both of these locations required maintenance of traffic with an online replacement.

TRAFFIC BENEFITS

Another benefit of SDCL construction is the positive effect on traffic control. For standard highway overpass structures, such as Three Springs Drive and Washington Avenue, installing girders as simple spans requires the closure of only one direction of a divided highway. If these structures were conventional continuous structures, both directions of traffic would have been closed and rerouted at times. As constructed, entrance and exit ramps were utilized to reroute traffic for closed lanes, minimizing the impact.

Another aspect of SDCL construction is the possibility of complete span-by-span construction. Due to staged construction in conjunction with the existing bridge, this was not possible at these locations. For structures constructed in one stage (such as a new alignment), one direction of traffic below the structure can be rerouted or shifted, and the span can be entirely constructed without live traffic underneath. This includes abutment, pier, girders and deck. If desired, the girder design could also accommodate the placement of the abutment diaphragm and barriers in the span before advancing. After completion of the span, traffic could be shifted from below the second span and the process repeated. The

Fig. 6. Three Springs Drive continuity splice.

final step would be the installation of the continuity splice and concrete diaphragm at the pier(s).

There are several cost and schedule benefits to this construction approach. First, because one entire span is constructed at a time, traffic only needs to be shifted once. This simplifies the maintenance and protection of traffic, minimizing construction time and cost spent on installation and subsequent adjustment of detour devices. Second, shifting traffic away from a span for its entire construction eliminates the time, cost, coordination and public relations associated with overnight or momentary traffic closures for girder erection and shielding. Finally, the removal of traffic under the span during the entire construction allows for versatility in material staging and crane placement, in addition to eliminating the need for shielding.

Also, for small spans and construction sites with large lay-down areas, complete spans can be constructed on temporary supports and lifted into place. This method would limit traffic disruption to a few night closures.

MAINTENANCE BENEFITS

The pier splice eliminates joints typical in simple span construction. The elimination of this joint prevents corrosion of the steel girders due to water. The concrete diaphragm also protects the girder ends and shields the pier cap from sediment buildup, which can lead to deterioration of the concrete, bearing pads and associated assemblies. These details, in combination with integral abutments, create jointless steel bridges with no exposed bearings or girder ends. This eliminates some of the primary areas of concern for maintenance going forward.

For smaller spans, the compression force in the bottom flange at the pier location could be transmitted through the concrete diaphragm alone, using end plates without steel shims between and relying on the compression strength of the diaphragm concrete. Additionally, the top flange tension splice could be carried through the reinforcement of the concrete deck. However, the use of simple steel connections between the top and bottom flanges in conjunction with the concrete diaphragm provides redundancy in the event of a component failure.

LESSONS LEARNED

The design and construction of these structures leads to several observations about SDCL construction. When integral abutments are used in conjunction with a continuity splice and reinforcement bar dowels at the pier, there is no lateral attachment of the superstructure to the substructure until the pier diaphragm is cast. If threaded anchor bolts through the girder flanges are not provided, then dimensions locating the girder ends relative to each other under the steel and steel plus concrete deck conditions should be provided on the design drawings, which account for girder end rotation under dead loads.

An alternate method would be to provide a temporary linkage connecting the girder webs at the neutral axis of the girders, as shown in Figure 9. A steel bar bolted to the webs could be used to maintain the proper distance between bearing centerlines. The bearing pad should be checked for the resulting deformation at the bottom flange from the deck pour. Additional ways of providing for construction

Fig. 7. Completed diaphragm.

Fig. 8. Temporary cross frames at supports.

flexibility would be to specify field drilling of the holes in the girder web for diaphragm reinforcement and also in the top flange for the splice plate connection.

Additional items of interest include detailing of deck reinforcement in the design drawings. In the vicinity of the top flange splice, reinforcement should be spaced to allow for field drilling and bolting. Also, consideration should be given to installing the pier diaphragm reinforcement cage after the temporary cross-frames have been removed and the steel continuity splice has been made.

Finally, instead of using flat shim plates to provide continuity between bottom flanges at the splice, "wedged kicker plates" could be used (Wasserman, 2005). These wedged shims can be driven in the field and will ensure a more complete contact of the plates.

CONCLUSION

The use of simple for dead–continuous for live load steel girders for the replacement of the Three Springs Drive and Washington Avenue Bridges in the northern panhandle of West Virginia proved successful. While the savings in steel weight versus conventional continuous girder construction proved negligible on these structures, benefits in fabrication, construction and future maintenance were evident. These projects also showed the advantages of SDCL construction regarding traffic control and the compatibility of SDCL construction with staged construction.

REFERENCES

Wasserman, E.P. (2005), "Simplified Continuity Details for Short- and Medium- Span Composite Steel Girder Bridges," *Transportation Research Record: Journal of the Transportation Research Board, CD 11-S,* Transportation Research Board of the National Academies, Washington, DC, pp. 197–202.

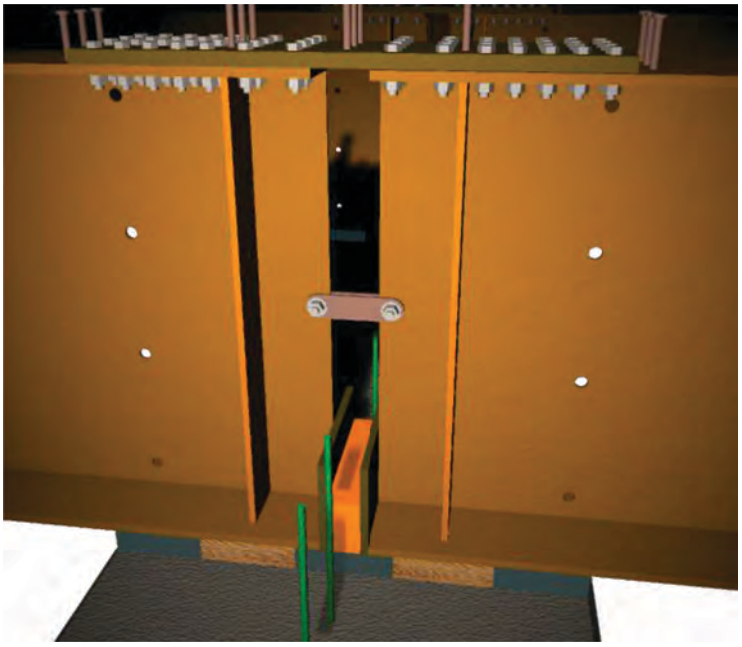

Fig. 9. Continuity diaphragm showing temporary linkage in web.

Current Steel Structures Research

No. 35

REIDAR BJORHOVDE

INTRODUCTION

This issue of "Current Steel Structures Research" for the *Engineering Journal* focuses on a selection of research projects at two French language universities: one from Canada and the other from France. The descriptions will not discuss all of the current projects at the schools—there are too many. But selected studies provide a representative picture of the research work and demonstrate the importance of the schools to their countries and their impact on industry and the profession worldwide.

The universities and their researchers and graduate students are well known in the world of steel construction: the École Polytechnique in Montréal, Quebec, Canada, and the National Institute of Applied Sciences of Rennes in Brittany, France. In France, the latter is normally referred to as INSA–Rennes (Institut National des Sciences Appliquées de Rennes). There are several INSAs in France, all of which are powerful centers of advanced study in engineering and applied science.

The sizes of the civil engineering faculties in general—and, especially, the structural engineering groups—are essential for these institutions. The studies that are presented in the next sections describe elements of the projects as well as other long-time efforts. As has been typical of American and European—and indeed worldwide—engineering research projects for years, many of the projects are multi-year; a number are also multi-partner and some are also multi-country efforts. The outcomes of the projects focus on industry needs and implementation in design standards.

The researchers in Montréal and Rennes have been active for many years, as evidenced by their leading roles in research and development in Canada, the United States and Europe, but they have also been frequent participants in the work in other countries and regions. Numerous high-quality papers, reports, design guides and conference presentations have been published, contributing to a collection of studies that continue to offer solutions to complex problems for designers as well as fabricators and erectors.

References are provided throughout the paper, whenever such are available in the public domain. However, much of the work is still in progress, and in some cases reports or publications have not yet been prepared for public dissemination.

Reidar Bjorhovde, Dr.-Ing., Ph.D., P.E., P.Eng., Research Editor of the AISC Engineering Journal, Tucson, AZ. Email: rbj@bjorhovde.com

SOME CURRENT RESEARCH WORK AT ÉCOLE POLYTECHNIQUE OF MONTRÉAL

A broad discussion of some of the ongoing research work in the Department of Civil Engineering at École Polytechnique of Montréal (ÉPM) was presented in the Fourth Quarter 2013 issue of the *Engineering Journal* (Bjorhovde, 2013). However, it was not possible to include a number of important projects at that time, and these are detailed in this paper.

Collapse Prevention of Low Ductility Concentrically Braced Frames

This is a collaborative research project led by Professors Larry Fahnestock of the University of Illinois at Urbana-Champaign and Eric Hines of Tufts University in Boston. It addresses the seismic performance of low-ductility steel braced frames designed with $R = 3.0$ and located in low and moderate seismic regions. The objectives of the project are to develop a fundamental understanding of the seismic performance of such structures. Further, it is essential to increase their reliability and resistance to seismic collapse by accounting for existing lateral capacity or to provide enhanced reserve capacity. In low-ductility braced frames, the failure of brace connections in tension is likely to occur early during a strong earthquake, prior to brace buckling in compression and yielding in tension. This can result in significant loss in lateral strength and stiffness and may lead to frame dynamic instability (Hines, Appel and Cheever, 2009). Upon reversal of loading, braces at failed connections may re-engage in bearing, as shown for a slotted HSS connection in Figure 1a. This behavior is generally ignored in seismic collapse assessment analysis. One means of enhancing reserve capacity of the frames is to introduce partial-strength beam-to-column connections with top and seat angles in the gravity frame of the building, as illustrated in Figure 1b. Nonlinear time-history analyses have shown that the moment frame action that develops in the gravity frame and the compression response of the braces after brace connection failures can contribute significantly to collapse prevention (Fell et al., 2009; Fell and Kanvinde, 2010).

As part of this project, a test program is being performed at ÉPM on beam-to-column connections with bolted web, top and seat angles. Cyclic push-pull static and dynamic tests are performed on isolated angles of various sizes and bolt diameters and patterns. The aim is to develop simple numerical models that are capable of predicting the hysteretic moment-rotation response of the beam-to-column connections, as illustrated in Figure 1c. The model accounts for the contribution of the beam web angles as well as fracture of the angles at large-story drifts. The test program also includes cyclic quasi-static testing of full-scale beam-to-column connections to further validate the numerical joint models. A parallel test program has been developed to generate data on the ductility capacity of welded brace slotted connections and the brace compression response after weld failure. A later phase of the project will test full-scale two-story and half-scale four-story braced frames at the Lehigh University RTMD NEES testing facility.

Shaking Table Testing of Advanced Seismic Force Resisting Systems

New cost-effective systems to achieve superior seismic performance compared to conventional seismic force resisting systems are now being studied. The work has focused on steel-braced frames designed to obtain uniform drift demand over the frame height, to minimize floor accelerations and permanent deformations and to confine any structural damage to easily replaceable components. The solutions generally include elastic braced-frame segments that are interconnected by means of conventional or advanced energy dissipating components such as ductile shear links, buckling restrained braces, self-centering braces and viscous dampers.

One braced-frame configuration currently being studied is illustrated in Figure 2a. It includes four-story elastic braced-frame modules that are linked together and to an exterior column using dedicated energy dissipating elements. Rocking response at the base or over the frame height is also studied. For a given typology, research essentially consists of performing numerical seismic simulations to understand the system response, refining the original concept and eventually developing simplified methods for its design. In the process, experimental validation may be needed to validate the numerical predictions, especially when the response involves complex dynamic phenomena such as sudden increases in stiffness induced by contacts or impacts, rapid strength and stiffness degradation behavior, dynamic instability, higher mode response in the inelastic range or components exhibiting nonlinear rate dependencies. Such validations generally need to be performed at the global system level so that the interaction between the various components is present, as would be the case in actual structures. This can be achieved using shaking table tests on reduced-scale models or real-time hybrid simulations with physical substructures that reproduce the critical phenomena.

Taking advantage of the 36-ft clear test height and the high overturning moment capacity of the earthquake simulator at ÉPM, a unique reconfigurable test setup was constructed over the last five years to perform shaking table testing of structural models up to eight stories. The setup includes a gravity/mass system that emulates the tributary floor seismic masses and weights for the lateral load resisting system being tested on the shaking table.

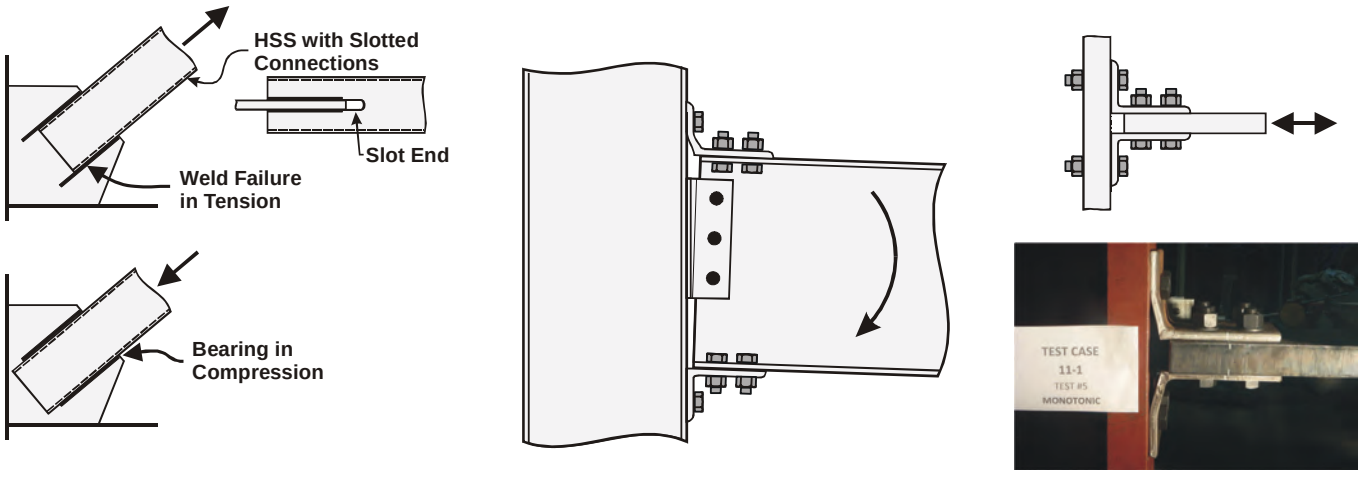

Fig. 1 (a) Re-engagement of a bracing member after weld failure in tension; (b) rotation demand; and (c) tests on isolated angles for beam-to-column connections with web, top and seat angles in the gravity system of low-ductility CBF structures (figures courtesy of Professor Robert Tremblay).

Figure 2b shows the setup that was recently used in a project with Professor Constantin Christopoulos of the University of Toronto for an eight-story braced frame. The frame was designed with two rocking interfaces and a self-centering brace fuse at the first level (Wiebe et al., 2013). As shown in this figure and in Figure 1, the mass/weight system is located on the laboratory ground floor, next to the earthquake simulator, so that the full payload capacity of the equipment is available for the testing. *P*-Δ effects are included in the tests and direct measurements of the applied inertia forces are obtained through the instrumented rigid arms connecting the masses to the specimen. In the future, it is planned to use the setup for similar test programs on other advanced steel seismic force resisting systems.

Future Experimental Research on Column Buckling under Seismic Demand

The potential for column instability under gravity plus seismically induced axial compression and flexural demands represents an important issue in several current research projects. This is the case for columns in multi-story braced frames where the primary axial load demand from gravity loads and brace axial forces is accompanied by in-plane flexural demand from the frame response. Large drifts develop due to the stiffness of the beam-to-columns connections where braces connect to columns, with unavoidable differences in drifts between adjacent stories. Both effects are schematically illustrated in Figure 3. While peak

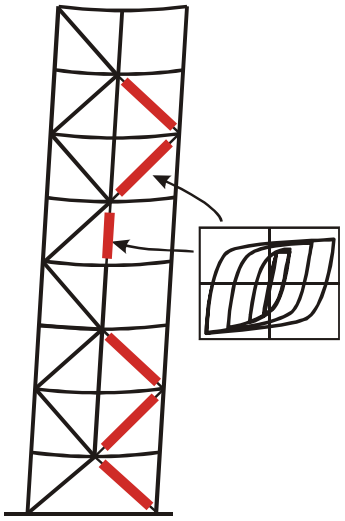

(a)

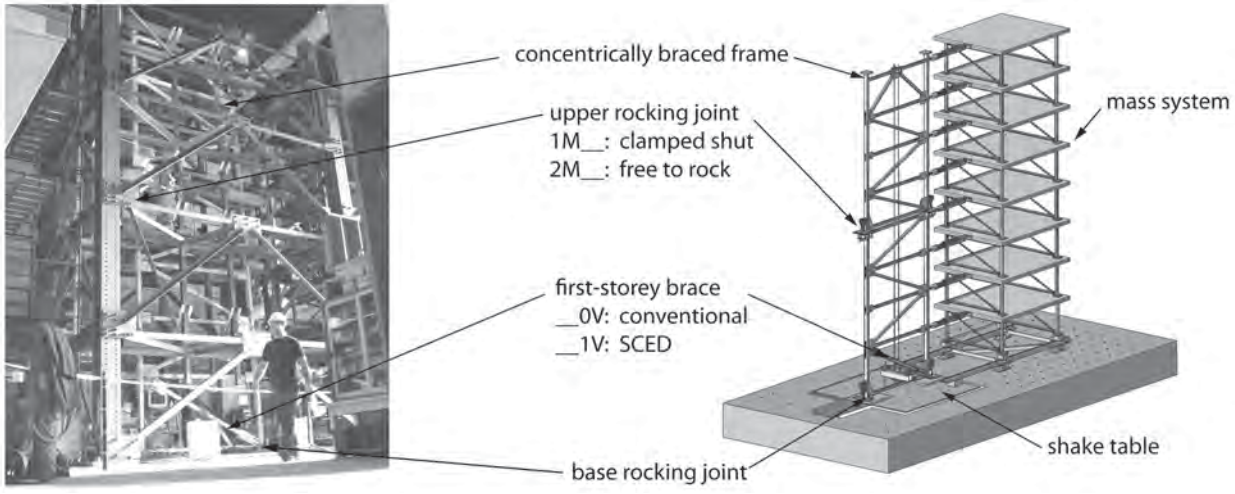

(b)

Fig. 2 (a) Innovative steel-braced frame for enhanced seismic performance; (b) reconfigurable shaking table setup for seismic testing of a rocking-braced steel frame with a base self-centering brace shear fuse (figures courtesy of Professor Robert Tremblay).

axial forces in columns of braced frames can be safely predicted by applying capacity design principles, the moment demand can only be assessed using nonlinear response history analysis as it depends on the amplitude and distribution of the frame inelastic deformations during earthquakes. Recent studies of multi-tiered braced frames used in tall single-story structures have been found to be particularly prone to pronounced variations of drifts over their height (Imanpour et al., 2013). Similar behavior is observed in moment frames and eccentrically braced frames with link-to-column connections. For such frames, the flexural demand from the beams or links can be determined from capacity design methods, but the prediction of column bending due to uneven story drifts remains a challenge for design. This response may lead to uneven distribution of the bending moments below and above the beam-to-column connections and the points of inflection that are far from the column mid-height, as is generally assumed in design.

Cyclic testing by Newell and Uang (2008) showed that stocky, fixed-ended W14 columns meeting the AISC section seismic compactness limits could develop plastic hinges at their ends without overall buckling, even when carrying high compressive loads. This suggests that excessive flexural demands on such columns can be accommodated through ductile inelastic flexural deformations. Numerical simulations indicate, however, that column buckling may be triggered when flexural demand not considered in design is applied to columns. As an example, this could be the case for slender columns subjected to flexure approaching single curvature.

Deep columns bent about their strong axis may also fail by lateral-torsional buckling. Buckling of gravity columns due to bending moments induced by large-story drifts concentrating in a given floor is another possible column stability failure example. This situation, which is not covered in current design provisions, may control the lateral deformation capacity of frames.

Column instability due to seismic effects is a complex problem as the axial and flexural demands are cyclic and vary in time, not necessarily in phase, and they are induced by a combination of loads and inelastic displacements. Further, column buckling typically involves large plastic deformations and local buckling. As part of this project, column testing is being planned at ÉPM to complement and validate current numerical work. In collaboration with Professor Charles-Philippe Lamarche of Sherbrooke University, tests will be performed on braced-frame columns with deep columns for moment frames. These studies are done in collaboration with Professor Dimitrios Lignos of McGill University and for columns of multi-tiered braced frames and gravity columns with Professors Larry Fahnestock of the University of Illinois and Christopher Stoakes of the University of Iowa. Realistic axial and uni- or bi-directional flexural demands will be applied to column specimens with the multi-axis loading apparatus shown in Figure 1, using either pre-defined protocols established from nonlinear response history analysis of prototype buildings or from hybrid simulation techniques.

SOME CURRENT RESEARCH WORK AT THE NATIONAL INSTITUTE OF APPLIED SCIENCE IN RENNES, FRANCE

Between 2002 and 2010, the French National Research Project MIKTI was undertaken to develop methods of analysis and design for composite bridges of small and medium spans. Under the leadership of department chair Professor Mohammed Hjiaj and project director Alain Lachal, the contribution of the Structural Engineering Research Group at INSA–Rennes was a major factor in the success of this project. Working in close collaboration with SNCF, the French national railroad organization, and with the companies ArcelorMittal and Vinci, the primary efforts focused on two topics: (1) innovative and economical solutions for continuous beams of composite bridges and (2) the mechanical behavior of groups of headed stud shear connectors with prefabricated slab and steel girders.

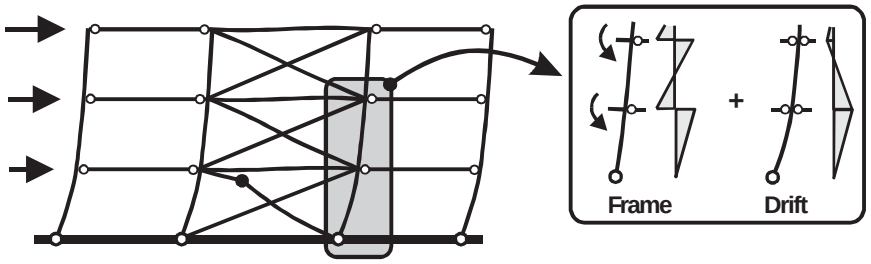

Fig. 3 In-plane flexural demand on columns of steel braced frames. Pinned column bases are shown for simplicity (figures courtesy of Professor Robert Tremblay).

Innovative Connection Solutions

For composite bridges of small and medium spans, the choice of a multi-beam deck with hot-rolled shapes connected to a reinforced concrete slab often appears to be an effective, economical, simple and fast solution for implementation on site. When the total length of the structure exceeds the limit for transport and handling, a beam-to-beam connection on site is necessary to ensure the continuity of the deck.

Three continuous joint solutions were selected, as shown in Figure 4. The first solutions uses bolted web cover plates and a direct contact between the compressed bottom flanges of the steel girders. The second solution uses butt plates anchored in the side faces of a transverse bridge piece of reinforced concrete. The third solution uses complete embedding of the two steel girder ends of the composite beam in a massive reinforced concrete transverse beam. Direct contact between the compressed steel girder flanges was also introduced in the third solution.

To connect the steel girder web ends inside the concrete embedding, two different arrangements were considered: on one side, eight-headed stud shear connectors were welded in pairs on each face of the steel girder web, and on the other side, eight transverse bars (to replace the shear connectors) would pass through predrilled holes in the web of the steel girder end.

For each connection solution, numerical modeling as well as large-scale laboratory and onsite tests were used to develop the design approaches.

Fabrication of Connections

For all the proposed solutions, the steel components of the composite beams are first prepared in the shop and equipped with steel elements for connections (plates, holes, welded headed studs, etc.). Then, the steel girders are transported to the construction site and placed on the supports. The connection components and the reinforcement are then installed. The concrete for the slab is poured and the continuity of the composite beam is completed by placing the concrete for the connection and the transverse beam over the pier at the same time (in the case of solutions 2 and 3). With the exception of solution 1, which requires a special team for the tightening of bolts, solutions 2 and 3 do not require any skilled labor. Some preliminary calibrations were carried out, such as those needed to develop the procedure to ensure good implementation of the material between the two ends of the girder flanges in order obtain the direct contact used for connections in solutions 1 and 3, as shown in Figure 5.

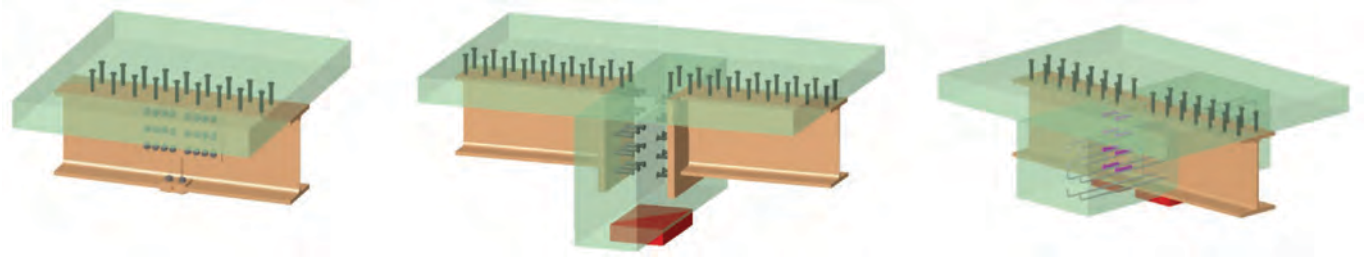

(a) (b) (c)

Fig. 4. Connection solutions, slab reinforcement not shown for clarity: (a) bolted connection with direct contact; (b) butt-plate connection; and (c) embedded connection (figure courtesy of Professors Mohammed Hjiaj and Alain Lachal).

(a) (b) (c)

Fig. 5. (a) ArcelorMittal fabrication; (b) INSA fabrication; (c) implementation of direct contact (photographs courtesy of Professors Mohammed Hjiaj and Alain Lachal).

Experimental and Numerical Studies

Test specimens were designed at approximately half-scale of typical medium-span bridges. They were fabricated and tested at the Structures Laboratory of INSA–Rennes, as shown in Figure 3. The specimens were first tested under fatigue loading and then the load was monotonically increased until failure. Moment-rotation characteristics were recorded, as shown in Figure 6, as were displacements, strains and stresses.

In addition, tests on a road bridge in service were also carried out over a period of eight years, to study the in-service behavior of the connections. This is illustrated in Figure 7.

(a) *(b)*

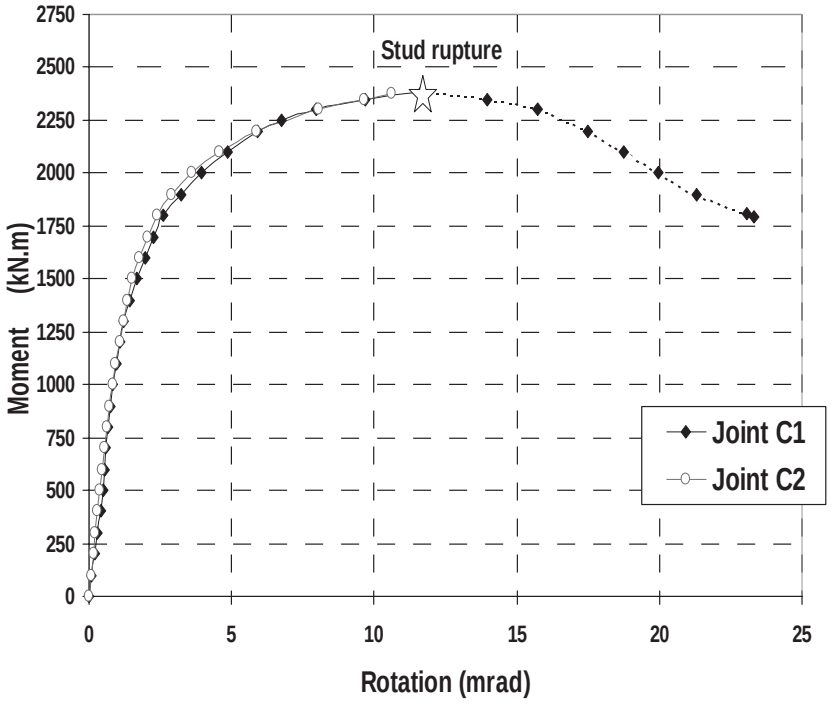

(c)

Fig. 6. (a) Connection 1; (b) connection 3; (c) moment-rotation curve for connection 3 (photographs and figure courtesy of Professors Mohammed Hjiaj and Alain Lachal).

To allow for an accurate interpretation of the test results, 2D and 3D finite element modeling was done for all of the connection types and calibrated against the experimental results. It was determined that the connections were able to achieve the continuity of the composite bridge desks with a satisfactory rotational stiffness and strength.

Connection Design

Simple design methods have been proposed for each of the three types of connections. As the basic design principle, it was decided to maintain a distribution of internal forces as close as possible to the distribution found in the beam cross-section close to the connection. This would maintain the same position of the elastic neutral axis. Because a connection is necessarily located near an intermediate support, only the negative bending moment that would be transmitted is considered. In French composite bridge design practice, the steel girder cross-sections are often slender (noncompact), such that only elastic analysis has been developed in this study.

Figure 8 provides a schematic illustration of this approach, with the normal and shear stress distributions in the composite section of the beam and the distribution of internal forces that the connection will have to transmit.

Grouped Shear Connection

A separate effort within the framework of the MIKTI project has dealt with the behavior and strength of groups of headed stud shear connectors in composite bridges. The main parameters were the material used to connect prefabricated slabs to steel flanges, the dimensions and characteristics of recesses in the prefabricated slabs, the placement of the reinforcing bars through the recesses and the number (four- or nine-headed studs per recess) and the spacing of the connectors. This is shown in Figure 9.

The interpretation of push-out test results mainly addressed the initial stiffness, the maximum strength and the ductile capacity of a group of shear connectors based on the experimental slip-shear force curves. The results have shown that the initial stiffness and the maximum strength of groups of

(a) *(b)*

Fig. 7. (a) Tested bridge; (b) loading of bridge (photographs courtesy of Professors Mohammed Hjiaj and Alain Lachal).

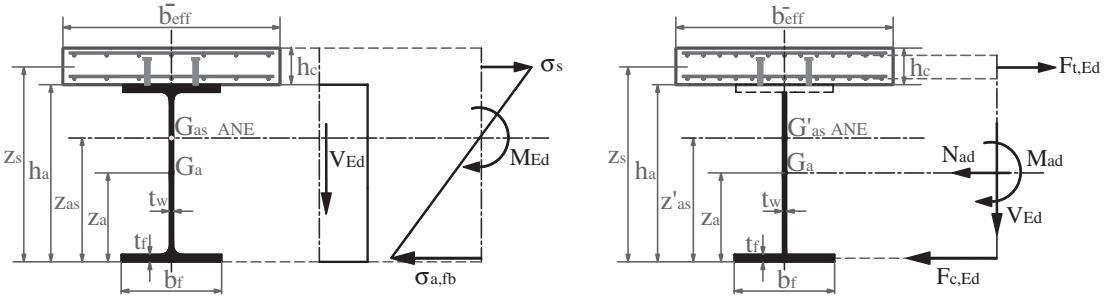

Fig. 8. Typical connection details and stress resultants (sketches courtesy of Professors Mohammed Hjiaj and Alain Lachal).

stud shear connectors increase with the performance of the concrete, whereas the slip capacity decreases.

Compared to standard test results, a reduction of about 10% of the initial stiffness and the maximum strength was observed, without a significant reduction of the slip capacity in the case of grouped stud connectors, with the same type of concrete as the concrete of the prefabricated slab.

ACKNOWLEDGMENTS

Professors Robert Tremblay, Mohammed Hjiaj and Alain Lachal have provided significant assistance in the development of this paper. Their efforts are sincerely appreciated.

REFERENCES

AISC (2012), *Seismic Design Manual,* 2nd ed., American Institute of Steel Construction, Chicago, IL.

Bjorhovde, R. (2013), "Current Steel Structures Research No. 34," AISC, *Engineering Journal,* Fourth Quarter, pp. 291-304.

Fell, B.V., Kanvinde, A.M., Deierlein, G.G. and Myers A.T. (2009), "Experimental Investigation of Inelastic Cyclic Buckling and Fracture of Steel Braces," ASCE, *Journal of Structural Engineering*, Vol. 135, No. 1, pp. 19–32.

Fell, B.V. and Kanvinde, A.M. (2010), "Tensile Forces for Seismic Design of Braced Frame Connections–Experimental Results," *Journal of Constructional Steel Research*, Vol. 66, pp. 496–503.

Hines, E.M., Appel, M.E. and Cheever, P.J. (2009), "Collapse Performance of Low-Ductility Chevron Braced Steel Frames in Moderate Seismic Regions," AISC, *Engineering Journal*, Third Quarter, pp. 149–180.

Imanpour, A., Stoakes, C., Tremblay, R., Fahnestock, L. and Davaran, A. (2013), "Seismic Stability Response of Columns in Multi-Tiered Braced Steel Frames for Industrial Applications," *Proceedings, 2013 ASCE Structures Congress,* Pittsburgh, PA, pp. 2650–2661.

Newell, J.D. and Uang, C.M. (2008), "Cyclic Behavior of Steel Wide-Flange Columns Subjected to Large Drift," ASCE, *Journal of Structural Engineering*, Vol. 134, No. 8, pp. 1334–1342.

Wiebe, L., Christopoulos, C., Tremblay, R. and Leclerc, M. (2013), "Mechanisms to Limit Higher Mode Effects in a Controlled Rocking Steel Frame. Part 1: Concept, Modeling and Low-Amplitude Shake Table Testing," *Earthquake Engineering and Structural Dynamics*, Vol. 42, No. 7, pp. 1053–1068.

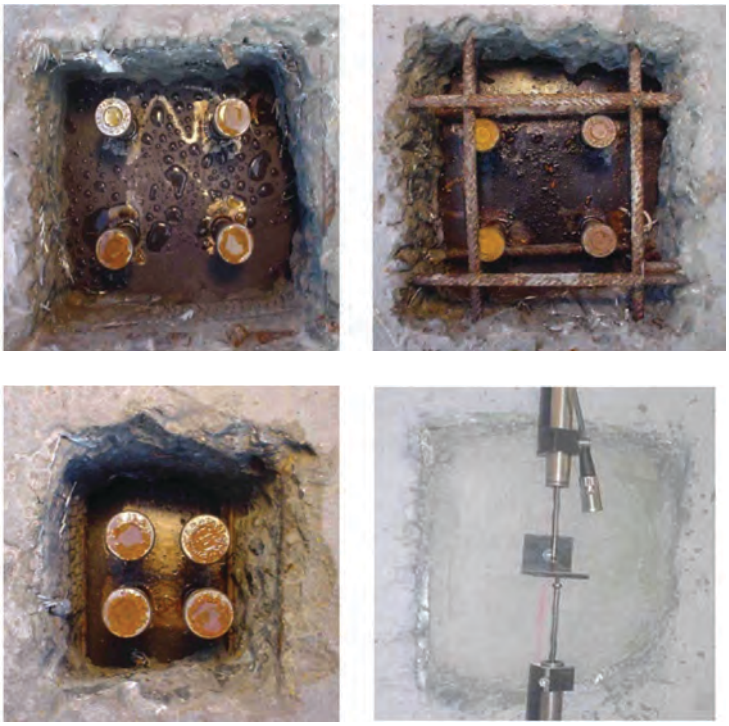

Fig. 9. Group arrangements of the stud shear connectors (photographs courtesy of Professors Mohammed Hjiaj and Alain Lachal).

GUIDE FOR AUTHORS

SCOPE: The ENGINEERING JOURNAL is dedicated to the improvement and advancement of steel construction. Its pages are open to all who wish to report on new developments or techniques in steel design, research, the design and/or construction of new projects, steel fabrication methods, or new products of significance to the uses of steel in construction. Only original papers should be submitted.

GENERAL: Papers intended for publication may be submitted by mail to the Editor, Keith Grubb, ENGINEERING JOURNAL, AMERICAN INSTITUTE OF STEEL CONSTRUCTION, One East Wacker Drive, Suite 700, Chicago, IL, 60601, or by email to grubb@aisc.org.

The articles published in the *Engineering Journal* undergo peer review before publication for (1) originality of contribution; (2) technical value to the steel construction community; (3) proper credit to others working in the same area; (4) prior publication of the material; and (5) justification of the conclusion based on the report.

All papers within the scope outlined above will be reviewed by engineers selected from among AISC, industry, design firms, and universities. The standard review process includes outside review by an average of three reviewers, who are experts in their respective technical area, and volunteers in the program. Papers not accepted will not be returned to the author. Published papers become the property of the American Institute of Steel Construction and are protected by appropriate copyrights. No proofs will be sent to authors. Each author receives three copies of the issue in which his contribution appears.

MANUSCRIPT PREPARATION: Manuscripts must be provided in Microsoft Word format. Include a PDF with your submittal. View our complete author guidelines at **www.aisc.org/ej**.

There's always a solution in steel.

ENGINEERING JOURNAL
American Institute of Steel Construction
One East Wacker Drive, Suite 700
Chicago, IL 60601

312.670.2400 www.aisc.org